School of Chemistry

[A study of Boron-Nitrogen clusters as an N-type co-dopant in diamond]

[Eduardo Requena]

This thesis is submitted in partial fulfilment of the requirements for the Honours Degree of MSci at the University of Bristol

Supervisor - Neil J Fox

Second Assessor - Paul May

Section - Physical Chemistry

Abstract

Diamond has shown enormous potential to be used as a material in high-speed electronics and energy conversion devices due to its superior properties over all other materials. The development of these devices has been slowed down due to the absence of a reliable and highly conductive n-type diamond material, which would allow a great advance in the matter. To achieve n-type conductivity, an element with more electrons than the parent element (Carbon) needs to be introduced into the lattice of diamond to form a dopant level near the conduction band.

In order to synthesise these diamond films, past computational studies have been reviewed to achieve information on the nature of the clusters that showed low donor levels and could be introduced in the lattice of diamond during growth. Nitrogen-rich Boron-Nitrogen clusters showed promising results as one way of achieving n-type conductivity by co-doping. Previous experimental work showed this method to work partially, decreasing the value of the donor level by around 50% in comparison to Nitrogen. Although this project is not strictly comparable to the previous work, as the Boron concentration was increased to achieve a conductive material at room temperature, in addition to using different reactors, growth parameters and geometry of substrates.

In this thesis, further investigation was made relating to the change from p-type to n-type semiconduction in CVD (Chemical Vapour Deposition) diamond films. Different growths were first made on Silicon substrates to inspect the surfaces and growth rate by Raman spectroscopy and Scanning Electron Microscopy (SEM). The parameters of the experiment were kept constant during growth, with molecular hydrogen kept at 500 sccm, methane kept at 20 sccm and diborane at 50 ppm in comparison to hydrogen. Nitrogen level was changed from 2% to 4.5% in 6 different growths, another growth was made with no Nitrogen to use as a comparison. The electrical properties were analysed first by two-probe contact measurements to get a rough estimate of the electrical resistance, and then by Hall effect measurements to achieve the resistivity, carrier concentration and mobility of the samples.

After completion of studies using Silicon as substrates, Single Crystal Diamond (SCD) substrates were used instead. This meant a change in the growth parameters but allowed to synthesise a more conductive material than on Silicon, with an homoepitaxial growth. After achieving the conductive Boron-doped diamond, Nitrogen was introduced in different growths at different concentrations, up to an N/B ratio of 500.

The same analytical tests were carried out for these samples as for the ones grown on Silicon. The electrical measurements, showed a decrease in resistivity upon addition of Nitrogen in the growth up to 180 N/B ratio, which is thought to be caused by the formation of BN-clusters. In these BN-clusters, Nitrogen atoms in substitutional positions are thought to be bonding to the Boron atoms that occupy interstitial positions due to the high level of doping, increasing mobility in the sample and hence, decreasing resistivity.

All the samples showed p-type carriers, but the formation of BN-clusters could have been proved by the decrease in resistivity upon addition of Nitrogen during growth. In this project, a detailed future work section describes what direction next experiments regarding co-doping of diamond should take.

Acknowledgements

I would like to thank my supervisor, Professor Neil Fox for all his help throughout the year and for making this project possible. I would also like to thank Professor Paul May for the advice and ideas for the project.

I wanted to give an especial thank you to Dr Hugo Dominguez and soon to be Dr Ramiz Zulkharnay for all their help at the lab and making time to answer all of my endless questions. I could not have done the project without their help and amazing knowledge on the subject.

Also, a final thank you to everyone in the diamond lab for all the help and being incredibly supportive at all times.

Table of contents

1. Introduction

1.1. Diamond and its synthesis

1.1.1. Diamond structure and its properties

Throughout history, diamonds have been associated with wealth, as precious stones, rather than having a scientific purpose. Natural diamonds are a rare mineral on Earth's surface; they are formed under high-pressure and high-temperature conditions that are generated in the Earth's mantle, deeper than ~150 km from the surface, or from dynamic compressions during meteoritic impacts to rocks on the crust of the Earth. Diamonds exhibits some extreme properties that makes them captivating for scientific research and a potential material in engineering applications, such as high-speed electronics and response systems as well as high-power laser windows, protective coatings, electrochemical sensors, and many more. Some of these exceptional properties include extreme mechanical hardness (-90 GPa), the highest known value of thermal conductivity at room temperature (2000 $Wm^{-1}K^{-1}$), high resistance to chemical corrosion, high radiation hardness, etc [i,ii].

Diamond, along with the crystalline form of graphite, are the most common allotropes of carbon, which makes for an exceptionally simple structure. Graphite consists of layers of sp^2 hybridised carbon atoms, each bonded to three equidistant carbon atoms, the layers are attracted to each other by Van der Waals forces and may be arranged in hexagonal or rhombohedral stacking sequences, with the former being the least frequent (shown in Figure 1). Diamonds, by contrast, consist of sp^3 hybridised carbon atoms, each bonded to four other bonded carbons in a tetrahedral arrangement (shown in Figure 1). This accounts for diamond being a much stronger compound than graphite and the lack of delocalised electrons in diamonds explains why it is an insulator at room temperature, with a band gap of 5.5 eV. Diamond contains ~$2*10^{23}$ C atoms per cm^3 in its lattice, and possesses a lattice constant of a=3.567Å, each carbon-carbon bond is equidistant with a distance between each neighbour atom of 1.545 Å [iii,iv].

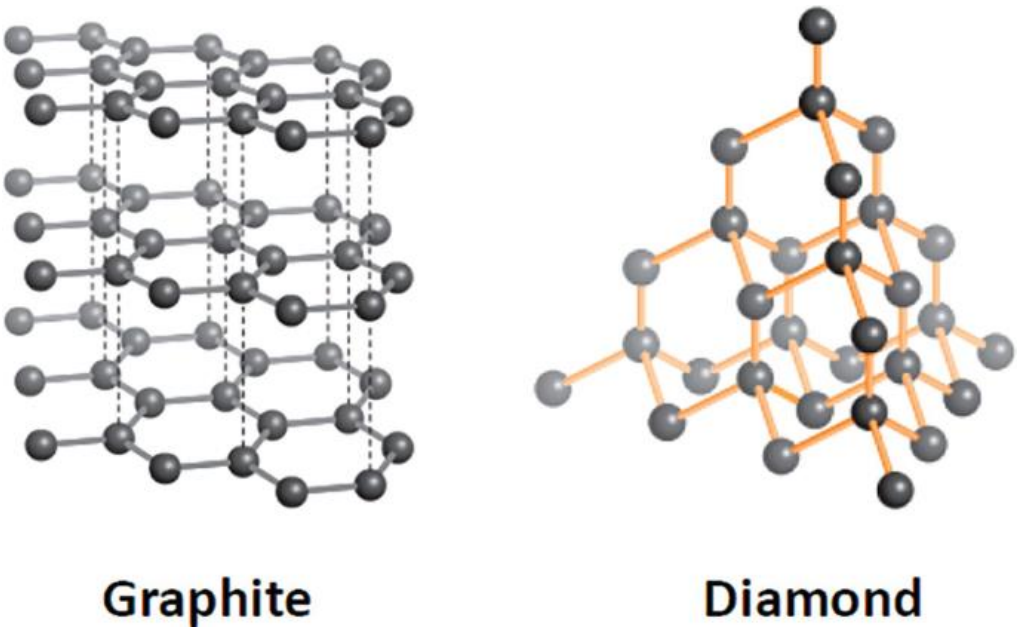

Figure 1: Structure of the most common allotropes of carbon, graphite and diamond. From the work of Kharisov, B.J. et al [v].

Diamonds can have different crystallographic structures with the (100) surface and (111) surface being the most important (shown in Figure 2). The differences in the type of surfaces can give different properties to the crystals; the growth of homoepitaxial diamond is much less prone to incorporation of stacking faults in case of (100) in comparison to (111) surfaces. The several types of surfaces can even be selectively grown if the appropriate parameters are controlled in a CVD type synthesis. At low temperature of the substrate and low CH_4 partial pressure (111) facets are more likely to appear, and (100) facets are more likely to appear if these two parameters are increased [vi].

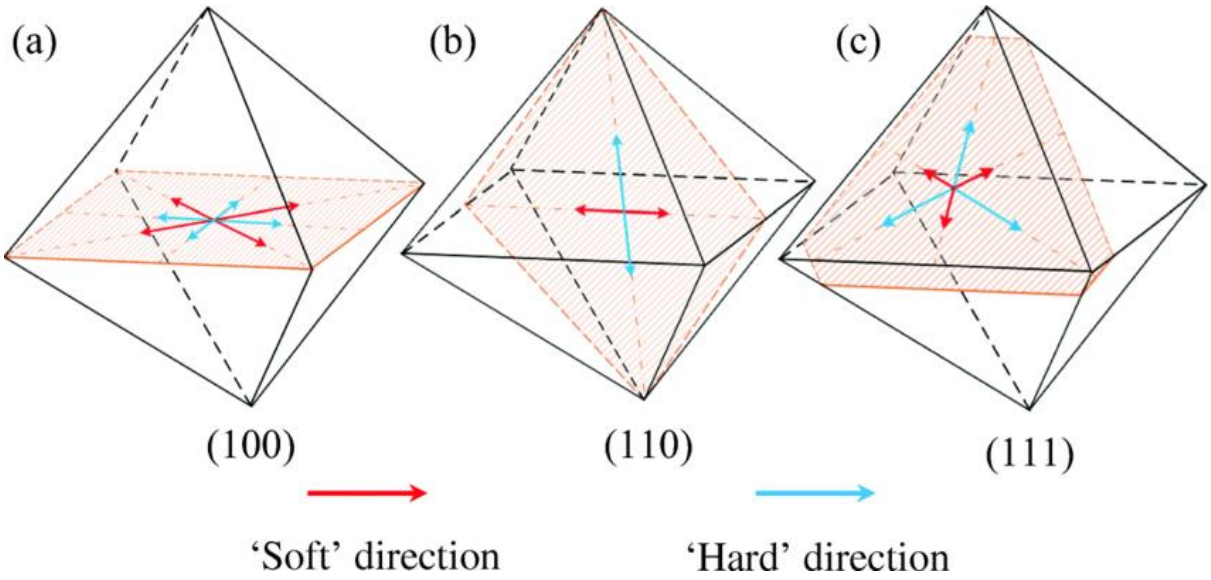

Figure 2: Differences in structure of (100), (110) and (111) orientation in diamond, showing a square surface in (100) and a triangle for (111) surfaces. From the work of Wang, J. *et al* [vii].

The different surfaces are known to have a big impact in the growing parameters and in the boron incorporation into the lattice. As shown in Table 1, the amount of carbon that is introduced compared to hydrogen during growth, can change from 1% in (100) to 0.1% in (110) to 0.136% in (111) in order for growth to happen. Studies also show a higher incorporation of Boron in (110) substrates than (100) and (111). The study also indicates by Secondary Ion Mass Spectrometry (SIMS) and Hall effect measurements that most of the incorporated atoms in (110) and (100) surfaces are electrically active, hence not depositing at interstitial positions or aggregates [viii]. Based on these favourable results towards the (110) surface, the Single Crystal Diamond substrates used for this project were (110) orientated, although not a lot of research has been done on these types of films, which hindered the finding of adjustable growth parameters.

Table 1: Data showing the difference in growing parameters for different crystallographic orientations. Based on the work of Mortet, V. *et al* [viii].

Substrates	(100)	(110)	(111)
Pressure (mbar)	110	130	110
MW power (W)	500	500	500
Temperature (°C)	1100	1100	1000
Total gas flow rate (sccm)	500	500	500
CH_4 concentration in H_2	1%	0.1%	0.126%
B/C ratio (ppm)	0-240	0-20	0-635

1.1.2. Diamond "types"

Gemmologists and science researchers have dedicated much time to classify the diverse types of diamonds that have existence. Gemmologists are interested in separating natural and synthetical diamonds, but their classification can also be useful for researchers. As stated before, diamonds are composed of only Carbon, but often they show impurities, like Nitrogen (N) atoms or Boron (B) atoms. These impurities can affect the colour, fluorescence, visible absorption spectra, and other properties of diamonds. Furthermore, it has been proved that diamonds with a minimal concentration of N impurities (0.3 ppm) exceed other diamond types with more impurity's concentration regarding to hardness and wear resistance. While other impurities can be incorporated into the lattice, the diamond type classification system focuses solely into Boron and Nitrogen impurities, as they are the ones most frequently found [ix,x].

The classification is divided into two broad categories (Figure 3): type I and type II. Type I diamonds are the ones that contain enough Nitrogen to be detected by IR absorption spectroscopy, whereas type II diamonds do not contain enough Nitrogen to be detected by the IR spectrometer. These broad categories are then subdivided into further subgroups regarding the nature of the impurities in them. Type I group subdivides into type Ia with aggregated N impurities and type Ib which contains isolated single N impurities. Type II group also subdivides into two categories; type IIa which contains no Boron or Nitrogen impurities and type IIb which mainly contains boron impurities [ix].

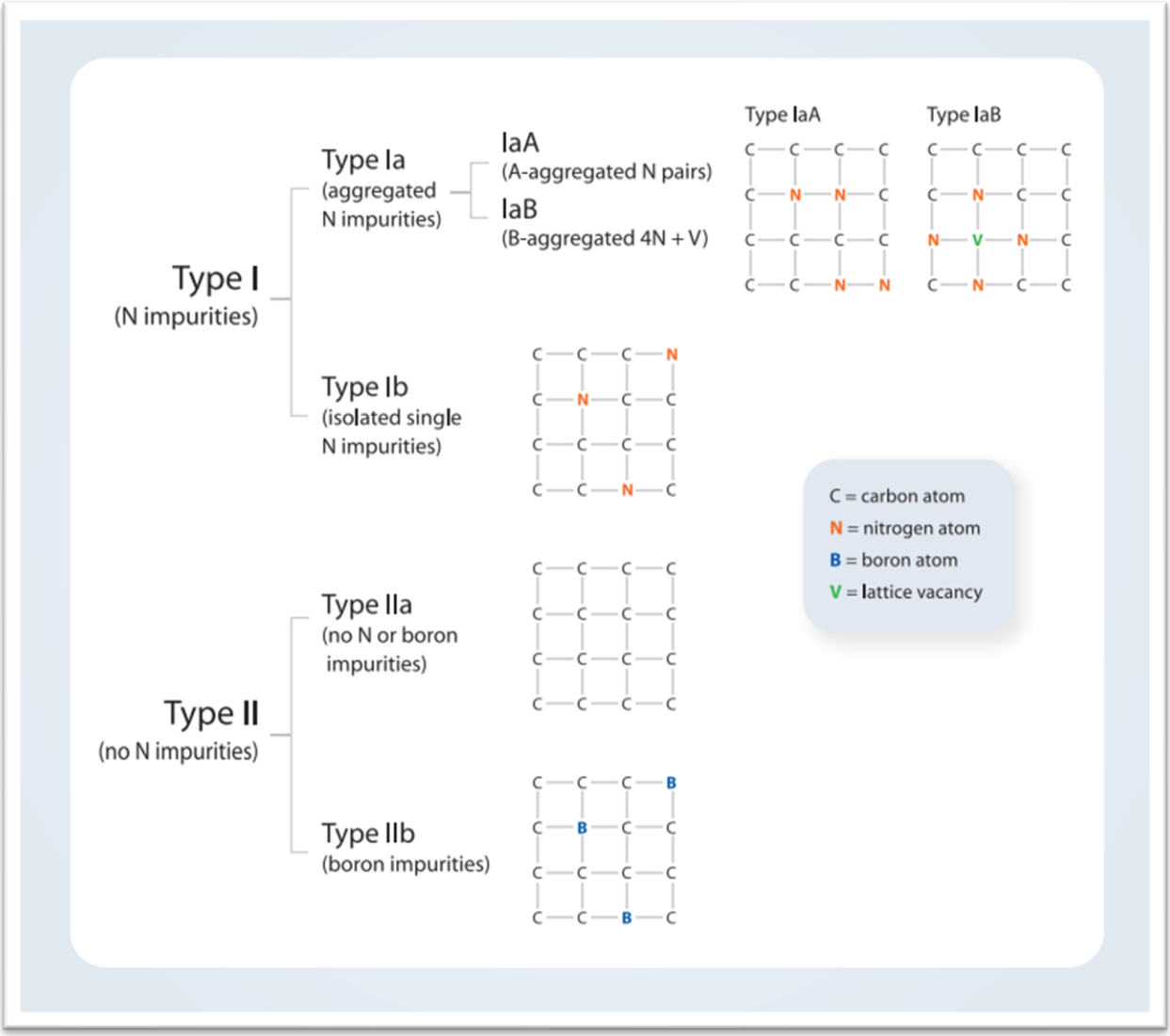

Figure 3: Diagram showing the two distinct categories of diamond and its subcategories, based on the impurities present on the lattice. From the work of Breeding, C.M. and Shigley, J.E. et al [ix].

1.2. Synthesis of diamond

1.2.1. History of synthetical diamonds

After the discovery by Antoine Lavoisier in 1792 and by Smithson Tenet in 1797 that diamond and graphite were indeed carbon allotropes, the search for methods on how to synthesise diamond or how to change abundant graphite into rare diamond initiated. Although it shows extreme properties, diamond is thermodynamically unstable compared to graphite. Delta G for diamond to graphite is negative and therefore spontaneous, but the transition from diamond to graphite has a large kinetic barrier, so diamond is not likely to transition on its own to graphite and is therefore kinetically stable. Also meaning that diamond crystals can be synthesised under appropriate conditions [xi,xii].

After many years of research, two different methods were issued in the 1950s, chemical vapour deposition (CVD) and high-pressure high-temperature (HPHT), and in 1956, the first synthetic diamond was made by H. Tracy Hall using a HPHT device designed by himself, while working for General Electric [iii, iv]. Figure 4 shows the pressure and temperature phase and the transition diagram of pure carbon, along with the conditions needed to carry out the various methods for diamond synthesis.

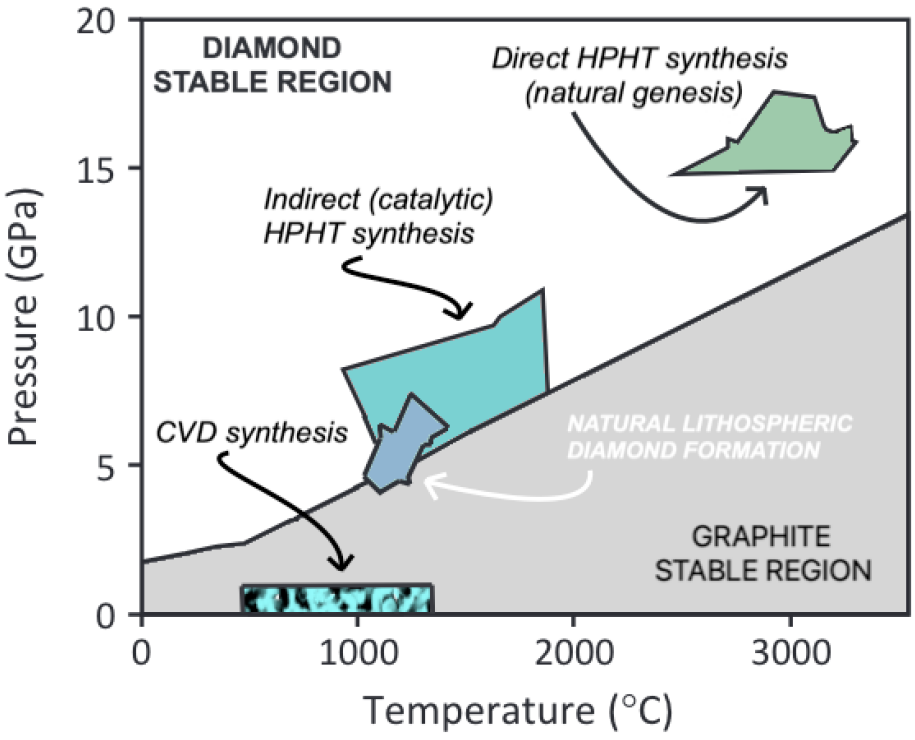

Figure 4: Graph showing the conditions needed in the three different pathways to form diamond: HPHT, CVD, and natural diamond formation. From the work of D'Haenens-Johansson, U.F., Butler, J.E. and Katrusha, A.N. et al [xii].

Both methods, HPHT and CVD are currently used nowadays for synthesis of diamonds, either for research of diamond films and coating or for industrial cutting tools or to be sold as gemstones [xii]. The two methods are different and have its own advantages and disadvantages, which will be discussed further in the report.

1.2.2. High pressure high temperature (HPHT) synthesis

As stated earlier, HPHT was the first method to synthesise diamond in the 1950s, which made it the only method of diamond growth until the 1980s. This method mimics the high pressures and temperatures of natural formation in the Earth's mantle. In further detail, HPHT diamond growth takes place in a capsule that can generate high pressures and temperatures (Figure 5). The standard temperatures used for the method are around 1200ºC – 1500ºC, with pressures going approximately around 4.5 x 10^7 Torr [xiii,xiv]. A diamond seed and a source of carbon, normally graphite, is used. A press is then used to crystallise the diamond at the mentioned temperature and pressure in which diamond is the thermodynamically stable allotrope of carbon [xii]. Process can either be direct or indirect (catalytic). The main disadvantages of this process are the high equipment and energy costs needed to obtain such temperatures and pressures. The indirect growth (Figure 4) improves one of the disadvantages, as it uses much fewer extreme conditions by using metal catalysts such as Iron, Nickel or Cobalt , reducing the expenses of the growth [xv].

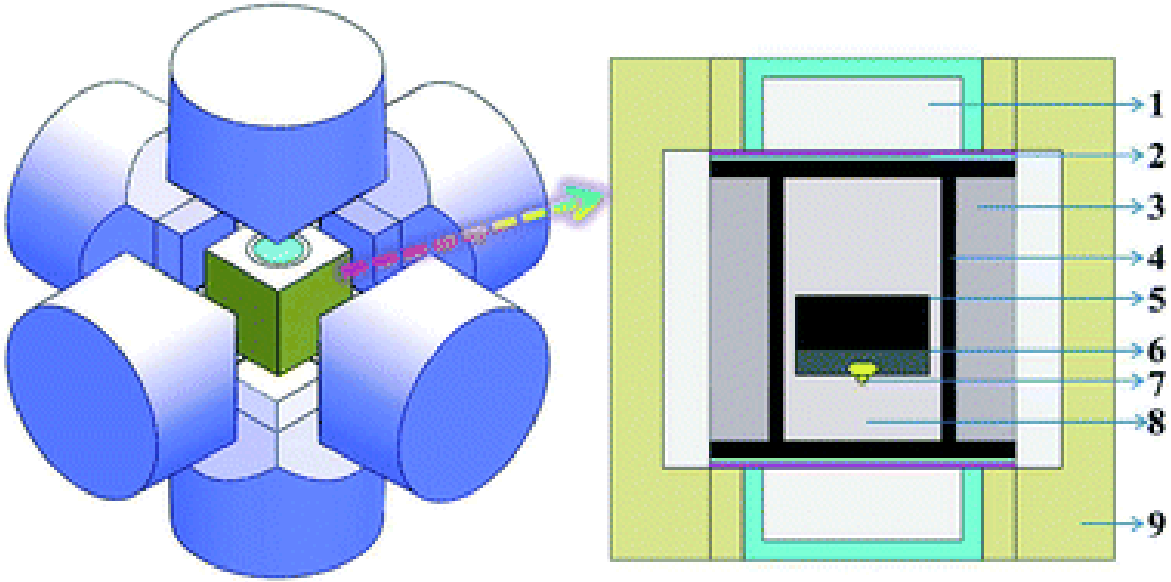

Figure 5: HPHT capsule for diamond growth: 1- steel cap; 2-Cu+Mo sheet; 3- NaCl + ZrO_2 sleeve; 4- graphite heater; 5-carbon source; 6- metal catalyst; 7- seed crystal; 8- ZrO_2 + MgO pillar; 9- pyrophyllite. From the work of Fang, C. et al. [xvi].

Another drawback of the HPHT method is the incorporation of Nitrogen into the lattice of diamond. The abundance of Nitrogen in the atmospheric air is responsible for the formation of HPHT diamonds with a few 100 ppm of N. These nitrogen atoms are also heterogeneously distributed in the lattice, as the concentration of nitrogen in the capsule decreases with time so does the incorporation of nitrogen into the lattice [xvii,xviii]. The ability to control the amount of impurities incorporated into diamond is a vital characteristic for utilizations past cutting tools or gemstones, which makes the HPHT method impractical for more advanced purposes.

Although HPHT is a common technique used for industrial and research purposes, it will not be discussed any further in this report.

1.2.3. Chemical vapour deposition synthesis of diamond

Patent for CVD was issued two years before HPHT was presented, in 1954. The CVD process does not mimic the natural production of diamond and does not require extreme pressures or temperatures, which made early researchers sceptical about the method. But the process did not get attention until the 1980s when the first reports of CVD growth of diamond were issued. These publications were made by a group in Japan, the National Institute for Research in Inorganic Materials which reported a series of papers in which diamond was deposited in various substrates at temperatures between 600ºC and 1000ºC and pressures of 0.5-750 Torr using different techniques, such as hot-filament CVD, RF-plasma CVD, and microwave plasma CVD. Since then, CVD gained much attention, and numerous research programs were spawned [xix,xx,xxi, xxii].

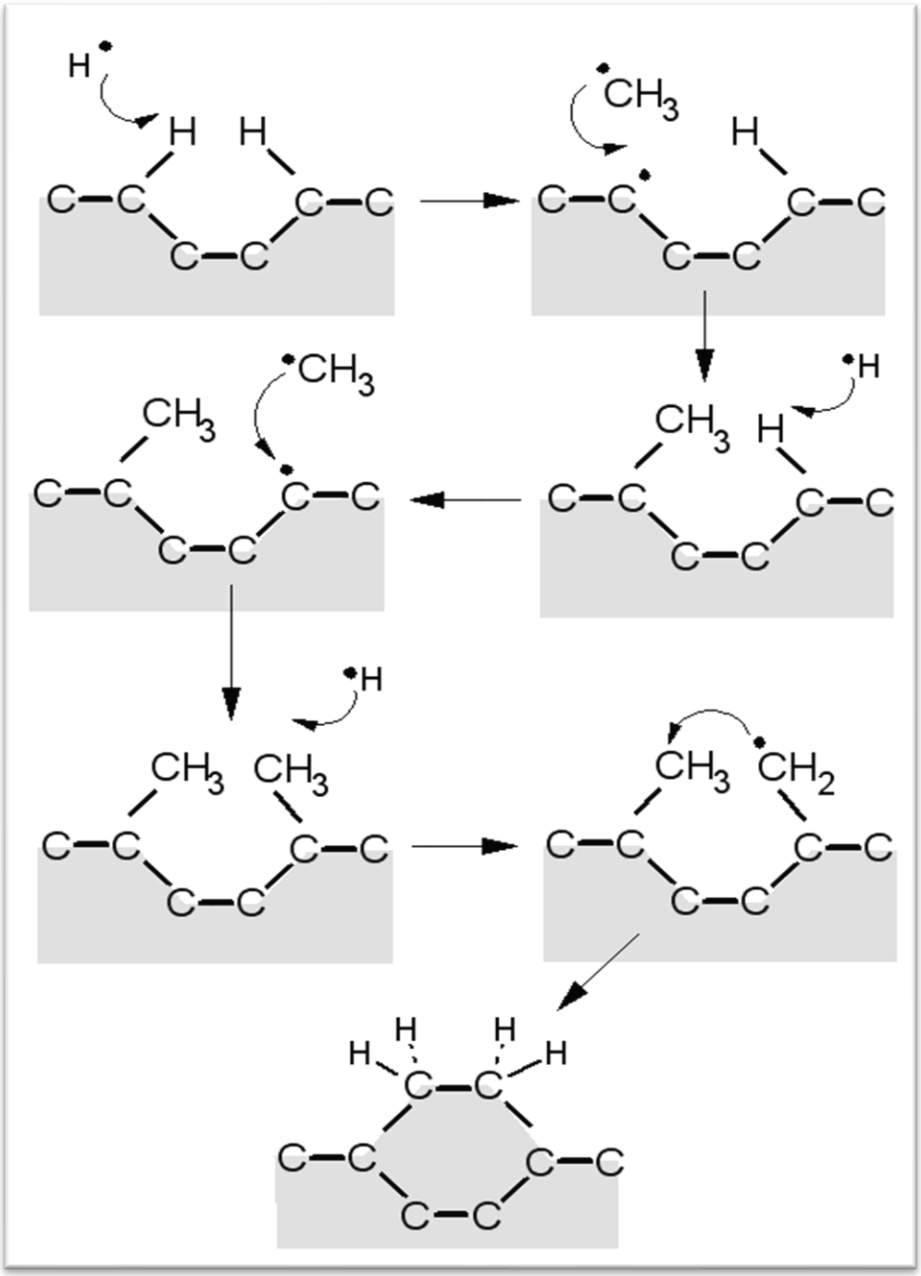

Figure 6: Mechanism of formation of diamond in CVD, activated by atomic hydrogen from [xxiii].

The CVD method grows diamond under thermodynamically metastable conditions, it involves the exposition of a substrate to carbon atoms that originate from the dissociation of a carbon-containing gas, normally methane (as shown in Figure 6). The substrate can either be bulk diamond (normally synthetic) or a non-diamond substrate, such as silicon or Germanium substrates. If the substrate used is bulk diamond, the resulting films are nominated as homoepitaxial or single crystalline, but if a non-diamond substrate is used instead, it is said to be heteroepitaxial or polycrystalline films (shown in Figure 7) [iv, xii]. The dissociation of the gases is activated by heat, light or plasma and atomic hydrogen, as it was discovered that diamond is more stable towards atomic hydrogen than graphite. More specifically, if two neighbours of a carbon atom in the diamond structure are replaced by hydrogen, the sp^3 hybridization remains, while a similar action in graphite would affect the electronic bonds in the whole graphite ring. Consequently, the growing of diamond in CVD consists in two steps. The first consists of carbon depositing essentially in the form of graphite with a slighter amount of diamond, and the second process consist of selective etching of graphite by atomic hydrogen. Based on this, the various enhanced CVD methods for the growth of diamond are developed to produce high amounts of atomic hydrogen from molecular hydrogen close to the surface of the growing sample [xxiv, xix].

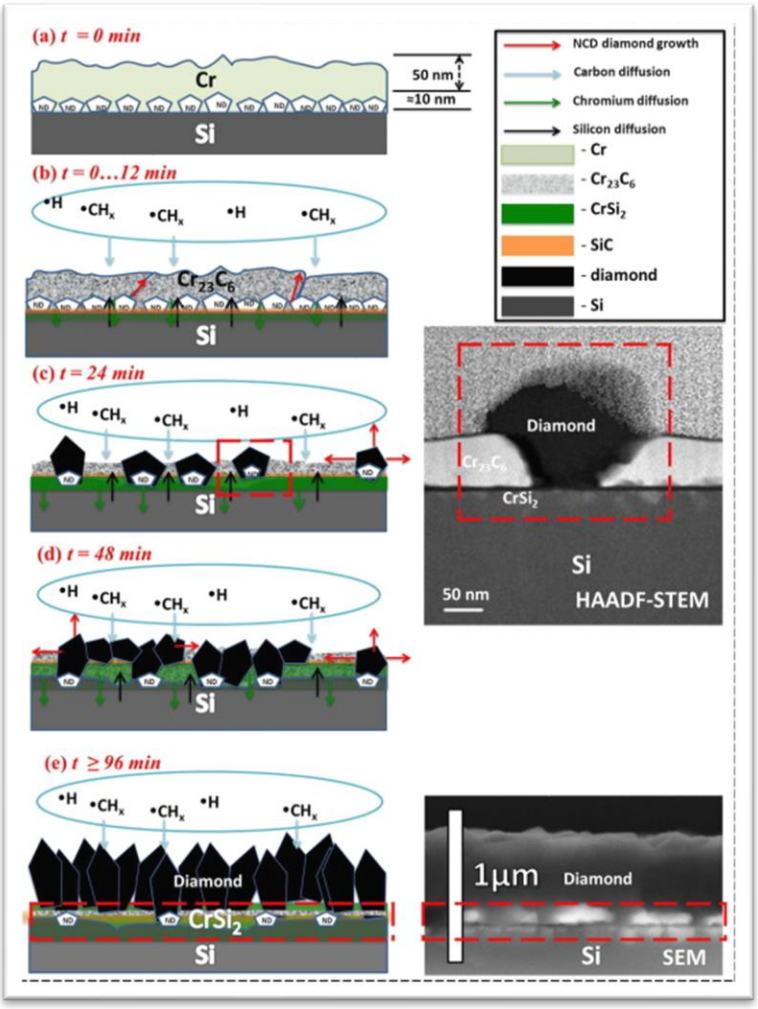

Figure 7: Physical representation of CVD polycrystalline diamond growth over a thin Cr layer in a Si substrate, from [xxv].

Since the first CVD method was issued, many techniques have been developed: filament-assisted thermal CVD, electron-assisted thermal CVD, laser-assisted thermal CVD, RF-plasma CVD, microwave-plasma CVD, combustion flame-assisted CVD and direct-current arc plasma jet CVD. Even though these techniques are different to each other, all current CVD methods have the following common features (shown in Figure 8):

Growth in the presence of atomic hydrogen as diamond is more stable towards atomic hydrogen than graphite, certifying the formation of diamond only.

Dissociation of carbon-containing source gases. Due to the high activation energy needed for methane's decomposition (230-243 KJ mol^{-1}), an external source, such as combustion or plasma processes, are used to dissociate the carbon source and produce the reactant species needed for diamond nucleation and growth. The ability of these reactant species to be transferred to the substrate, determines the growth rate of the film.

Growth at moderate substrate temperatures due to formation of graphite at temperatures above 1200 ºC and the formation of diamond-like-carbon (DLC) deposits at temperatures below 500 ºC [xxvi].

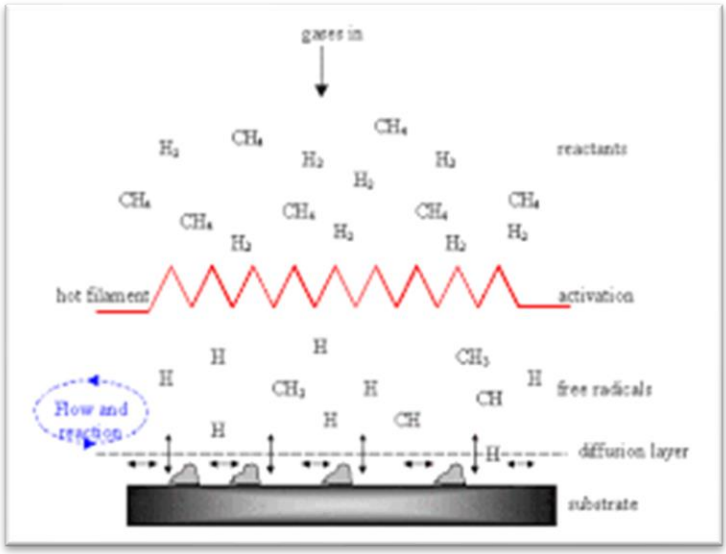

Figure 8: Physical representation of formation of atomic hydrogen and dissociation of methane gas in hot-filament CVD from [xxvii].

The growth parameters can be adjusted, which can change the type of diamonds formed in a sample. By increasing the amount of carbon compared to atomic hydrogen, diamond nucleation is increased, and fine-grained diamond coatings are formed. In the case of extreme changes in process parameters, nanocrystalline diamond (NCD) and ultra-nanocrystalline diamond (UNCD) films are formed [xxviii,xxix]. These coatings are formed by diamond crystals which are in the nanometre scale and contain grain boundaries consisted of amorphous carbon. The number of grain boundaries can affect the content of the diamond phase, if there are a high number of grain boundaries, the diamond phase is reduced, leading to difficulties to distinguish between diamond (crystalline) and amorphous carbon. Therefore, the layer growth rates are low due to the higher amount of sp2 carbon and increased etching by atomic Hydrogen [xxx, xxxi] .

1.3. Diamond as a semiconductor

1.3.1. Semiconductivity (Band gap theory)

To understand the electronical properties of solids, the band theory is applied, which provides a useful way to visualize the differences between metallic conductors and semiconductors. The main difference between these two types of solid structures is their effect on conductivity with temperature, with metallic conductors' electrical resistivity increasing with increasing temperature, and semiconductors' resistivity decreasing with temperature, as shown in Figure 9 [xxxii, xxxiii].

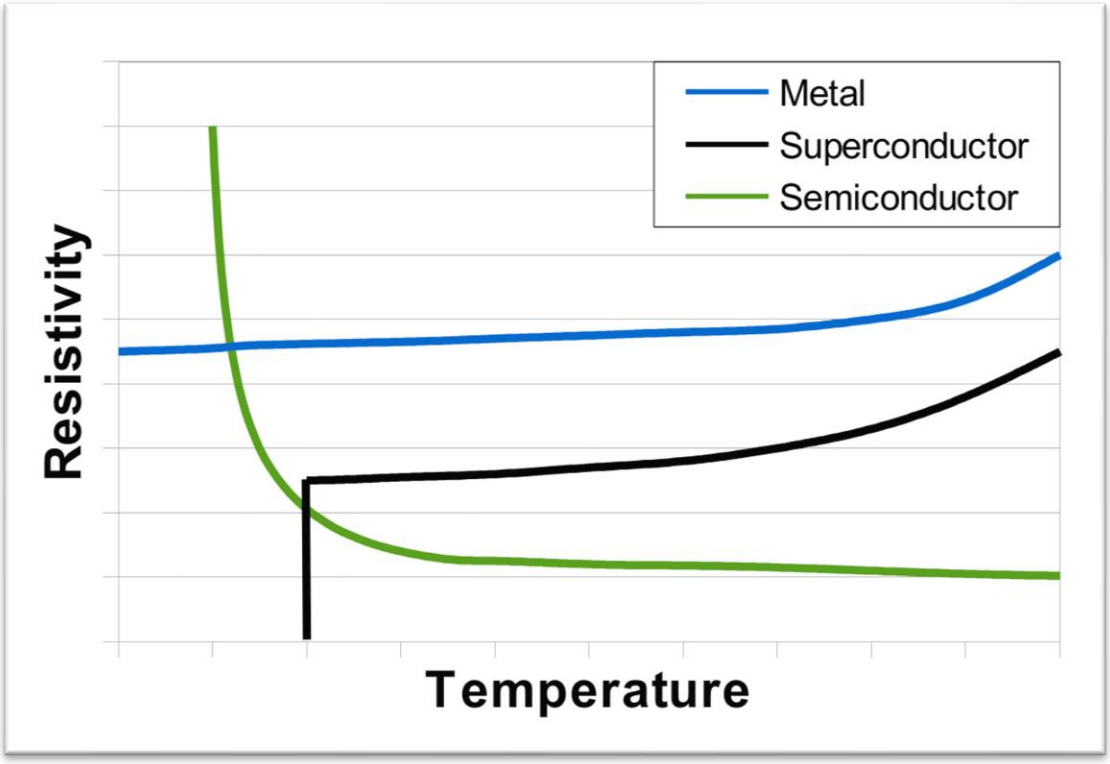

Figure 9: The variation of the electrical resistivity of different substances with temperature. As stated before, metals' resistivity increases with increasing temperature and semiconductors' resistivity decreases with increasing temperature. From [xxxiv].

The main idea of the bands of energy levels formation is that many atomic orbitals in a compound lead to many molecular orbitals that are closely spaced in energy, almost continuous (forming bands). These bands are separated by band gaps, which are energy gaps for which there is no present molecular orbitals (Figure 10). A band can be formed of s orbitals, which is called **s band** or, if available, p orbitals or even d orbitals, named **p band** and **d band**, respectively. As p orbitals lie higher in energy than s orbitals of the same valence shell, there is often an energy gap between the two bands. However, if the bands span a wide range of energy and the two atomic energies are similar, then the two bands overlap (Figure 11), which can happen also with p bands and d bands [xxxii, xxxv, xxxvi].

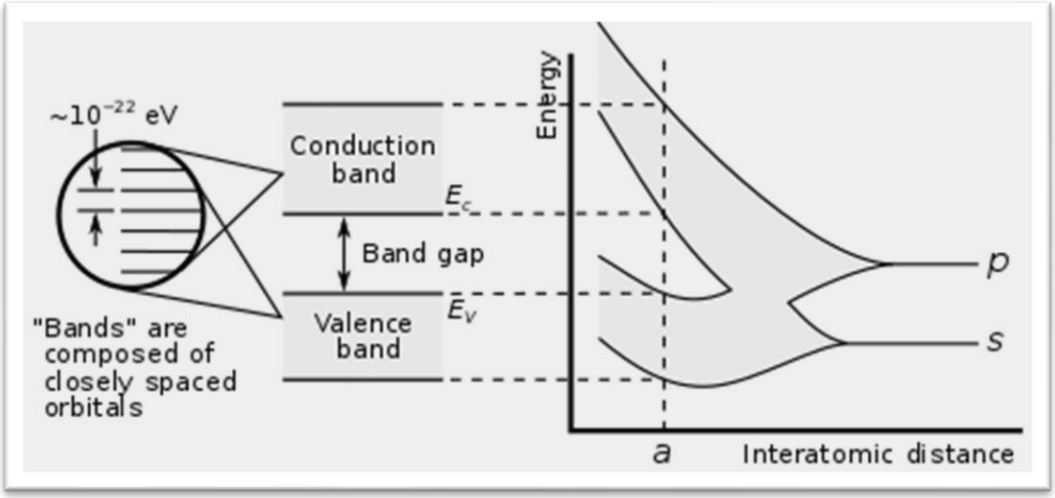

Figure 10: Diagram showing the electronic structure of a solid, with an **s band** and a **p band** from [xxxvii].

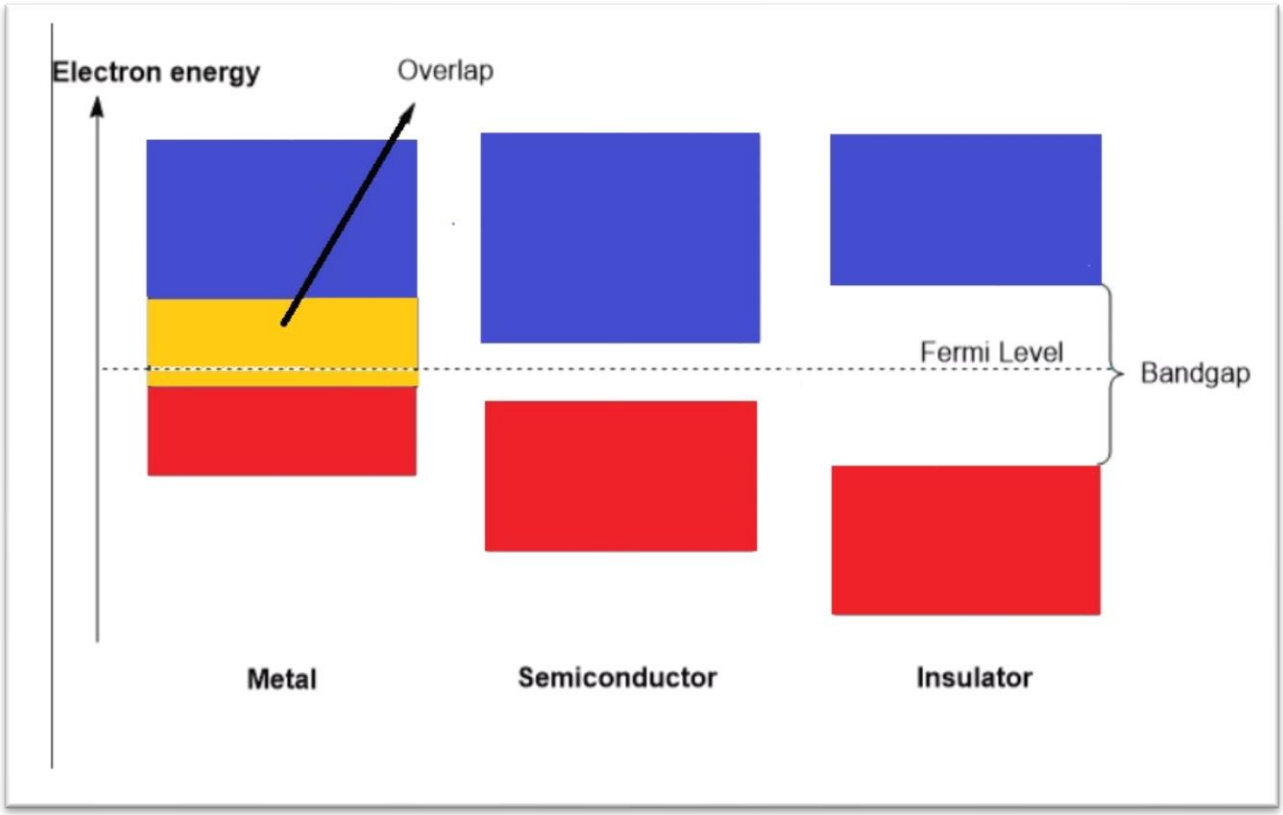

Figure 11: Diagram showing the difference in electronic structures of different solids and the Fermi level.

The density of states, ρ (Figure 12), can be calculated by dividing the number of energy levels in an energy range by the width of the range. Also, the density of states is not uniform across a band, in most cases, the states are densest close to the centre of the band [xxxii].

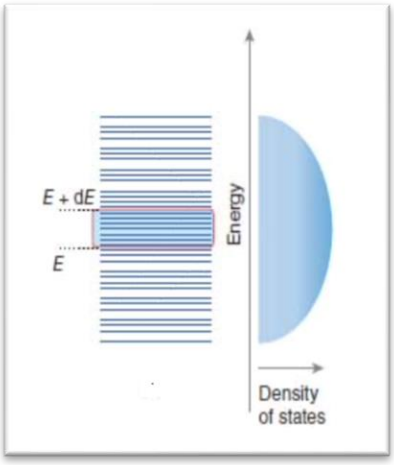

Figure 12: Diagram showing the density of states in a metal as the number of energy levels in an infinitesimal range of energies between E and E+ dE, from [xxxii].

When T=0K, electrons occupy the individual molecular orbitals of the bands in accordance with the Aufbau principle. If each atom supplies one **s** electron, then at T=0K only the lowest orbitals are occupied. The Fermi level is the highest occupied energy level at T=0K, and it lies near the centre of the band (Figure 11). When a band is only half full, the electrons can move freely through the solid, as they can be easily promoted to empty levels near the Fermi level, forming a metallic conductor. When a band is completely filled, and there is a considerable energy gap before an empty level, the solid is considered an insulator or a semiconductor. As stated before, the characteristic physical property of a semiconductor is that its electrical conductivity increases with increasing temperature. The difference between insulators and semiconductors is the size of the band gap, not the conductivity, as the conductivity of a given substance can vary with varying temperature. There are two types of semiconductors: intrinsic and extrinsic semiconductors. Intrinsic semiconductors have no impurities intentionally added, hence their electrical properties are determined solely by the material itself. In an intrinsic semiconductor, the number of free electrons is equal to the number of holes, resulting in a balanced distribution of charge carriers. At room temperature, some electrons in the material gain enough thermal energy to jump into the conduction band, where they become free to move and conduct electricity (Figure 13). Diamond is not an intrinsic semiconductor, so these types of semiconductors will not be discussed any further in this report [xxxii].

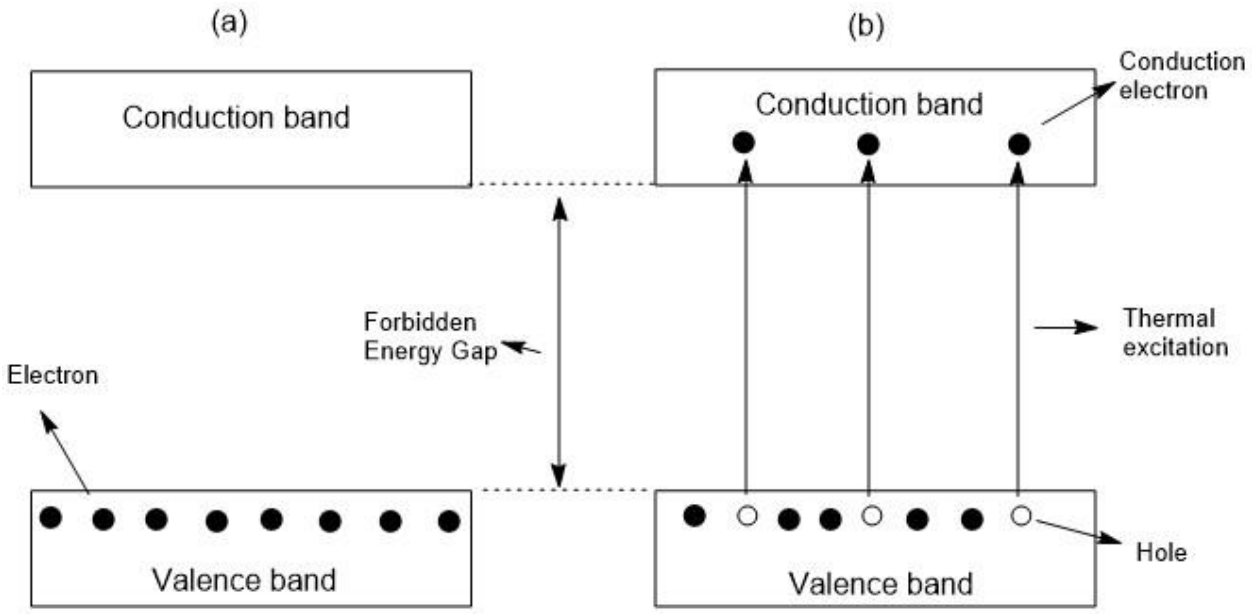

Figure 13: Energy Band diagram of intrinsic semiconductor at (a) 0K and at (b) T>0K.

Extrinsic semiconductors are only semiconductors because of the presence of intentionally placed impurities, which are called dopants. Dopants are substitutional, as the dopant atom takes the place of a parent atom in the crystal lattice and only low levels of dopant concentration are needed (about one atom per 10^9 of the host material) so it is necessary to achieve extremely high purity of the parent element initially. There are two possible ways of doping a semiconductor: p-type and n-type doping.

In p-type doping, an atom with fewer electrons than the parent element is introduced into the lattice. These atoms form a narrow and empty level that lies above the valence band, called the acceptor level (Figure 14a). At T=0K, the acceptor level is empty, but at higher temperatures it can accept electrons from the valence band. By doing so, it causes holes to form in the lattice structure, which allows the other electrons to be mobile [xxxii].

In n-type doping, the number of electron carriers are increased with atoms with more electrons than the parent element. The foreign atom levels will be at a higher energy than the valence electrons, which forms a dopant level, which is a filled narrow level just below the conduction band (Figure 14b). For T>0, some of the electrons in the dopant level can be thermically excited into the conduction band, from there they will be able to migrate through the structure in the band formed by parent atoms overlap [xxxii].

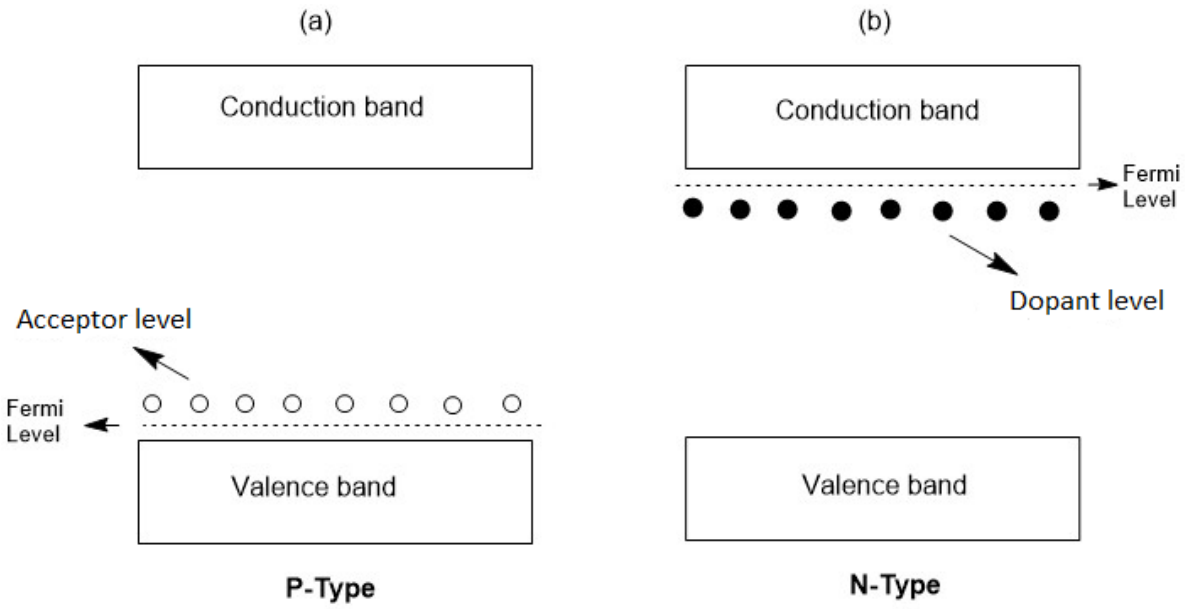

Figure 14: The band structure of (a) a p-type semiconductor and (b) an n-type semiconductor.

1.3.2. Electronical properties of diamond

Silicon is the most used material for semiconductor applications nowadays, and it has been so for more than 50 years (Figure 15). It is widely known that a notable improvement in power electronics would be obtained from the use of wide bandgap semiconductor materials. These types of materials have improved physical and electronical properties for its use in power devices compared to silicon [xxxviii]. Power electronic devices subject to wide bandgap semiconductors are now emerging as an advancement in the performance of power electronics systems by offering higher blocking voltages, improved efficiency, and reliability (higher performance/cost ratio), easier paralleling, and reduced thermal requirements, thus leading to the realization of more efficient sustainable electronic systems [xxxix xl xli].

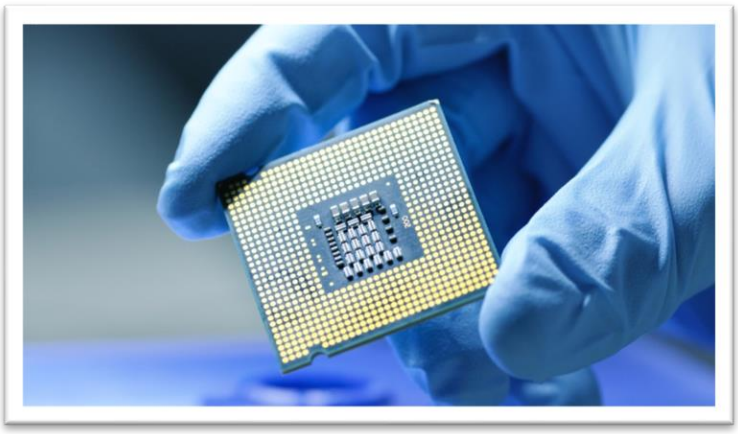

Figure 15: Silicon used as a microchip. Taken from [xlii].

Diamond is a wide-bandgap semiconductor (E gap = 5.5 eV) with enormous potential as an electronic device material in both active devices, such as high-frequency field-effect transistors (FETs) and high-power switches, and passive devices, such as Schottky diodes. Its electronical and physical properties (Table 2) are superior to every other semiconductor available, which is why it has been researched to gain accessible conductivity. It could potentially enable devices that are beyond the scope of current systems in terms of operating frequency, power handling capacity, operating voltage, and operating environment [xliii, xliv].

Table 2: Comparison of the electronic properties of diamond and other semiconductors.

Properties	Si	GaAs	6H-SiC	4H-SiC	GaN	Diamond
Band gap (eV)	1.12	1.43	3.03	3.26	3.45	5.45
Dielectric constant	11.9	13.1	9.66	10.1	9	5.5
Electrical breakdown field (kV cm^{-1})	300	400	2500	2200	2000	10,000
Electron mobility (cm^2 V^{-1} s^{-1})	1500	8500	500	1000	1250	2200
Hole mobility (cm^2 V^{-1} s^{-1})	600	400	101	115	850	850
e-drift velocity (x107 cm s^{-1})	1	1	2	2	2.2	2.7
Thermal conductivity (W cm^{-1} K^{-1})	1.5	0.46	4.9	4.9	1.3	22

1.4. Doping of diamond

1.4.1. Boron doping

As many other solids, impurities can be introduced into the diamond lattice with different elements. Boron is arguably the most technologically relevant impurity in diamond. It is the only known shallow dopant with activation energy of 0.368 eV, which is also found in natural diamond (type IIb). Boron can be introduced into the diamond lattice by CVD using gases such as B_2H_6 (diborane) or $B(CH_3)_3$ (trimethyl borane), which decompose in the hot plasma into active BH_x species and incorporate into the lattice, substituting C atoms (Figure 16). In order to show semi-metallic properties, the dopant densities should be greater than ~10^{20} B atoms per cm^{-3} (Figure 17). For dopant densities less than this value, the diamond will show hopping conduction features and for even smaller values of dopant, p-type semiconduction properties [xlv, xlvi, xlvii, xlviii].

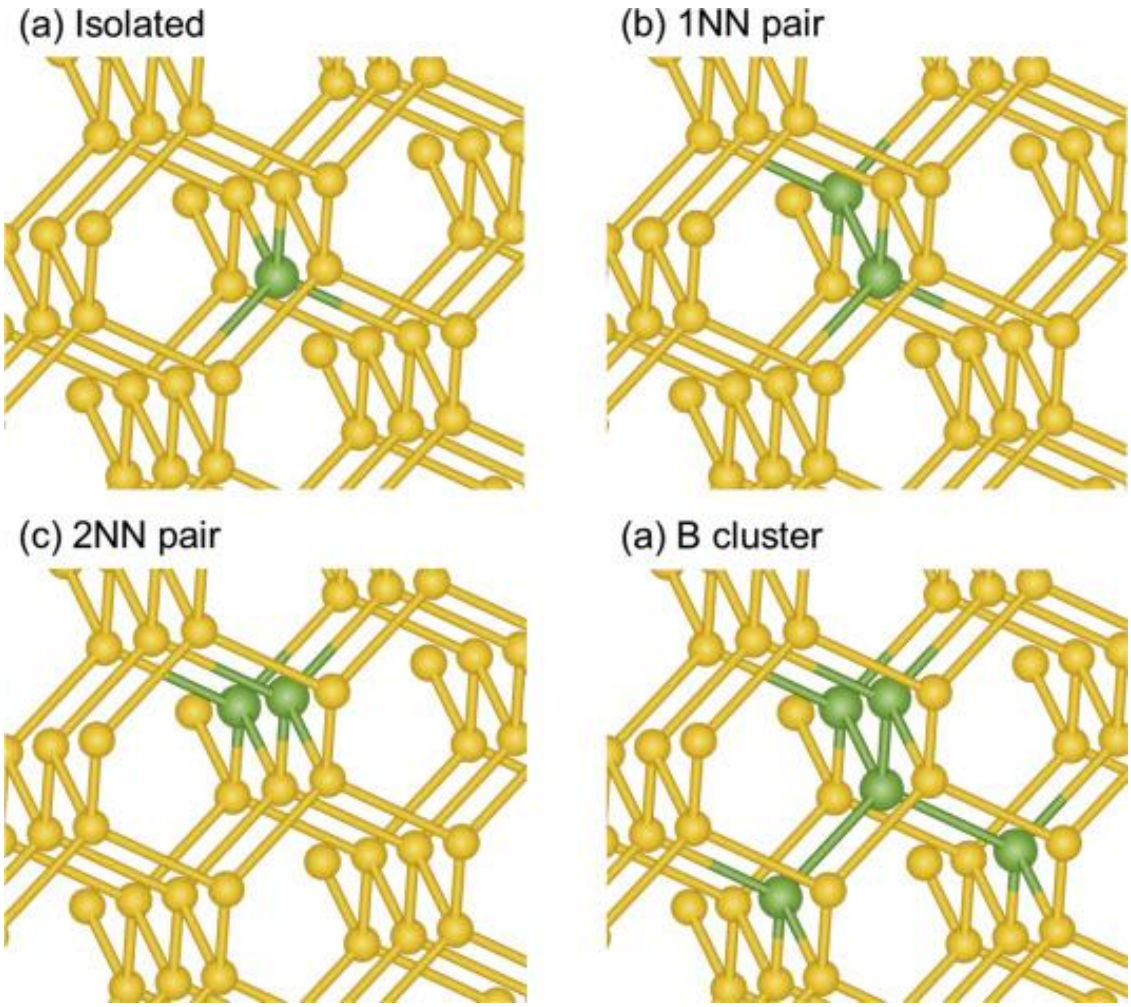

Figure 16: Crystal structures of boron doped diamond (BDD). The large spheres (green) and small spheres (yellow) show boron and carbon, respectively. Taken from the work of Watanabe, T. et al. [xlix].

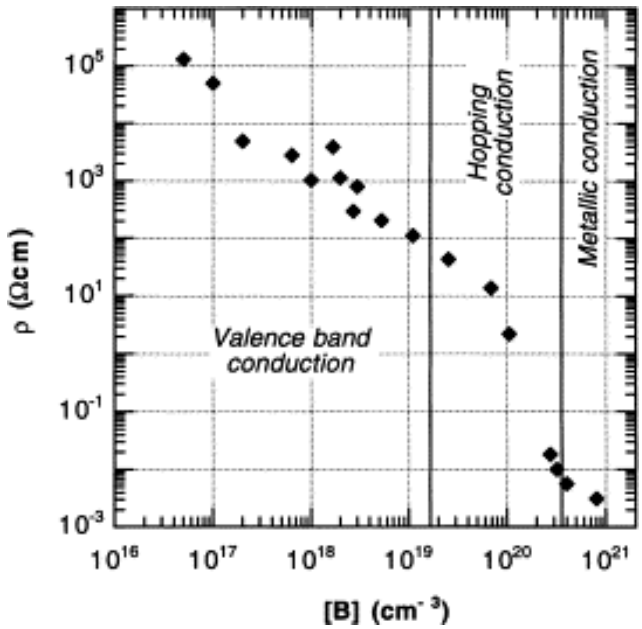

Figure 17: Room temperature resistivity as a function of Boron doping concentration. At low-medium level of doping, valence band conduction is shown, at elevated level, hopping conduction is shown instead and at heavy doping levels, metallic conduction is shown. Taken from the work of Lagrange, J.-P., Deneuville, A. and Gheeraert, E. et al. [xlviii].

As shown earlier, boron doped diamond shows great increases in conductivity, which allows it to act as an excellent p-type conductive material not only in electrochemical applications but also for high-temperature, high-power and radiation-proof photoelectronic devices thanks to its physical and electronical properties [l].

1.4.2. Nitrogen and other n-type dopants doping

Although p-type diamond has been widely reported with boron-doping, highly conductive n-type diamond films have not been produced yet. This fact has slowed down the development of diamond-based devices. Although n-type conductivity has been reported from different methods, these films have not been widely reproduced [li].

Nitrogen, which possesses more electrons than carbon unlike boron, can also be introduced into the diamond lattice, although its relevance to technology is considerably lower than boron's, as studies suggest that the donor level is situated 1.7 eV below the conduction band. This makes the nitrogen-doped diamond (NDD) essentially impracticable for any device operating at room temperature [lii]. NDD can be formed naturally or by HPHT, due to the high concentration of nitrogen in air, and by CVD, adding a source of nitrogen such as N_2 or NH_3 [liii, liv]. NDDs also give place to a point defect in diamond, the nearest neighbour nitrogen-vacancy (NV) centre (shown in Figure 18a). The detection of NV single centres demonstrated photostable single photon generation which contains applications in quantum optical networks as well as in applications for optical preparation and readout of the centre's electronic spin [lv].

Furthermore, the addition of Nitrogen into the diamond lattice causes an increase in electrical resistance (Figure 18b). This is due to the high ionization energy of Nitrogen which does not allow its ionization at room temperature and hence, the flow of electrons throughout the lattice of the material [lvi].

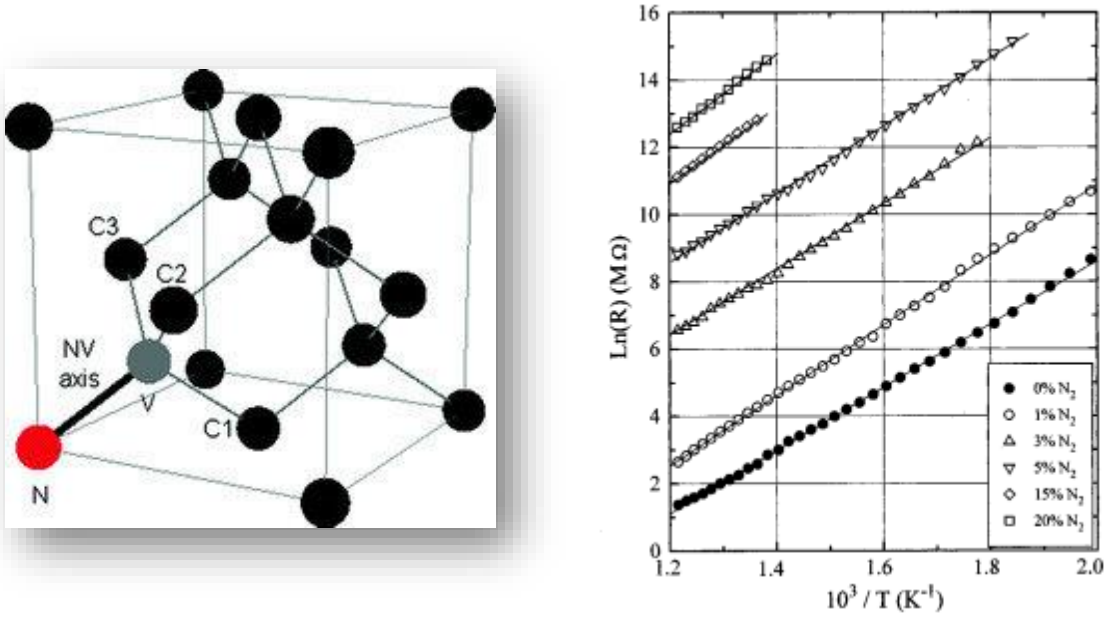

Figure 18a: Diamond crystal lattice showing an NV centre defect. The vacancy, nitrogen atom, and nearest-neighbour carbon atoms are labelled in the image. Taken from the work of Jensen, K., Kehayias, P. and Budker, D. et al. [lvii]. Figure 18: Logarithm of resistance vs reciprocal temperature for diamond samples produced with different Nitrogen concentrations. Taken from the work of Baranauskas, V. et al. [lvi].

Phosphorus is below nitrogen in the periodic table and can also be introduced into the diamond lattice. Studies suggest a donor level situated 0.6 eV below the conduction band, in contrast with the deeper donor level of nitrogen [lviii]. However, the donor level is still not shallow enough for room temperature electronics, and the electron density in the diamond lattice is too little as the phosphorus concentration in the lattice is low due to chemical kinetics limitations [lix]. Lithium is also a dopant with enormous potential to act as a shallow dopant when in an interstitial position in the lattice. Calculations show that, when in a substitutional site, it introduces a compensating acceptor level. However, because of the diffusivities and solubilities of Li being so low, these atoms are not expected to enter the diamond crystal under thermodynamic equilibrium conditions [lx]. Other candidate substitutional donors are arsenic (As) and antimony (Sb), but there is a lack of experimental data on these dopants and have not been proven suitable for n-type doping [lxi].

1.5. Co-doping of diamond

As none of the individual n-type dopants give the necessary results to construct a highly conductive n-type diamond, research is now focused on using combinations of elements in order to achieve a reliable n-type donor.

Many computational studies have been made trying to find, theoretically, the nature of the n-type donor. In theory, LiN_4 [lxii], BN_2 [lxiii], Si_4N [lxiv] and HN_2 [lxv] all show donor levels shallower than nitrogen, and some, like Si_4N, even shallower than phosphorus. Despite the promising results, these studies made no attempt to produce the co-doped material.

Although co-doping shows very promising results, it has generally failed to deliver the material [lxvi]. There are distinct reasons why this approach is challenging and why researchers try to avoid this route if possible:

- The route to form these complexes may lead to several processing steps.
- The individual dopants may lead to compensation, populating scattering sites, which would reduce the mobility of the film, thus its conductivity.
- The useful form of the complex may not be the lowest in energy, leading to a low efficiency of formation of the shallow dopant.
- Diamond does not allow diffusion unless elevated temperature treatments are used, which means the only efficient way to co-dope is during growth. As implantation doping in diamond leads to implantation damage which compensates donors.
- The thermal stability of the complexes may not be consistent with operational lifetimes required for device applications [lxvii].

As co-doping is a hard technique to achieve results with, little research has been done on mixing combination of elemental gases to the CVD growth. The most common elements added, as mentioned before, are boron, nitrogen, and phosphorus. Sulphur and oxygen are claimed to also form shallow donors, but they remain to be proved [lxviii]. Oxygen has been previously introduced into growth of diamond but not as a dopant. It is found that oxygen interacts strongly with boron and boron-containing gases, which forms boron oxides that cannot be introduced into the crystal lattice. Hence, oxygen can be used to decrease the very feasible introduction of boron into diamond, as boron causes contamination into the reactor with one sole use [lxix, lxx].

1.5.1. Boron-Nitrogen co-doping

As boron and nitrogen are the most common dopants for diamond, they can easily be used to start experimental research in co-doping of diamond. As stated before, their individual introduction to the lattice can be easily achieved so they seem like an excellent choice of elements to co-introduce. Furthermore, accidental co-introduction of boron and nitrogen has already been experienced as some level of nitrogen is almost impossible to avoid (because of its high concentration in air) in both HPHT and CVD even when boron doping. And, as stated before, boron can contaminate a reactor permanently with one sole use, which means that a nitrogen doping attempt in such reactor will be introduced along with boron [lxx].

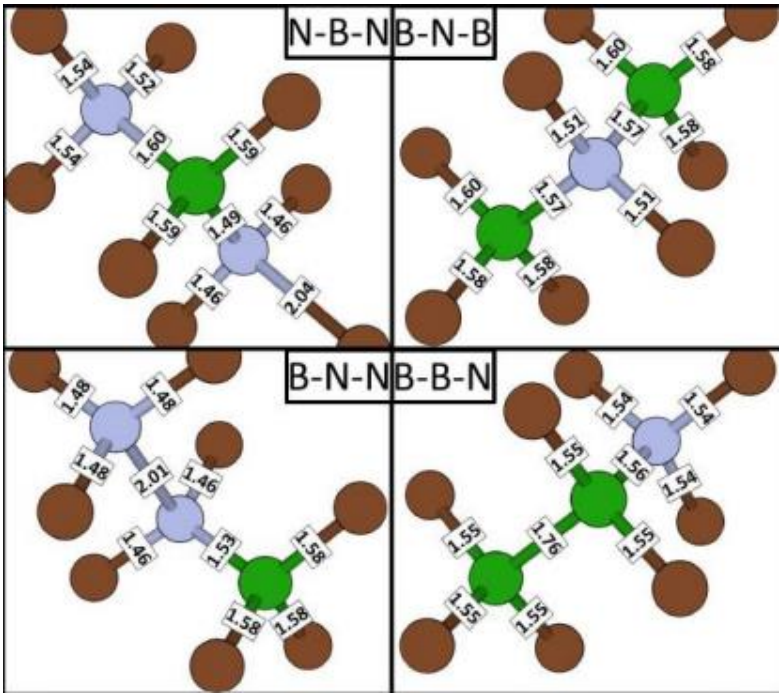

Figure 19: Diagram with different BN clusters inside the diamond structure, including the BN_2 cluster. Taken from [lxxi].

Various computational studies have been made on the co-doping of boron-nitrogen clusters in the structure of diamond (Figure 19). Katayama-Yoshida, H. *et al.* [lxiii] introduced the BN_2 complex, which showed a theoretical donor level of 1.17 eV, decreasing the already mentioned 1.7 eV donor level of individual nitrogen. Furthermore, Alex Croot et al.[lxxii] showed BN_2 and BN_3 complexes to be the most promising to achieve n-type conductivity, although not improving the donor level of phosphorus, hence proving hard to be conductive at room temperature. This work also showed that B-rich clusters will have no part in the synthesis of the n-type material as they have electronic energy levels comparable to that of boron.

Liu, D.Y. *et al.* [lix] published experimental work regarding the synthesis of n-type diamond by introduction of N-rich boron-nitrogen clusters. Its work kept a constant flow of gases containing a source of H_2, C and B, while changing the concentrations of nitrogen to investigate the resistance of the samples and the type of conductivity. The results showed a successful synthesis of the n-type material reducing the activation energy of the donors by around 50%. The work suggests that the change from p-type to n-type conductivity (Figure 20) is due to a change in the clusters going from B-rich clusters to N-rich clusters, but it is not investigated any further.

This project is not strictly comparable to the work carried out by Liu, D.Y. *et al.* due to the usage of a different reactor, different geometry in the substrates which, as mentioned earlier, has a big influence in the growing parameters and the boron incorporation, there are also differences between the two experiments due to the limitations in the MFCs for the reactor used for my experiment. The project carried out used different growing conditions to adjust it to the reactor used and increasing the Boron concentration in order to achieve better results at room temperature. It is also worth mentioning that the Hall effect measurements taken on the work of Liu, D.Y. *et al.* are at a temperature of 773 K,

while the ones taken on this project were at room temperature. The difference in temperature can influence highly in the ionization of Nitrogen atoms in the lattice, which would enhance n-type conductivity.

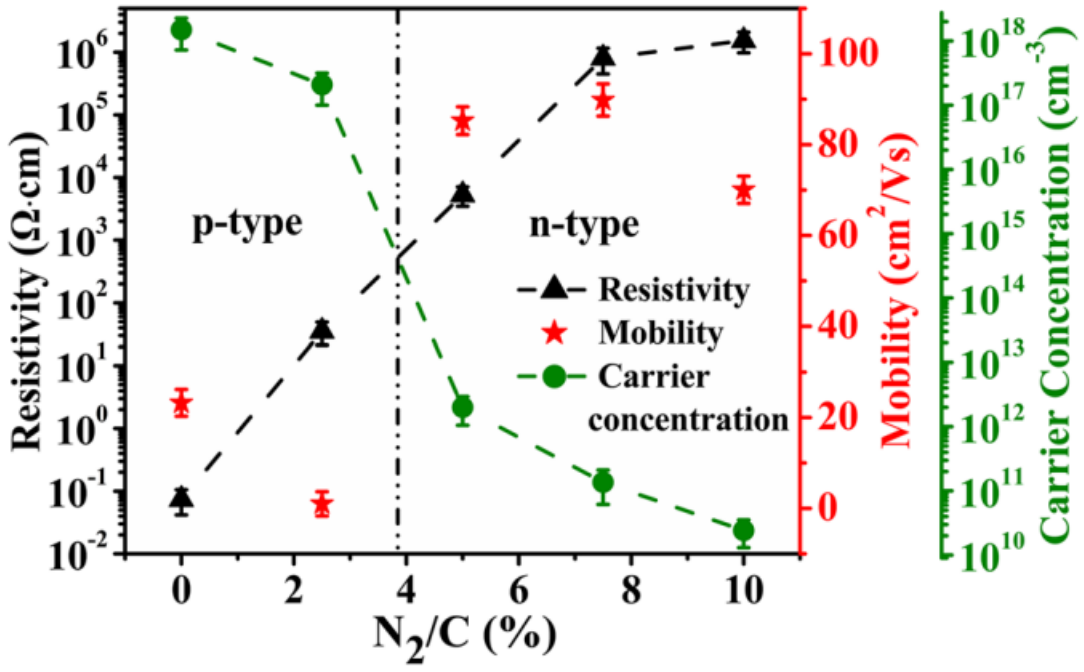

Figure 20: The resistivity, mobility, and carrier concentration at 773 K of boron-doped and boron–nitrogen co-doped diamond films. It shows a clear change from p-type to n-type material. From the work of Liu, D.Y. *et al.* [lix].

1.6. Aim of the thesis

The aim of this thesis will be to further investigate the formation of BN clusters in the diamond lattice by co-doping of single crystal diamond (SCD) following the work done by Liu, D.Y. *et al. lix* and Alex Croot et al. [lxxii]. An attempt to synthesise an n-type conductive layer at room temperature will be carried out by co-doping of Boron and Nitrogen in the growth phase.

In order to synthesise these diamond films, past computational studies will be reviewed to achieve information on the nature of the clusters that showed lower donor levels and could be introduced in the lattice of diamond during growth. Nitrogen-rich Boron-Nitrogen clusters in substitutional showed promising results as one way of achieving n-type conductivity by co-doping. Previous experimental work showed this method to work, decreasing the value of the donor level by around 50% in comparison to Nitrogen. In this project, the level of Boron will be raised in order to achieve a more conductive material at room temperature.

In this thesis further investigation will be made relating to the change from p-type to n-type semiconduction in CVD diamond films. Different growths will be made first on Silicon substrates, to inspect the surfaces and growth rate by Raman spectroscopy and Scanning Electron Microscopy (SEM). Hall effect measurements will be taken of all the samples, to learn about the mobility, carrier concentration and the resistivity of the grown layers.

Right parameters will be found to grow on SCD with an orientation of (110), to achieve a conductive Boron-doped layer of diamond at room temperature. Then, Nitrogen will be added to these parameters in different N/B ratios to achieve an n-type material. The electrical properties will be measured using a two-probe contact analysis and Hall effect measurements to learn about the resistance, the mobility, the carrier concentration and the resistivity of the grown layers.

All the samples will be inspected using SEM in order to measure the thickness and grain mean size of the polycrystalline layers and the thickness of the SCD samples, in order to achieve more accurate Hall calculations.

2. Experimental and analytical techniques

2.1. Experimental apparatus

2.1.1. Microwave-plasma CVD reactor

The reactor used for this experiment is shown schematically in Figure 21. It has been used to introduce both Boron and Nitrogen into the plasma, for introduction into the substrate. A new Nitrogen line was installed, as the reactor did not possess one prior to the experiment. The reactor is made by high-vacuum components which ensured minimal air contamination into the reactor.

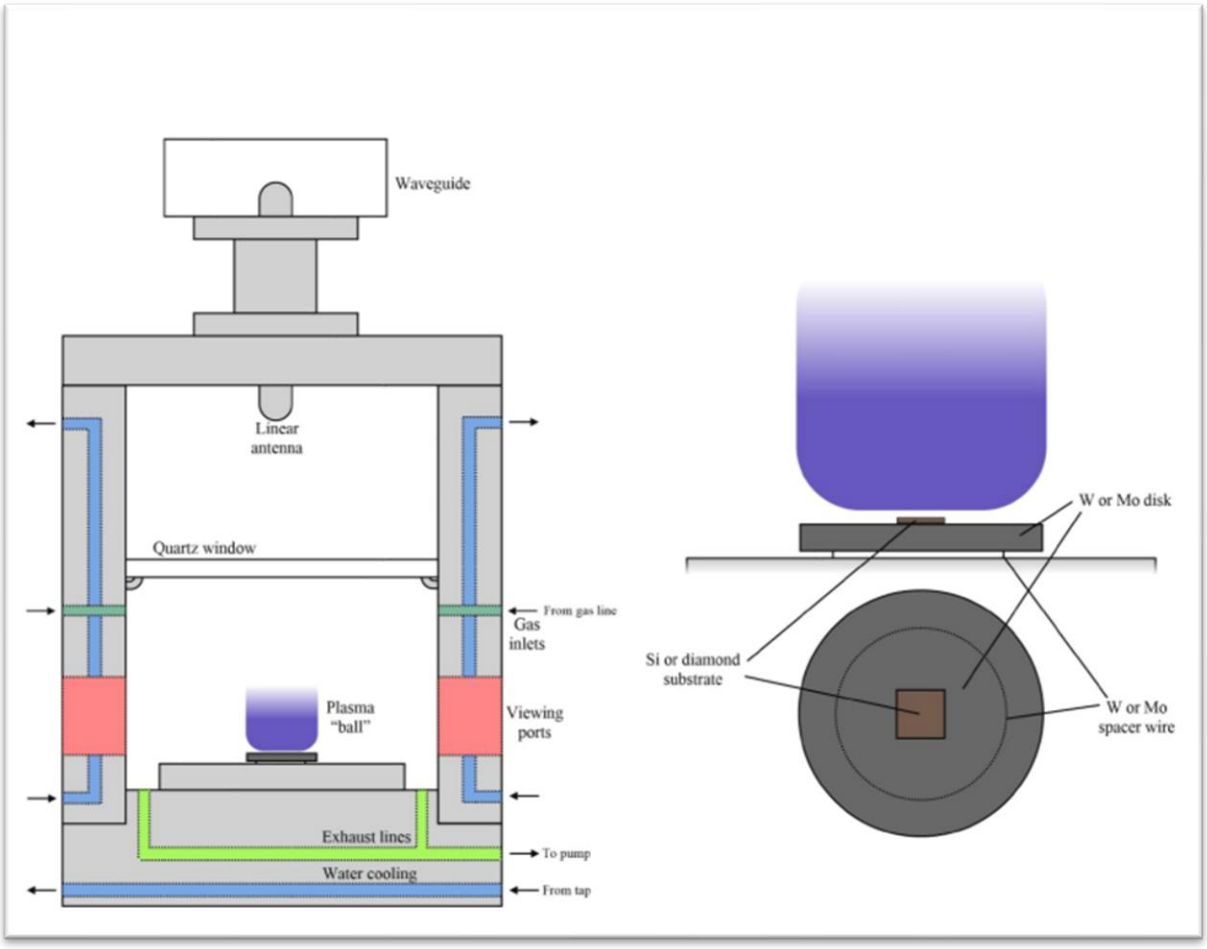

Figure 21: Schematic figure of the MW-CVD reactor. The image on the left shows the whole reactor chamber, and the image on the right shows an amplified diagram of the substrate sitting on the disk and on top of the spacer wire. From the work of Alex Croot et. Al.

As shown in Figure 21, the chamber of the reactor is where the substrate is positioned. The substrate is put on top of a metallic disk (Mo or W), which is also put on top of a circular metallic wire (Mo or W). These components rest on top of a water-cooled Aluminium base-plate. The thickness of the wire reflects directly on the temperature of the substrate, a thicker wire will result in a higher temperature of the substrate. This allows to use different power and pressure on the growth while keeping a similar temperature. The temperature of the substrate was measured by a pyrometer attached on top of the chamber.

2.1.2. Electrospray seeding apparatus

The Silicon substrates used in the first part of the experiment needed to be seeded with nanodiamond for the growth of diamond to be successful. The seeding apparatus (shown in Figure 22) consists of two parts: the power supply and the electrospray chamber. The power supply which can go up to 50kV, is connected to the chamber by conducting tweezers. The current provided from the power supply makes the needle spray the nanodiamond solution directed into the substrate rotator. The substrate rotator is a circular and sticky surface where the Silicon substrates are attached and start rotating during the spraying, to get uniform seeding.

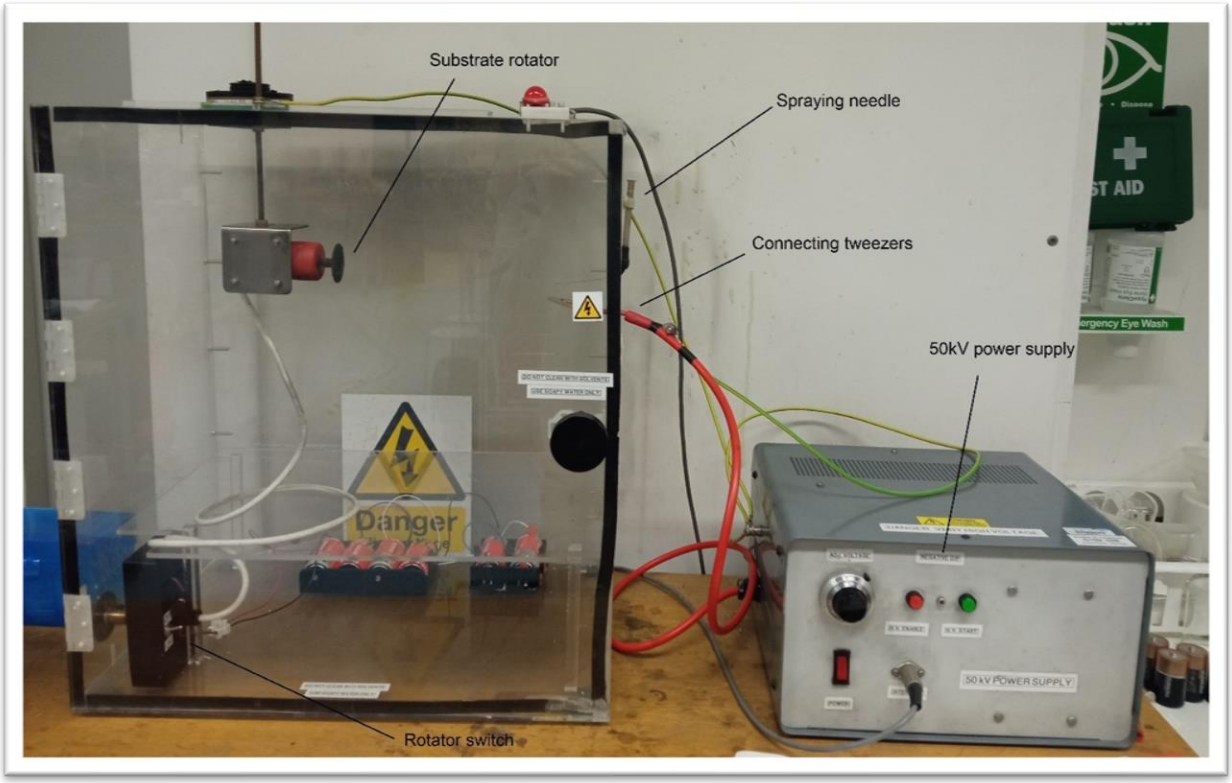

Figure 22: Picture of the apparatus used for seeding of Silicon substrates. Most important parts of the apparatus are labelled in the picture.

2.2. Analytical techniques

2.2.1. Raman spectroscopy

Laser Raman spectroscopy is widely used as an analytical tool to assess diamond and CVD diamond films. It is a non-invasive technique, which requires none or truly little preparation and it can be used even with exceedingly small volumes of sample. It proves to be very efficient as every carbon allotrope displays an identifiable Raman peak, as shown in Table 3. Diamond appears as a single sharp line at 1332 cm^{-1}, whereas graphite can be shown in two different shifts depending on its structure (Figure 23). Disordered graphite peak is at 1546 cm^{-1} and monocrystalline graphite appears at 1580 cm^{-1}. Raman spectroscopy also shows an amorphous carbon phase composed of two peaks: the first one is at a shift of 1345 cm^{-1}, called D band, and the second one is in the range of 1500-1600 cm^{-1}, called G band. The D line is due to an sp^2 hybridised carbon structure and the G peak is known to appear due to the in plane stretching motion between sp^2 carbon atoms [lxxiii,lxxiv].

Table 3: Positions of Raman bands for different forms of carbon. Based on the work of Anna Dychalska *et al* [lxxv].

Raman shift (cm^{-1})	Interpretation
1580	Monocrystalline graphite
1546	Disordered graphite
1500-1600	Amorphous carbon sp^2 (G-band)
1430-1470	Trans-polyacetylene laying in the grain boundaries
1345	Amorphous carbon sp^2 (D-band)
1332	Diamond band
1220	Disordered diamond
1150, 1237	Nanodiamond
1100-1150	Trans-polyacetylene segments at the grain boundaries

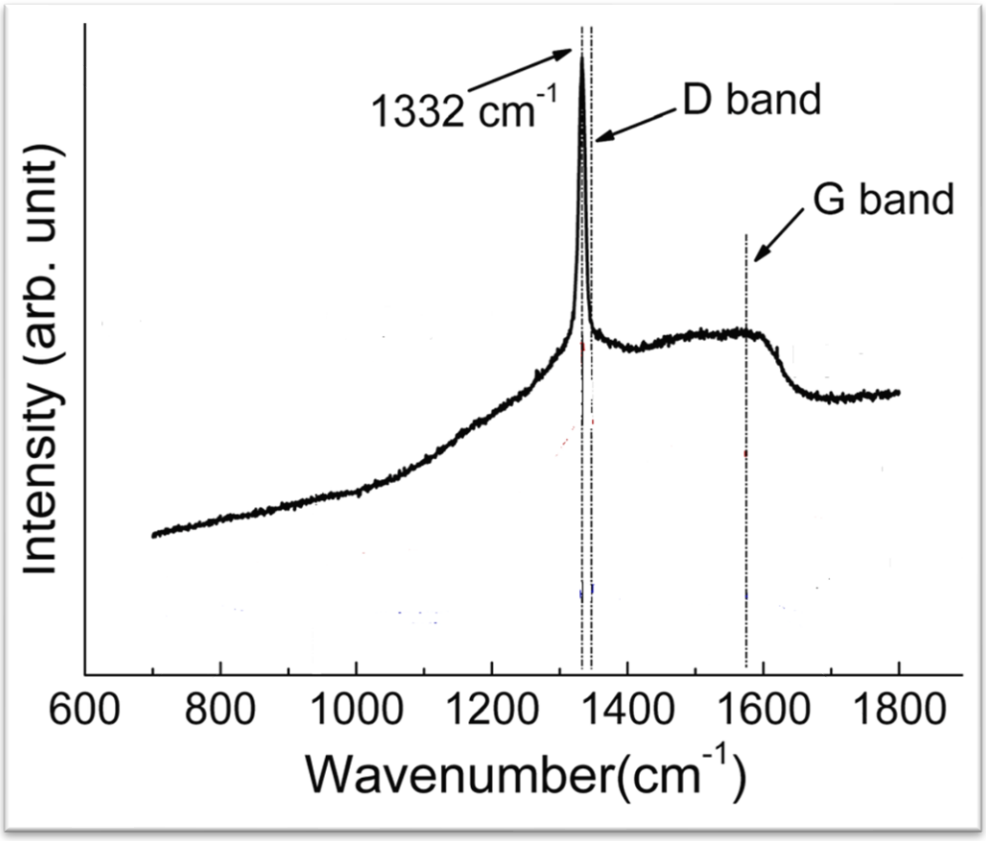

Figure 23: Raman spectra of pure diamond, from the work of Zhuang, H. *et al* [lxxvi].

The width of a natural diamond is around 2 cm^{-1} and has a broader linewidth for polycrystalline CVD diamond films (from 5 to 15 cm^{-1}), this is caused by chemical defects and micro-stains. The diamond peak is often shifted relative to that of natural diamond, due to temperature or lattice strain effects, so Raman spectroscopy can be used to measure the purity of the diamond sample [lxxvii].

2.2.2. Hall effect measurements

The Lorentz force is the physical principle underlying the Hall effect, which combines two separate forces: the electric force and the magnetic force. The Hall effect (Figure 24) is the deflection of electrons or holes (depending on whether the sample being tested is an n-type or a p-type) in a semiconductor with current (x-axis) flowing perpendicular to a magnetic field (z-axis). The deflection of these charged carriers in the negative y-axis direction, sets up a voltage, known as Hall voltage. The polarity of the voltage is dependent on the effective charge of the carrier (negative for an n-type and positive for a p-type semiconductor). And the magnitude of Hall voltage depends on the strength of the magnetic field, the current given, and the carrier density.is determined from the Hall voltage and resistivity [lxxviii].

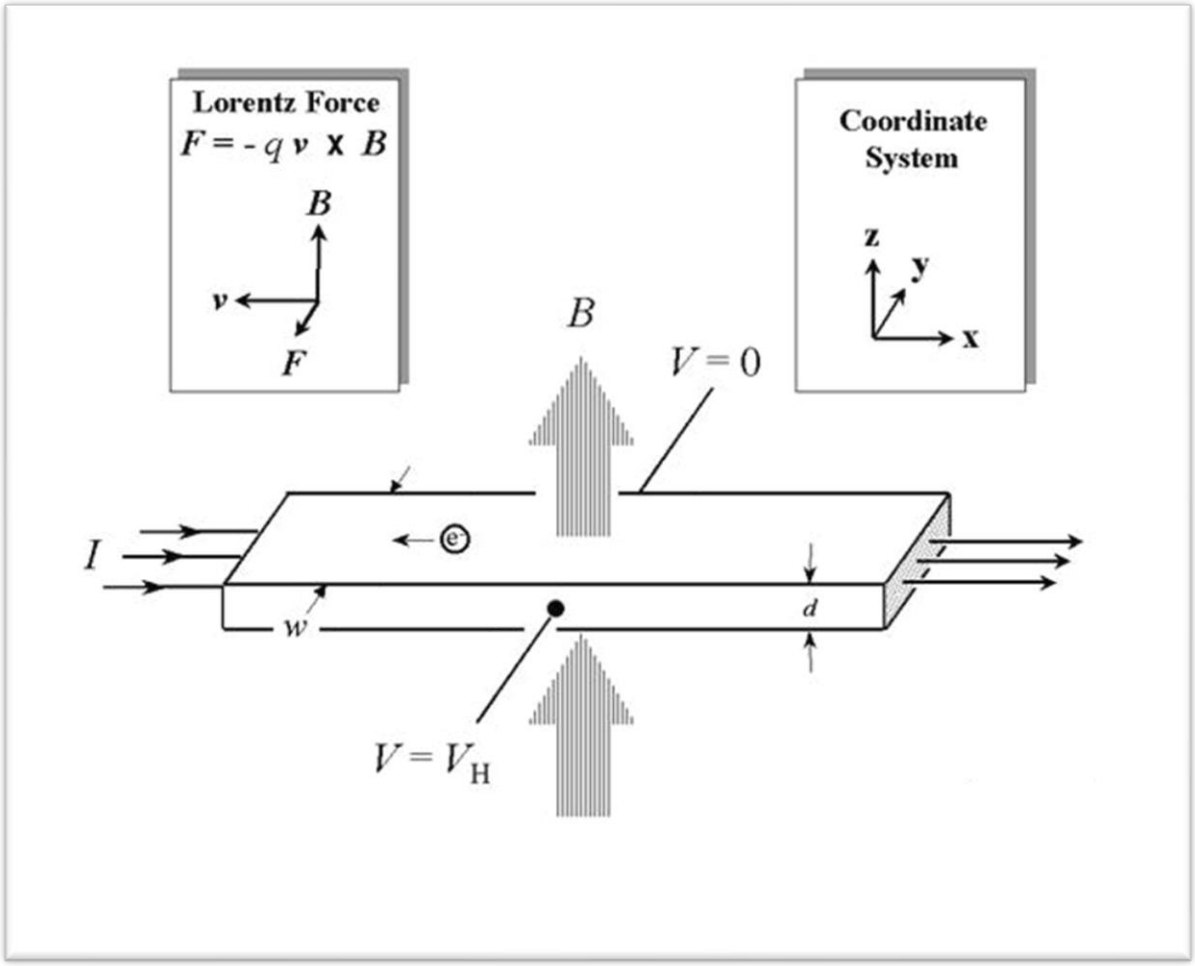

Figure 24: Schematic figure of the Hall effect in a rectangular semiconductor with four ohmic contacts. The direction of the magnetic field B is along the z-axis, with the current applied going along the x-axis. The sample has a finite thickness d. From the work of NIST [lxxix].

The Hall effect measurements were used in the experiment to estimate the values of resistivity for all the samples synthesised using the Van der Pauw (VDP) technique, and to estimate the values of the Hall voltage, the carrier type, the carrier concentration and the mobility of the samples.

2.2.3. Scanning electron microscopy

Scanning electron microscopy (SEM) is an analytical technique that can provide information on surface topography, crystalline structure, chemical composition, and electrical behaviour of organic and inorganic materials. It works from the nanometre to the micrometre scale, at a high magnification that can even reach 1000000x in producing images of a material on some of the most modern models. The analysis works through SEM equipment, shown in Figure 25. In order to analyse the material, electrons are accelerated to high energies between 2 and 1000 keV, and if the samples are thick enough, particles emerging from the surface (e.g., electrons, x-rays, and photons) can give information about the surface of the sample [lxxx].

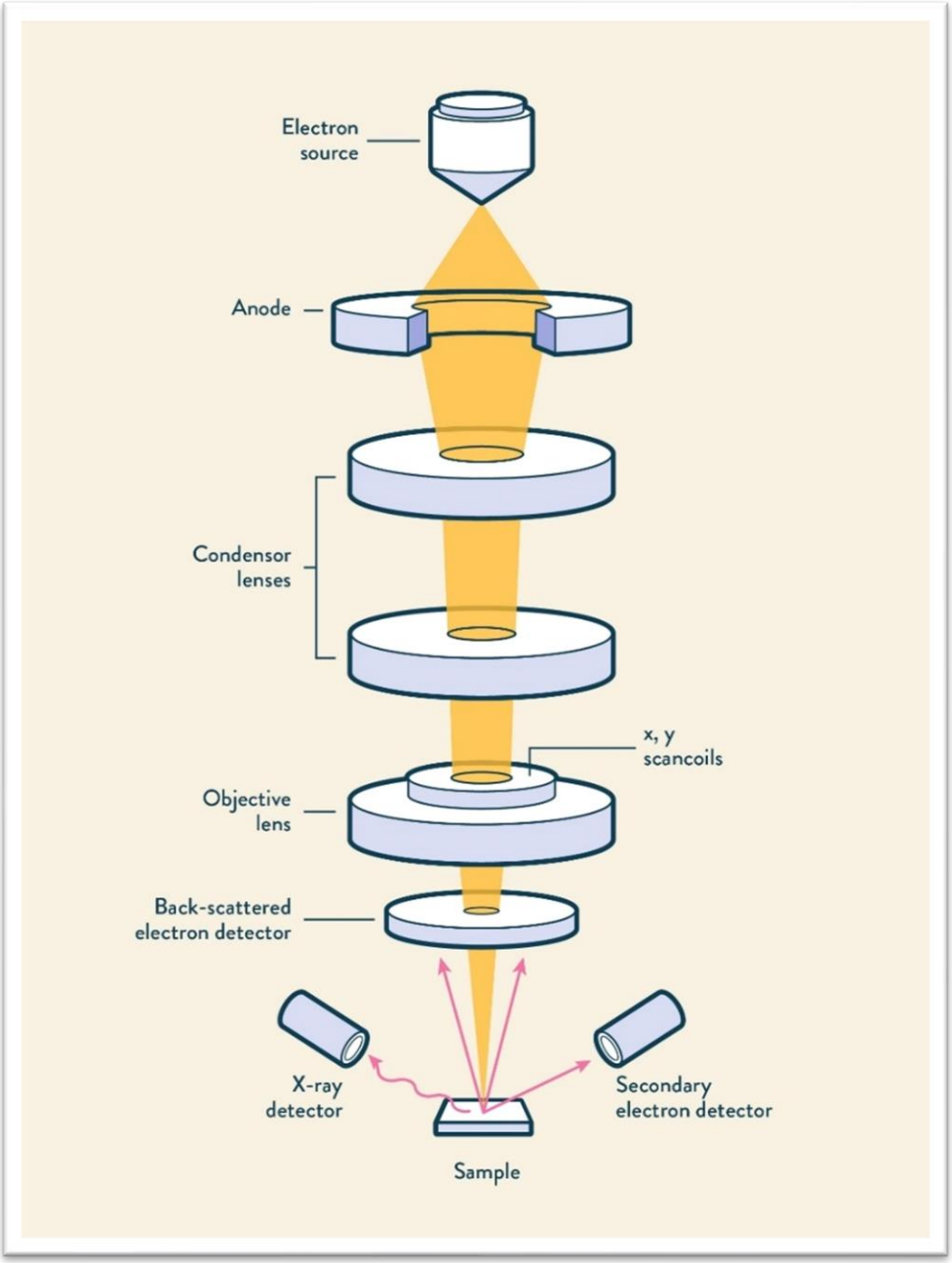

Figure 25: Schematic figure of an SEM apparatus, from the work of Gleichmann, N. *et al* [lxxxi].

In more detail, the analysis is done through applying a beam of high-energy electrons, often with a thermal source. The gun produces a spot size that is too large to give a sharp image of the material, so the SEM is equipped with condenser lenses which compress the spot and direct the electrons beam. This forms an image of the material point by point depending on the movement of the scan coils, which can cause the electron beam to move to distinct positions in the form of straight lines in a rectangular geometry. If a higher magnification is required, the scan coils make the beam to deflect a smaller area in the sample. The emitted electrons are detected by the Electron detector to form an image, both secondary electrons and backscattered electrons are used in SEM image production [lxxxii].

For these study, the secondary electron detector (SED) and the backscattering electron detector (BED) were used. The secondary electrons give information about the topography of the surface, and were also used to perceive the distribution of dopants in the films. This is possible due to insulator areas charging up with electrons and giving a bright white image, in opposition with conductive areas that give darker images. The backscattering electron detector is often used to obtain high-resolution images of the elements present in the sample, nevertheless it was used as a way to observe whether any scratches were present in the films grown on SCD [lxxxiii]. Difference between the images of both detectors can be seen in Figure 26.

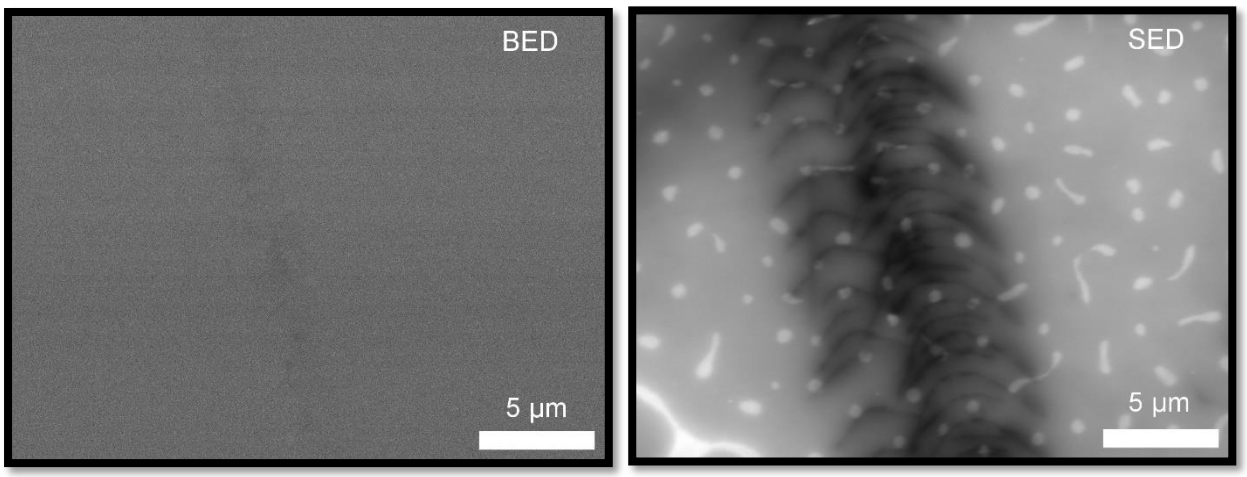

Figure 26: On the left, an image taken with the backscattered electron detector, showing a smooth surface. On the right, an image taken with the secondary electron detector, showing different shapes along the film, with some areas showing charging of electrons and others showing dark images. Both images are of the same are in the film with an accelerating voltage of 15kV and a magnification of x5000.

SEM analysis was also used to measure the thickness of the samples grown on Si substrates, as well as to inspect the surface and the growth patterns.

3. Experimental method

3.1. Electrospray seeding of Silicon substrates

A solution of 40 ml of methanol and 5 drops of a solution of primary crystals of detonation nanodiamond dispersed in water (2.0 w/v %) was made and introduced into a vial. The vial was fixed into an ultrasonic probe, which was left to run for one hour at 30% power.

Meanwhile, the Silicon substrates were washed, first with acetone and then with isopropanol, both for 15 min each in an Ultrasonic cleaning bath. After the bath, the samples were air dried and stick into the rotating surface in the Electrospray apparatus (Figure 22), 1 mL of the nanodiamond solution was introduced into the needle of the apparatus. The machine was left working at 65 KV until the needle was emptied out twice. All the samples showed uniform seeding of nanodiamond.

3.2. Growth on Silicon substrates

Silicon substrates were placed in the reactor chamber, which was then closed and pumped into pressures of approximately 7.5×10^{-6} Torrs. The parameters shown in Table 4 were used to grow the different samples, altering the concentration of Nitrogen introduced in each of them. The temperature was measured by a 1-colour pyrometer and displayed on a readout in the rack. The surface temperatures of the substrates were around 900 ± 20 ºC, at a microwave power of 1.2 Kilowatts and a pressure of 120 Torrs for all the samples. A separating wire of 0.25 mm of diameter and Mo disk were used for all the growths. Each sample was deposited for 120 minutes before the non-hydrogen gases were turned off.

Table 4: Different concentrations of gases used to grow seven different samples. The sample with 0% N_2 was used as a reference to compare with the other six samples.

CH_4 (sccm)	H_2 (sccm)	B_2H_6 (sccm)	N_2 (N_2/C %)
20	**489.835**	**9.999**	**0**
20	**489.835**	**9.999**	**2**
20	**489.835**	**9.999**	**2.5**
20	**489.835**	**9.999**	**3**
20	**489.835**	**9.999**	**3.5**
20	**489.835**	**9.999**	**4**
20	**489.835**	**9.999**	**4.5**

3.3. Acid cleaning of Single Crystal Diamond substrates

A 100 ml solution of H_2SO_4 (95% w/w) was added to 6.5 g of KNO_3 and left to dissolve under reflux conditions at approximately 200ºC. After the solution was fully dissolved (solution turned yellow), SCD substrates were introduced into the acidic solution and were left under reflux for 3 hours (Figure 27).

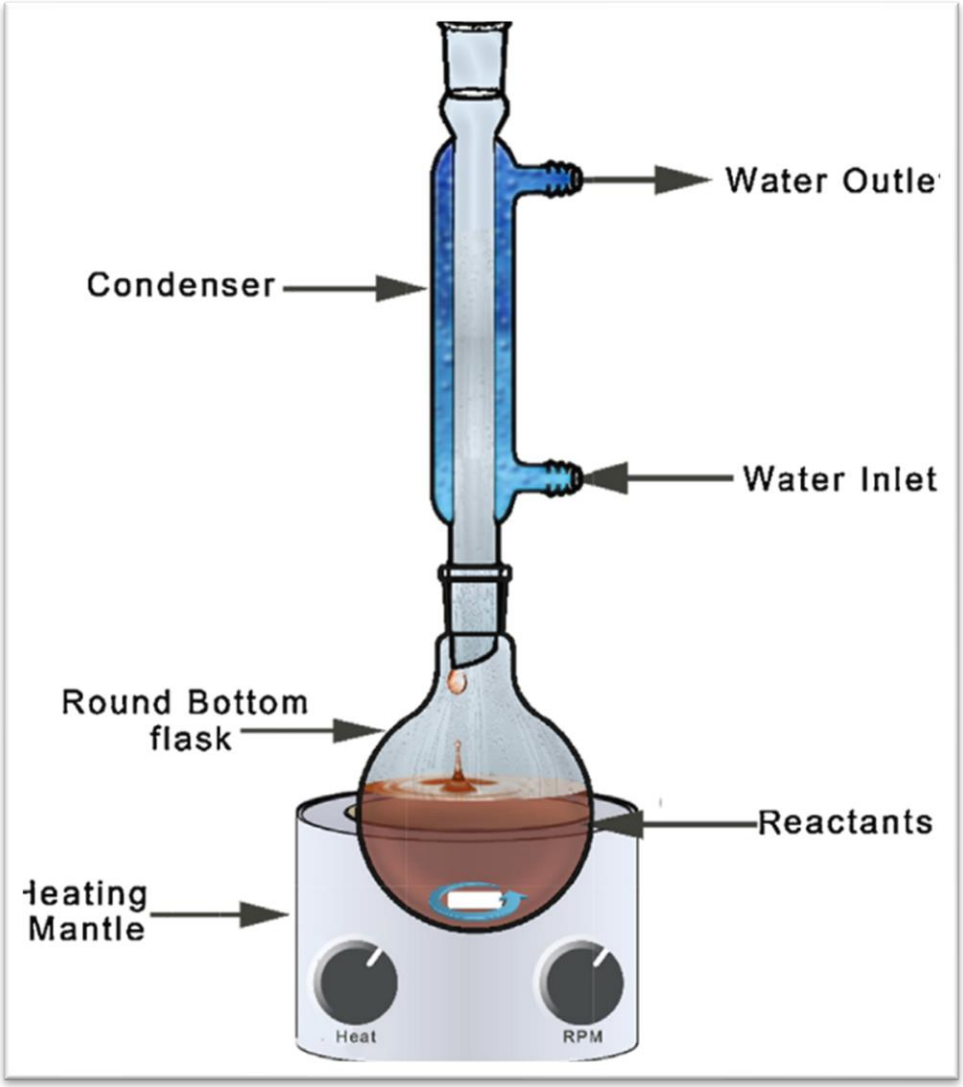

Figure 27: Schematic figure of a round-bottomed flask under reflux conditions, as it was carried out in the experiment.

After 3 hours, the flask containing the acidic solution and substrates was left to cool. When it was cooled down; the acid was neutralised and disposed of; the substrates, were further washed with acetone and isopropanol for 15 min each in an Ultrasonic cleaning bath. The substrates were then air-dried.

3.4. Growth on Single Crystal Diamond substrates

Single crystal diamond substrates were placed in the reactor chamber, which was then closed and pumped into pressures of approximately $7.5x10^{-6}$ Torrs. The parameters shown in Table 5 were used to grow the different samples, altering the concentration of Nitrogen introduced in each of them. The temperature was measured by a 1-colour pyrometer and displayed on a readout in the rack. The surface temperatures of the substrates were around 1085 ± 10 ºC, at a microwave power of 1.35 Kilowatts and a pressure of 100-95 Torrs for all the samples, changing pressure after 60 minutes of growth to keep the temperature stable. A separating wire of 0.5 mm of diameter and Mo disk were used for all the growths. Each sample was deposited for 120 minutes before the non-hydrogen gases were turned off.

Table 5: Different concentrations of gases used to grow seven different samples. The sample with 0% N_2 was used as a reference to compare with the other six samples.

CH_4 (sccm)	H_2 (sccm)	B_2H_6 (sccm)	N_2 (N_2/C %)
7.5	**690**	**50**	**0**
7.5	**690**	**50**	**6.7**
7.5	**690**	**50**	**8**
7.5	**690**	**50**	**10.5**
7.5	**690**	**50**	**20**
7.5	**690**	**50**	**33.3**

4. Results and discussion

4.1. Polycrystalline diamond samples grown on Silicon substrates

The samples grown on Silicon substrates had a range of N_2/C from 0% up to 4.5%, each showing different electrical characteristics. The first analytical technique used on them was a two-probe contact test to get a rough estimate of the electrical resistance for each substrate. The results shown on Figure 28, show first a decrease of the electrical resistance upon addition of Nitrogen into the gas phase up to 2.5% N_2/C. After those levels, the electrical resistance increases linearly with a slight decrease between 3% and 3.5% N_2/C , until reaching a higher resistance than the BDD sample. The decrease in electrical resistance was highly unexpected, as every sample had the same levels of Boron and resistance has been reported to show an increase in electrical resistance upon addition of Nitrogen with similar levels of the dopant, as mentioned earlier (shown in Figure 18b).

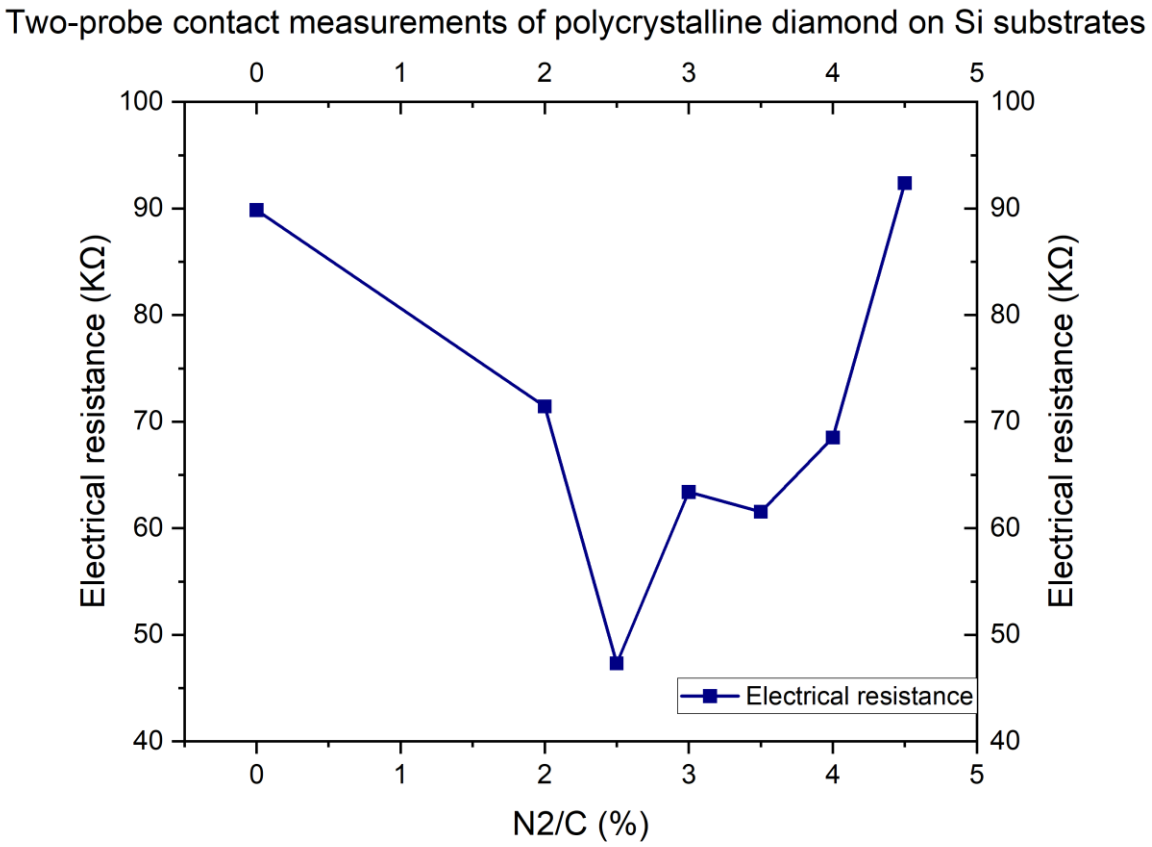

Figure 28: Graph showing the different electrical resistance of 7 different polycrystalline diamonds, with different N_2/C ratios.

The samples were analysed by Raman spectroscopy, which indicated the growth of diamond showing a peak at 1332 cm^{-1} on each of the samples (Figure 29 and Figure 30). The Raman data also indicates the increase in impurities addition (or dopants incorporation) into the lattice. This is shown by the peak at around 1600 cm^{-1} increasing in intensity as more Nitrogen was being added into the growth phase. As shown in Table 3, this peak indicates the presence of amorphous sp^2 hybridised carbon atoms, which form in the lattice due to the

presence of impurities in substitutional positions, preventing the formation of sp^3 hybridised carbon atoms.

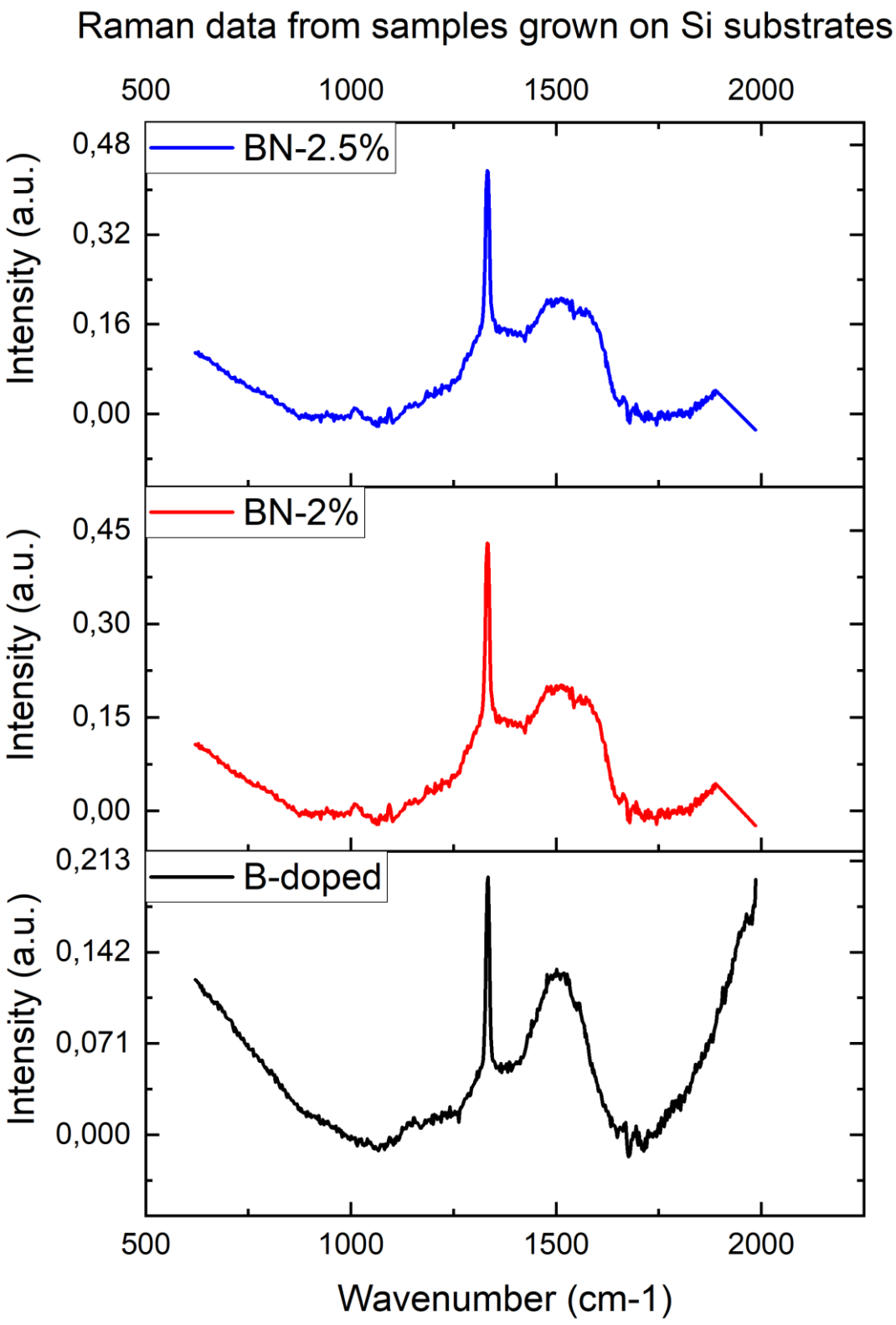

Figure 29: Three different stacked graphs showing the Raman data from the samples with a 0%, 2% and 2.5% N_2/C ratio. All the samples were grown on Si substrates after being seeded by electrospray

with a nanodiamond/methanol solution. All data was normalised and the baseline was subtracted to show a flat baseline.

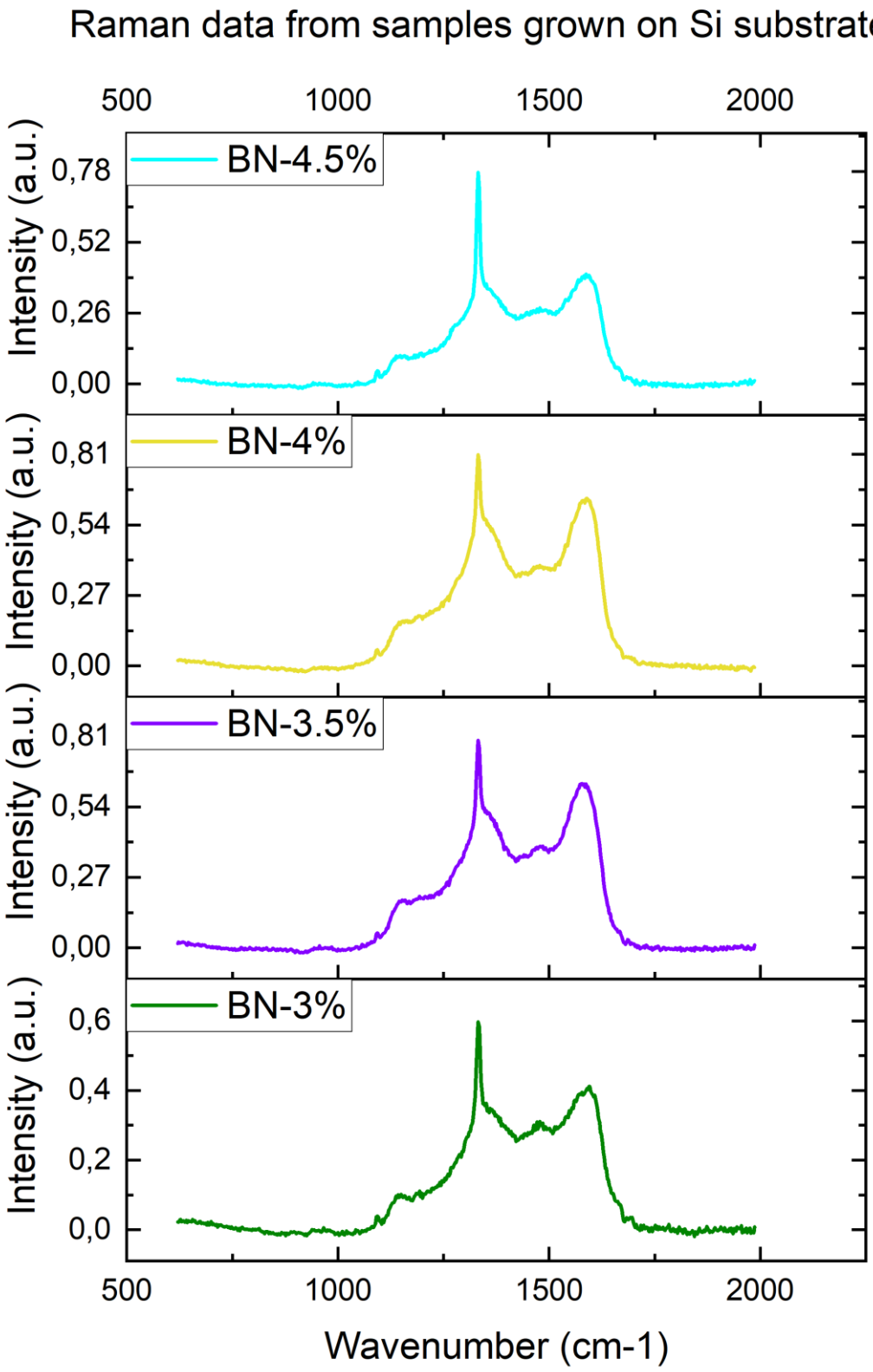

Figure 30: Four different stacked graphs showing the Raman data from the samples with a 3%, 3.5%, 4% and 4.5% N_2/C ratio. All the samples were grown on Si substrates after being seeded by

electrospray with a nanodiamond/methanol solution. All data was normalised and the baseline was subtracted to show a flat baseline.

The baseline was subtracted for all the data displayed and then, was plotted onto the same graph in Figure 31 to perceive the difference in Relative Intensity in all of the samples. As it can be seen, the intensity of the peaks at around 1600 cm^{-1} increases upon addition of Nitrogen, showing an increase in introduction of dopants in substitutional positions in the lattice.

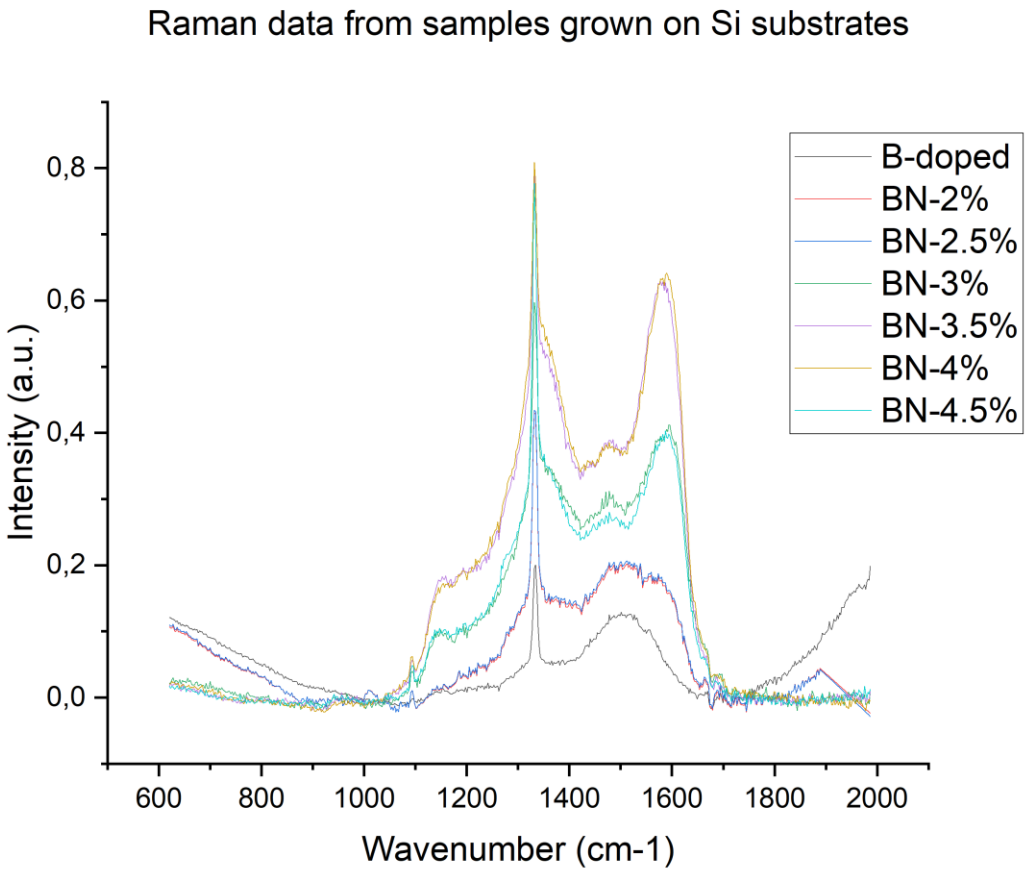

Figure 31: Raman data from all polycrystalline samples plot onto each other. All data was normalised and the baseline was subtracted to show a flat baseline.

SEM images showed different thickness across the samples, as it is expected when using different growing parameters. The thickness was measured taking an average of different points across the surface in cross-section images of the samples. As stated before, the samples were grown under the same conditions and duration. As shown in Figure 32, the growth rate increased in the sample with 2% of Nitrogen compared to carbon by approximately 70%, which is in accordance with the work of Yiming, Z., Larsson, F. and Larsson, K et al [lxxxiv]. The growth rate then decreased down to 0.8 µm with 3.5% of nitrogen on carbon and then increased again up to 1 µm with 4.5%. The decrease was not expected at such a low concentration of nitrogen of carbon, as studies show an increase in the growth rate up to 20% of N_2/C. The increase is attributed to the formation of CN radicals at low concentrations of Nitrogen, followed by a reduction of CH_x radicals at high concentrations of

Nitrogen [lxxxv]. As the concentration used in these experiments are much lower than the concentrations reported to decrease the growth rate, there is reason to believe that the Boron and Nitrogen incorporation are decrementing the growth rate, as the samples with concentration higher than 2% show a lower growth rate than the sample with no Nitrogen.

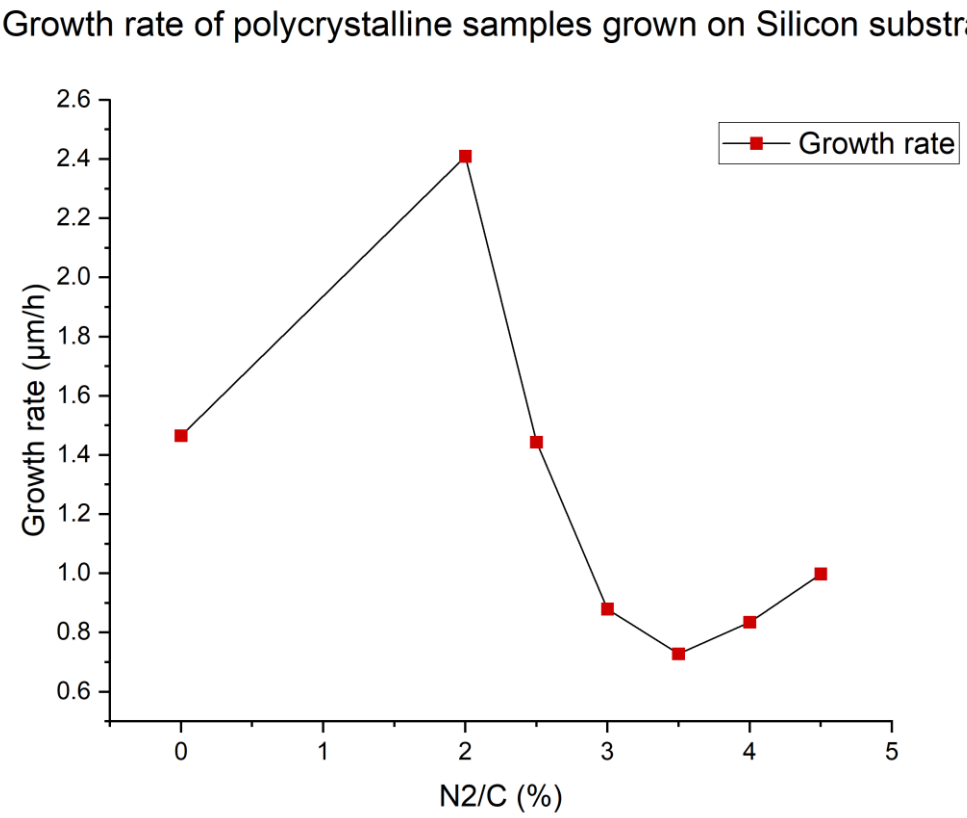

Figure 32: *Graph showing the growth rate of polycrystalline samples grown on Silicon substrates, calculated with SEM images.*

The SEM images also showed a variety of grain shapes, meaning different geometries in the samples. As shown in Figure 2, the different grain shapes can manifest the type of crystallographic orientation of the surface crystals. A triangular shape means a (111) orientation, while a (100) orientation is seen as a square shape. As it can be seen in Figure 33, there was an overall trend showing more 111 crystallographic orientations upon more nitrogen concentration. This trend is due to epitaxial growth, in which a crystal is grown on a substrate such that the crystal lattice of the growing crystal aligns with the lattice of the substrate. The strain that is cause by the incorporation of Nitrogen atoms into the lattice can cause the diamond to grow preferentially in the (111) plane, which is particularly stable thermodynamically.

The remainder of the SEM surface figures are available at the appendix, from Figure 49 to Figure 51.

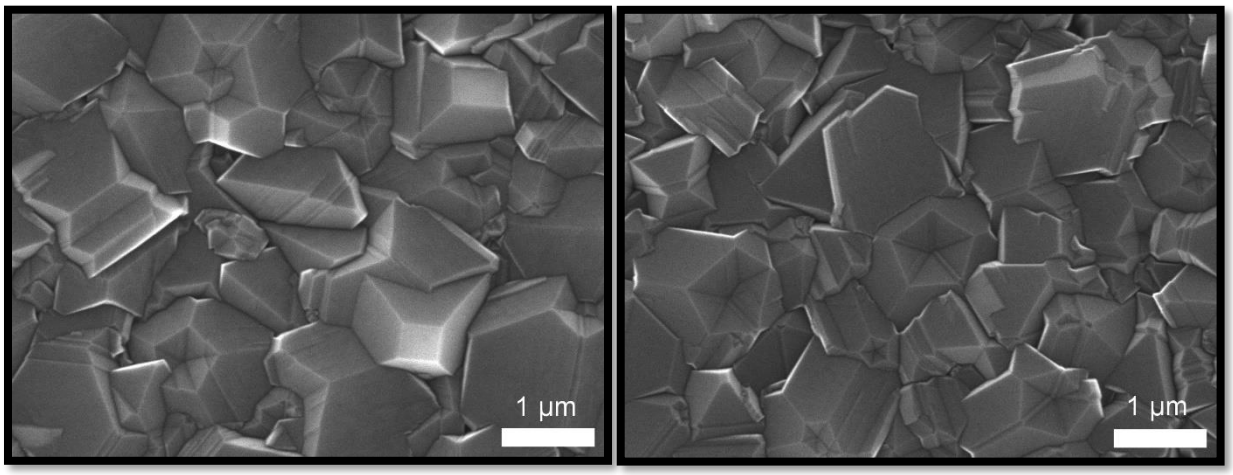

Figure 33: On the left, image of 0% N_2/C sample showing 111 and 100 orientations. On the right, image of 2.5% N_2/C sample showing mainly 111 orientations. All pictures have a magnification of x20000, and *an applied potential of 15.0 kV.*

Hall effect measurements were taken for the samples, despite some inaccuracies that have been reported on this sort of measurements for polycrystalline semiconductors on conductive substrates. Some of the inaccuracies that occur can be the contact resistance of the samples, as it can differ between grains, leading to non-constant measurements; the presence of grain boundaries can affect the carrier concentration and the mobility of the charge carriers leading to differences in the Hall effect measurements; they can also have a high density of surface states which can confine charge carriers and again affect the measurements. The conductive substrate, Silicon in this case, can provide a parallel conduction for path carriers, which can lead to an inaccurate estimation of the mobility and the carrier concentration of the samples [lxxxvi].

The measurements showed non-ohmic contacts in the current-voltage (I-V) line, which has also been reported to affect the accuracy of the results. Despite all this, the samples showed consistent results in all four contacts, the I-V graphs are available in the appendix from Figure 52 to Figure 58.

The results (Figure 34) of the Hall effect measurements showed p-type carriers for all the samples, but it did demonstrate some surprising results. The resistivity of all the co-doped samples decreased in comparison with the Boron-doped sample. This is an unexpected result as the introduction of Nitrogen is reported to increase the resistivity in diamond layers. A plausible explanation for this, is the formation of BN-clusters in substitutional positions, by bonding of Nitrogen atoms to Boron atoms in interstitial positions, moving them into substitutional positions. This release of Boron atoms from interstitial positions would signify an increase in mobility for the charged carriers, hence lowering the resistivity of the sample. As it can be seen in Figure 34, the mobility of the samples decreased slightly in the 2% N_2/C, and then linearly increased up to the 3.5% N_2/C sample, achieving a maximum of ~240 cm^2/ Vs, and then decreasing again linearly up to ~166 cm^2/ Vs in the 4.5% N_2/C sample. The carrier concentration of all the co-doped samples remained in the same scale of 10^{18} cm^{-3} and staying nearly stable. The reference BDD sample showed a carrier concentration ~$7*10^{16}$ cm^{-3}, which then increased for the co-doped samples as it was expected by the addition of more dopants into the growth phase. The maximum carrier concentration was

~4*10^{18} given by the 3% N_2/C sample, but not showing a considerable increase in comparison with other co-doped samples. These results have been analysed acknowledging the possible inaccuracies of this type of measurement in the samples measured, especially for mobility and carrier concentration.

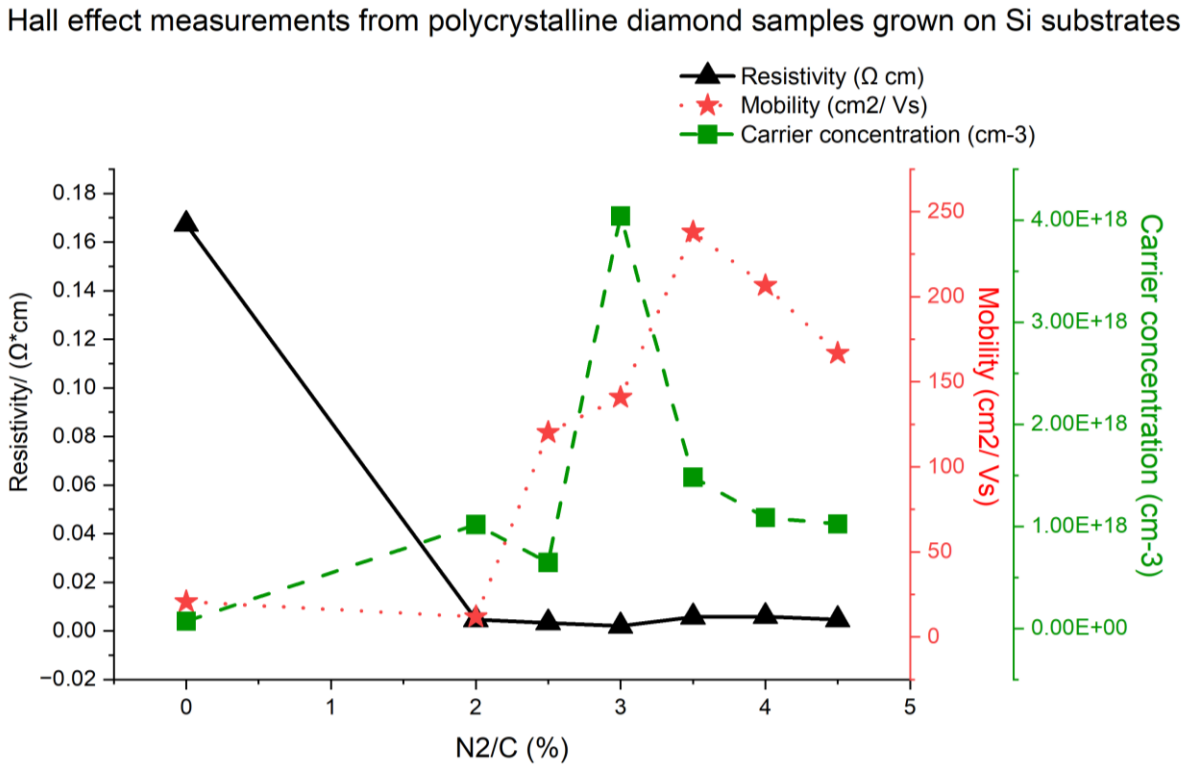

Figure 34: Graph with three different Y axis, showing results from the Hall effect measurements taken of the polycrystalline diamond samples grown on Si substrates. The graph shows the values and trends of the resistivity measured in Ω*cm, the mobility of the carriers measured in cm^2/Vs and the carrier concentration measured in cm^{-3}.

4.2. Diamond samples grown on single crystal diamond substrates

The samples grown on SCD substrates had a range of N_2/C from 0% up to 33.3%, each showing different electrical characteristics. The first analytical technique used on them was a two-probe contact test to get a rough estimate of the electrical resistance for each substrate. The results shown on Figure 35, show first a decrease of the electrical resistance upon addition of Nitrogen into the gas phase, with a minimum of 2.99 kΩ on the sample with 8% N_2/C. After those levels, the electrical resistance increases linearly up to the sample with 20 % N_2/C, which shows a resistance of 3.78 kΩ, lower than the BDD sample. The decrease in electrical resistance was highly unexpected again, as every sample had the same levels of Boron and resistance has been reported to show an increase in electrical resistance upon addition of Nitrogen with similar levels of the dopant, as mentioned earlier (shown in Figure 18b). The same trend observed in the Silicon experiments (electrical resistance decreasing at low concentrations of nitrogen and then increasing upon heavy nitrogen doping) has occurred when growing on SCD substrates, showing a pattern in the electrical behaviour of co-doped samples.

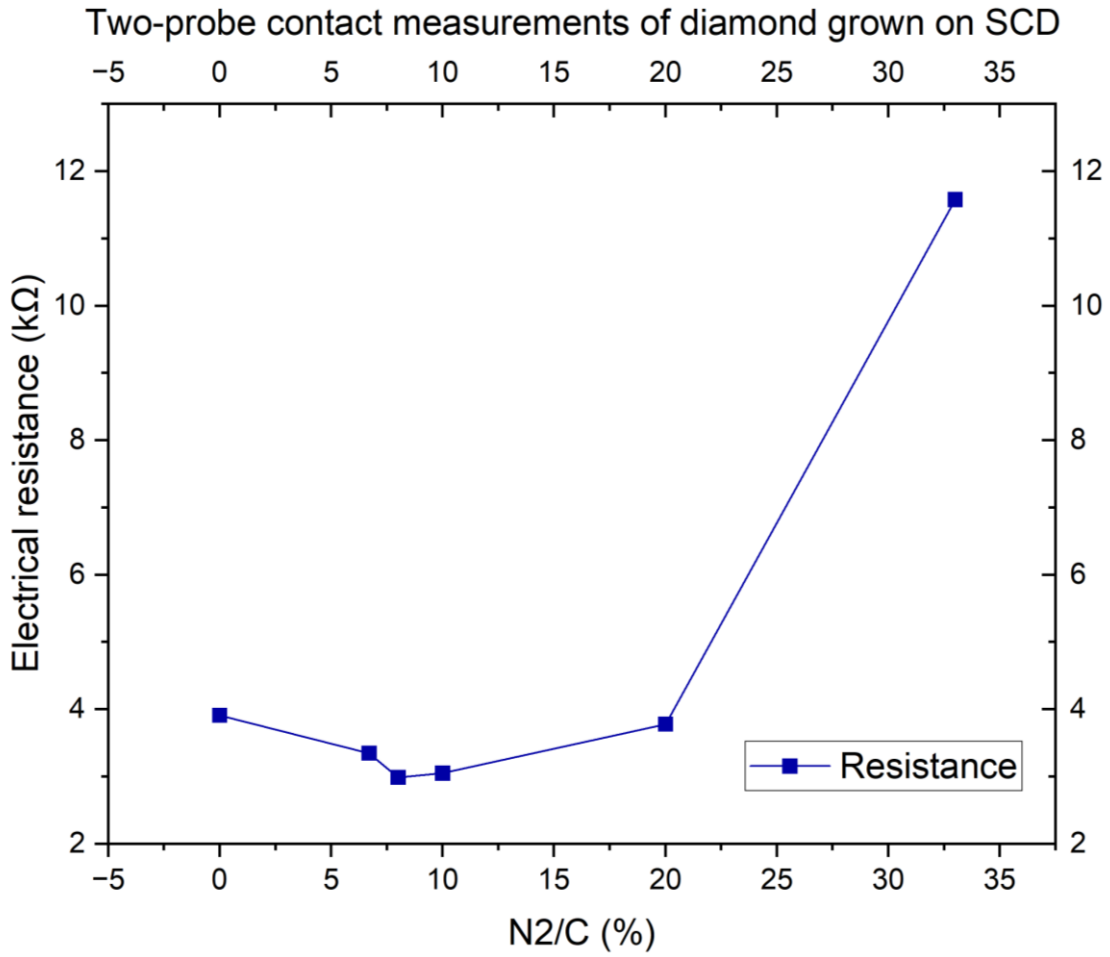

Figure 35: Graph showing the electrical resistance measured with a two-probe contact for diamond samples grown on SCD substrates with different N_2/C ratios.

As it was expected, the SC samples showed no significant peaks apart from the 1332 cm^{-1} diamond peak, shown in Figure 36 and Figure 37. Assuming the Raman laser did not go

through the doped layer into the bulk diamond substrate, the data is useful to confirm that the samples are in fact, epitaxial films with a near-continuous crystal in the grown layer.

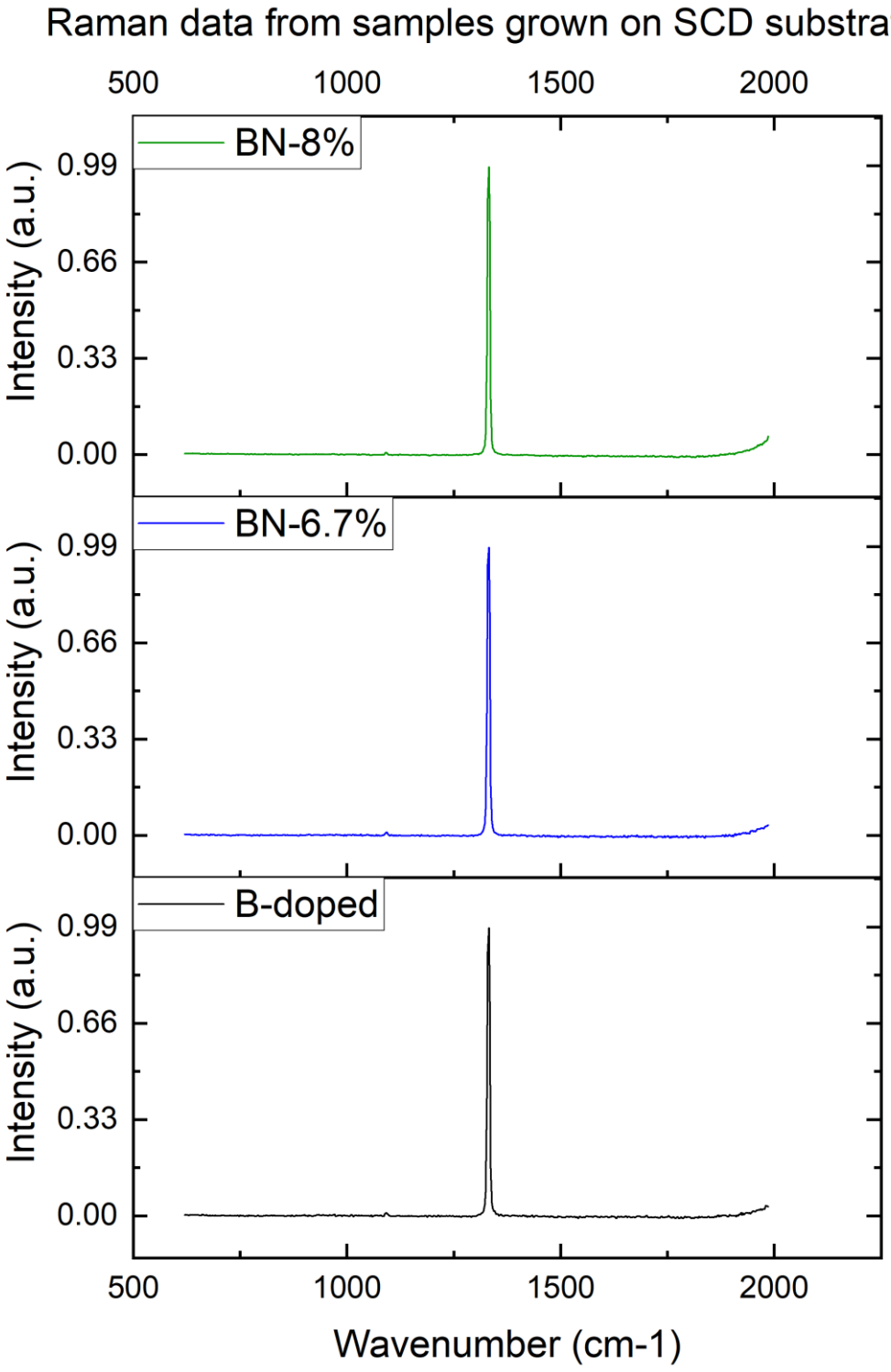

Figure 36: Three different stacked graphs showing the Raman spectroscopy data of three different samples grown on SCD substrates with different N_2/C ratios varying from 0% to 8%.

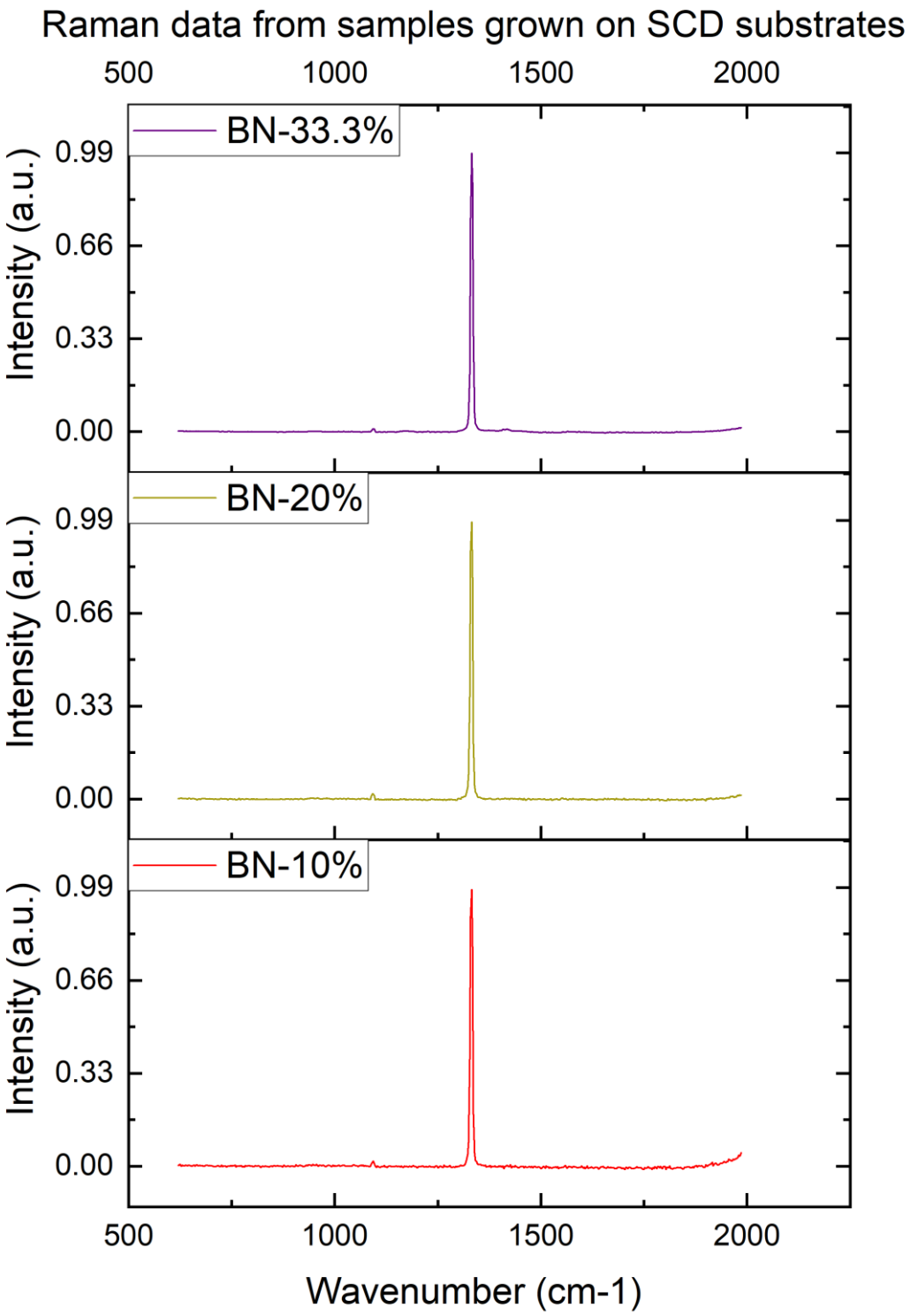

Figure 37: Three different stacked graphs showing the Raman spectroscopy data of three different samples grown on SCD substrates with different N_2/C ratios varying from 10% to 33.3%.

The measuring of the thickness was originally thought to be done by using a mask during growth to avoid lateral growth and then measuring the thickness of the doped layer, which is seen darker in the SEM due to its higher conductivity. Nevertheless, the mask used was found to be unsuitable for this practice, as its high thickness, avoided the plasma to sit on top of the SCD substrate which meant no growth of diamond on the substrate but on the mask instead. Hereby, the growths were carried out on unmasked substrates which produced lateral growth on them.

As expected, the SEM images were not useful to estimate the thickness of the samples, although they showed some unexpected results in the uniformity of the doping in the films. The distribution of doping can be shown by SEM owning to the secondary electrons moving throughout the films, if an area is not conductive enough there is a charging in the area resulting in a brighter white light in the picture.

First, a SCD clean substrate was imaged to inspect the surface (Figure 38) both with BED and SED to inspect the surface. As expected, it showed a smooth and cleaned surface with no scratches or substances on the film.

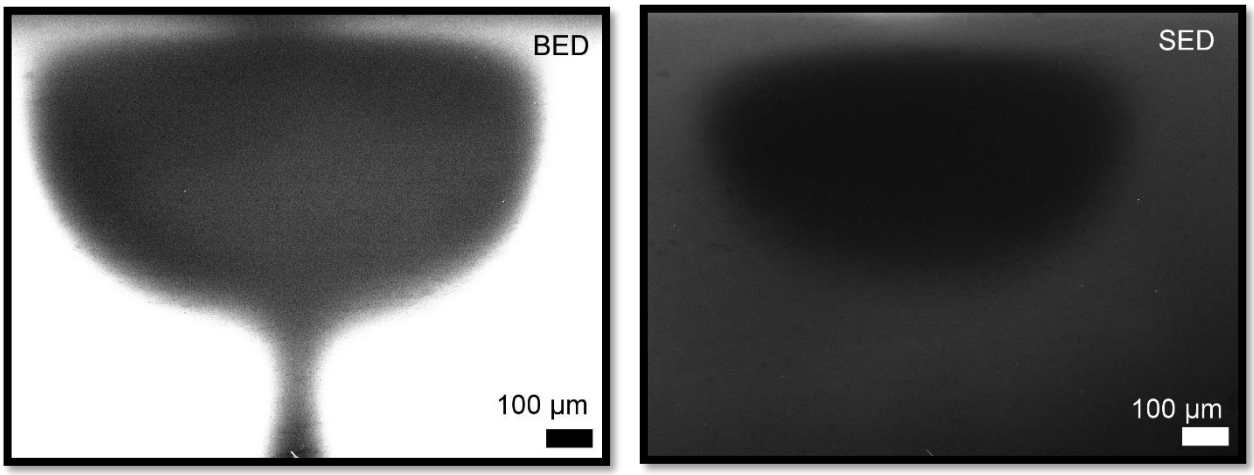

Figure 38: On the left, an image of the top of the SCD substrate with BED, on the right, an image of the same area of the substrate with SED. Both images were taken with an acceleration voltage of 15 kV, and a magnification of x100.

The Boron-doped films showed a non-uniform distribution of the dopants using the SED, as it can be seen in Figure 39. This type of distribution of dopants in the film means the film is not uniformly conductive, as the electrons can flow better in some regions than others. The BED image shows, on the contrary, a smooth surface with no physical scratches on the film.

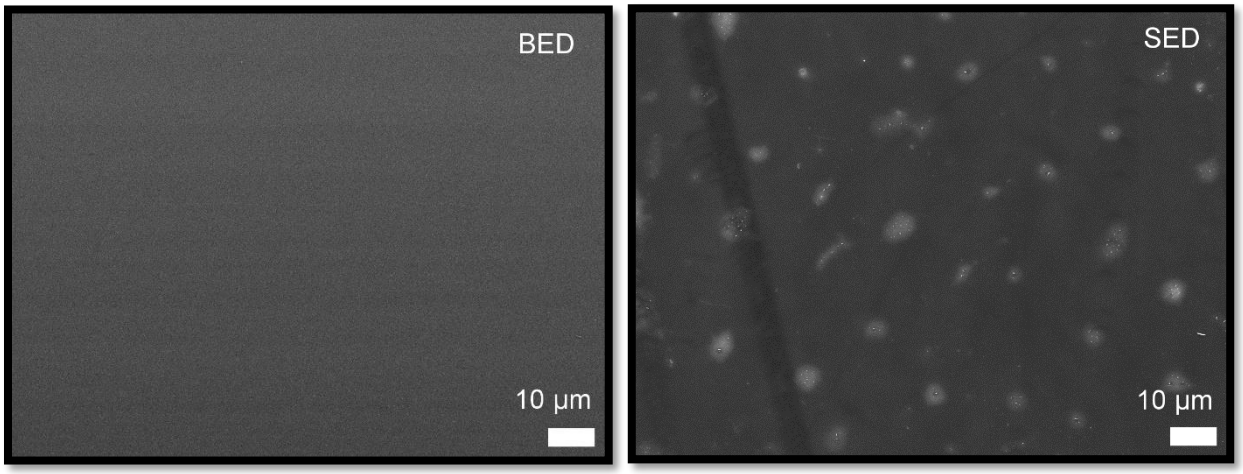

Figure 39: On the left, an image of the top of a BDD film using BED, on the right, an image of the same region of the film using SED. Both images were taken with an acceleration voltage of 15 kV, and a magnification of x1000.

The co-doped sample with a 6.7% of N_2/C (Figure 40) showed again an uneven distribution of the dopants with regions charging up on the SED, and dark regions showing better flow of electrons. The BED image showed again, a smooth surface on the film, with a few dots on the image that are probably little scratches or dust that had deposited on the sample.

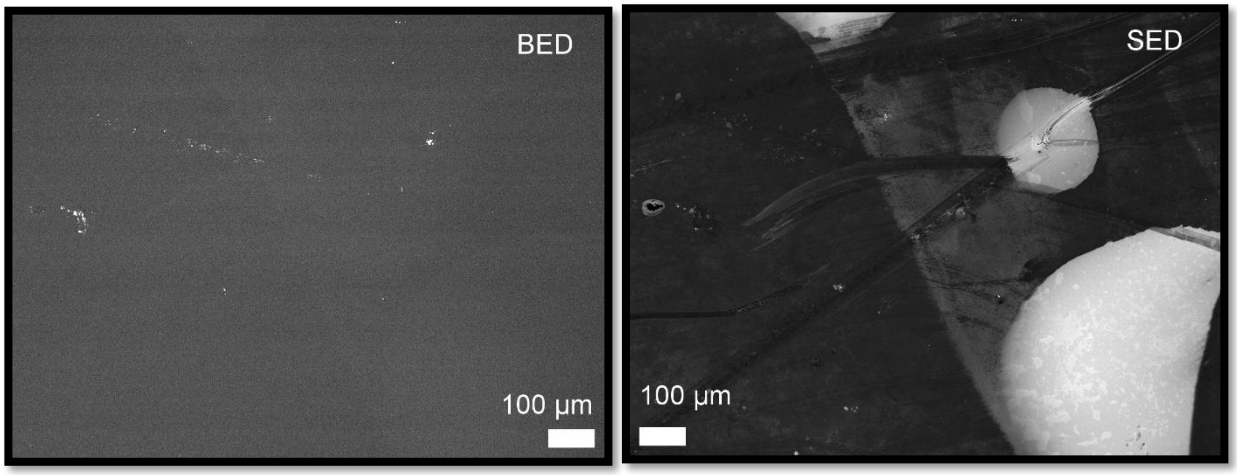

Figure 40: On the left, an image of the top of a BN co-doped diamond film with 6.7% N_2/C using BED, on the right, an image of the same region of the film using SED. Both images were taken with an acceleration voltage of 15 kV, and a magnification of x100.

The co-doped sample with an 8% of N_2/C (Figure 41) showed very similar results to the previous sample (6.7% N_2/C), nonetheless, the image taken with SED shows a different pattern in the distribution of dopants in the film, being this sample more uniform, with smaller 'charging' areas. The image taken with the BED shows a smooth film with no physical scratches again.

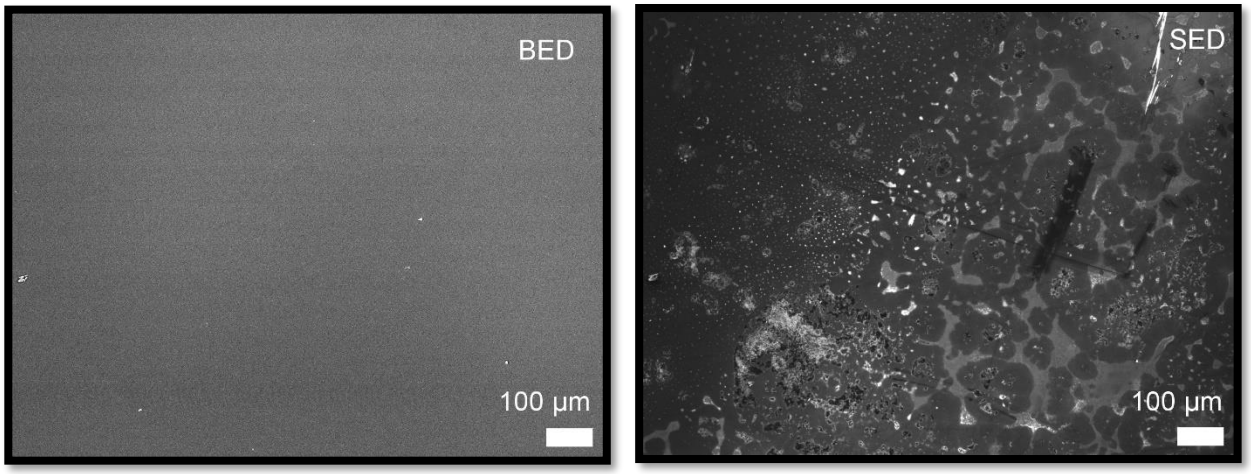

Figure 41: On the left, an image of the top of a BN co-doped diamond film with 8% N_2/C using BED, on the right, an image of the same region of the film using SED. Both images were taken with an acceleration voltage of 15 kV, and a magnification of x100.

The co-doped sample with a 10% of N_2/C (Figure 42) showed mainly uniformity in the flow of electrons in the images with BED and SED. However, the sample showed a crystal in a region of the film that was surrounded by less conductive material, as it can be seen in Figure 43. The reason for this crystal formation is unknown, but it is thought that a particle could have landed on the film before growth, stimulating nucleation. It is suspected that the distribution of dopants was affected due to the formation of the crystal amid the film, explaining the less conductive surroundings of the crystal.

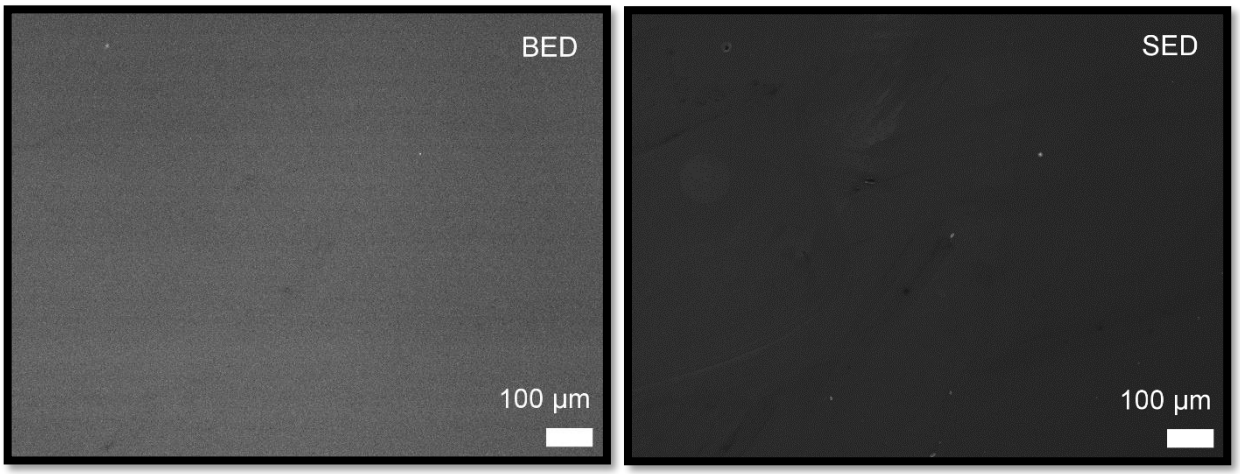

Figure 42: On the left, an image of the top of a BN co-doped diamond film with 10% N_2/C using BED, on the right, an image of the same region of the film using SED. Both images were taken with an acceleration voltage of 15 kV, and a magnification of x100.

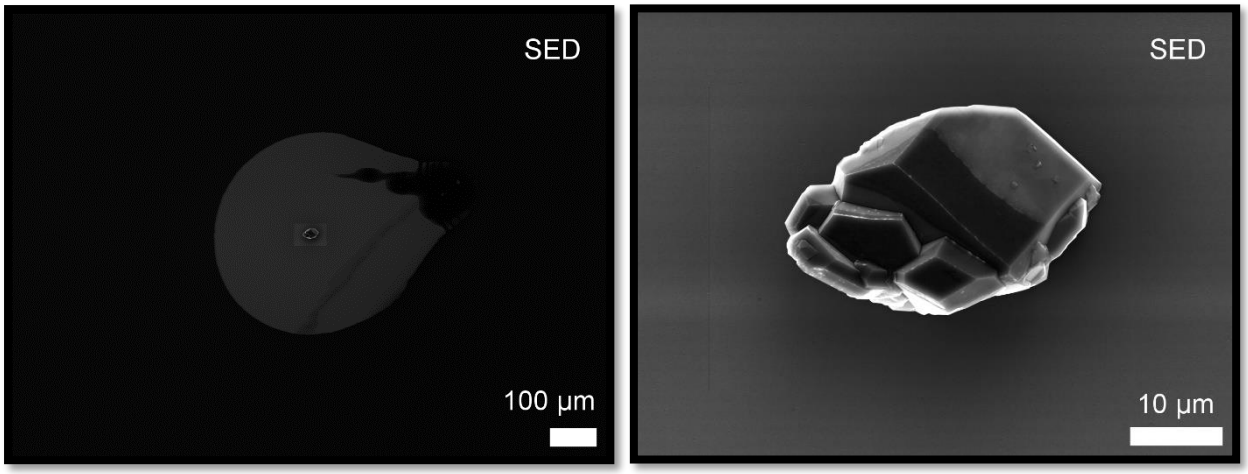

Figure 43: On the left, an image of the crystal found in the 10% N_2/C film, showing less conductive surroundings around the crystal. The image was taken with a x100 magnification and a 15kV of acceleration voltage. On the right, a closer image of the crystal formed. The image was taken with a x2000 magnification and an acceleration voltage of 15 kV.

The co-doped sample with a 20% of N_2/C (Figure 44) showed a dopant distribution similar to the sample with 8% N_2/C, the BED image showed no species on the surface, meaning the patterns in the SED image were not due to physical scratches.

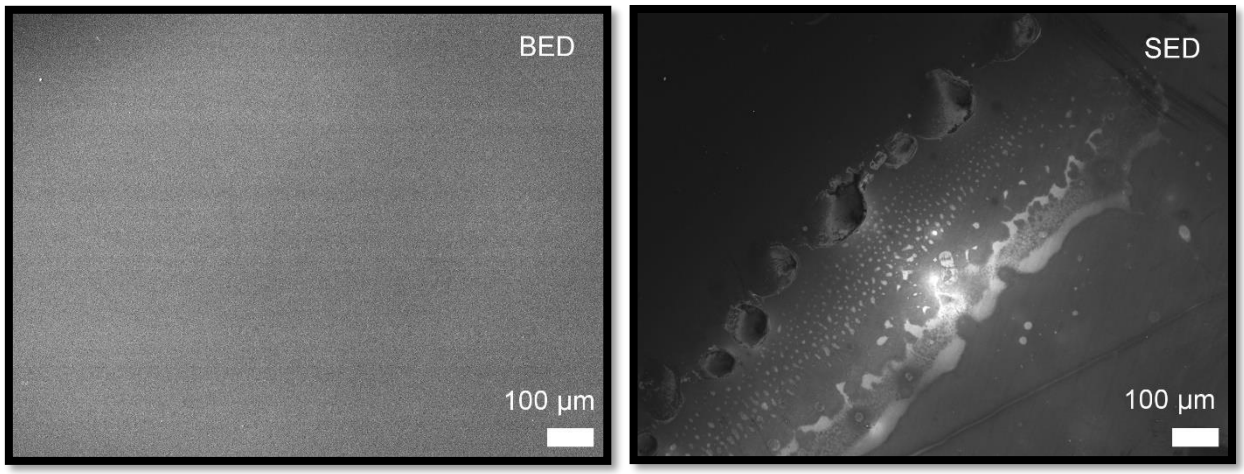

Figure 44: On the left, an image of the top of a BN co-doped diamond film with 20% N_2/C using BED, on the right, an image of the same region of the film using SED. Both images were taken with an acceleration voltage of 15 kV, and a magnification of x100.

The co-doped sample with a 33.3% of N_2/C (Figure 45) manifested similar patterns of non-uniform distribution of dopants as the sample with 8% N_2/C. It formed areas with a high flow of electrons, but also areas where charging of electrons was happening after the electron beam started. Again, the image with BED showed a smooth surface on the film with no physical scratches or other species on it.

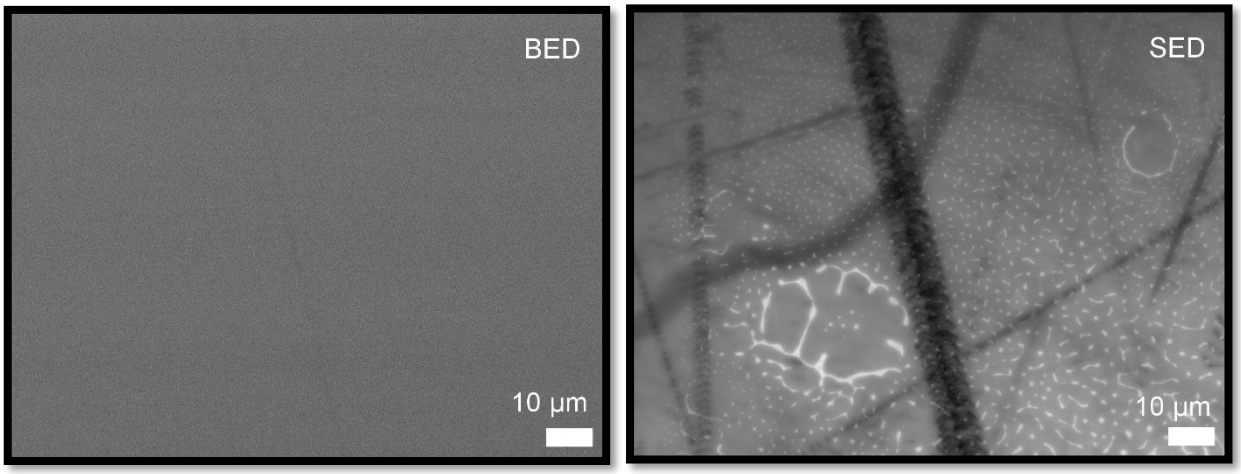

Figure 45: On the left, an image of the top of a BN co-doped diamond film with 33% N_2/C using BED, on the right, an image of the same region of the film using SED. Both images were taken with an acceleration voltage of 15 kV, and a magnification of x1000.

A further unexpected characteristic found on the samples worth mentioning, is the appearance of an 'edge effect' in the samples with 0%, 8%, 20% and 33% N_2/C, shown in Figure 46. This was highly unexpected as the films were not masked when growing, but the SED images show a clear difference of flow of electrons capacity between the edges and the centre of the samples. The images of this areas taken with BED are available in the appendix, Figure 59.

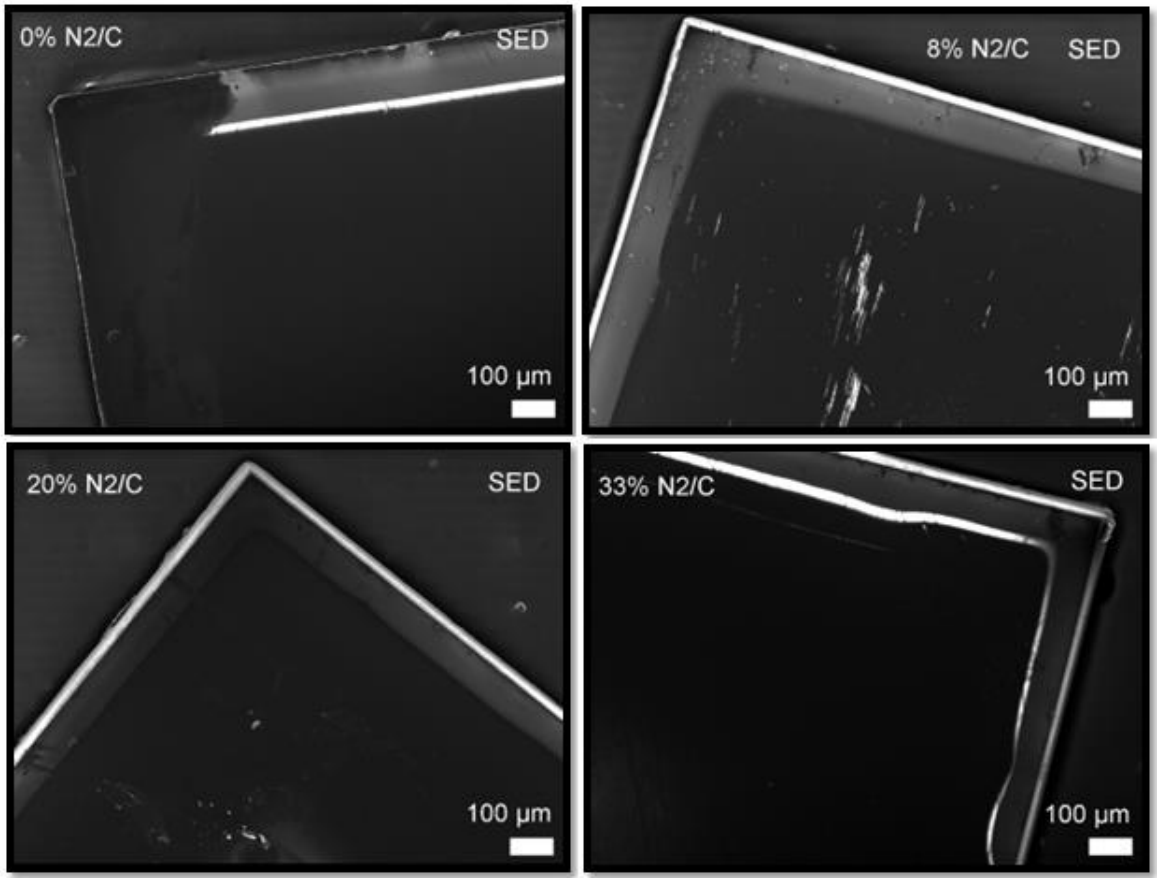

Figure 46: Four different images of the edges of four different films, showing the 'edge effect'. All images were taken with an acceleration voltage of 15 kV and a magnification of x100.

Hall effect measurements were taken for all the samples grown on SCD substrates. As the thickness of the samples was unknown, 1µm thickness was assumed for all the samples for consistency. It was also assumed that the rectangular-shaped films did not behaved differently than square-shaped geometries factor for Hall effect measurements, as a rectangle is not a Van der Pauw geometry.

The samples showed to be Ohmic-contacts in the current-voltage (I/V) line, allowing charge to flow easily in the films, proving a lower resistance than the samples grown on Si substrates. The I/V graphs are available in the appendix from Figure 60 to Figure 65.

The results (Figure 47) of the Hall effect measurements showed again, p-type carriers for all the samples, nonetheless showing unpredicted results. The resistivity of the co-doped samples decreased in comparison to the Boron-doped sample, apart from the sample with a 33.3% N_2/C, which was expected as the Nitrogen concentration was very high. These results conforms a trend in the decrease of resistivity of films co-doped with Boron and low levels of Nitrogen, as it happened with films grown on Si substrates. Again, a feasible explanation for these results would be the formation of BN-clusters in substitutional positions, by bonding of Nitrogen atoms to Boron atoms in interstitial positions, moving the Boron atoms into substitutional positions. This release of Boron atoms from interstitial positions would signify an increase in mobility for the charged carriers, hence lowering the resistivity of the samples.

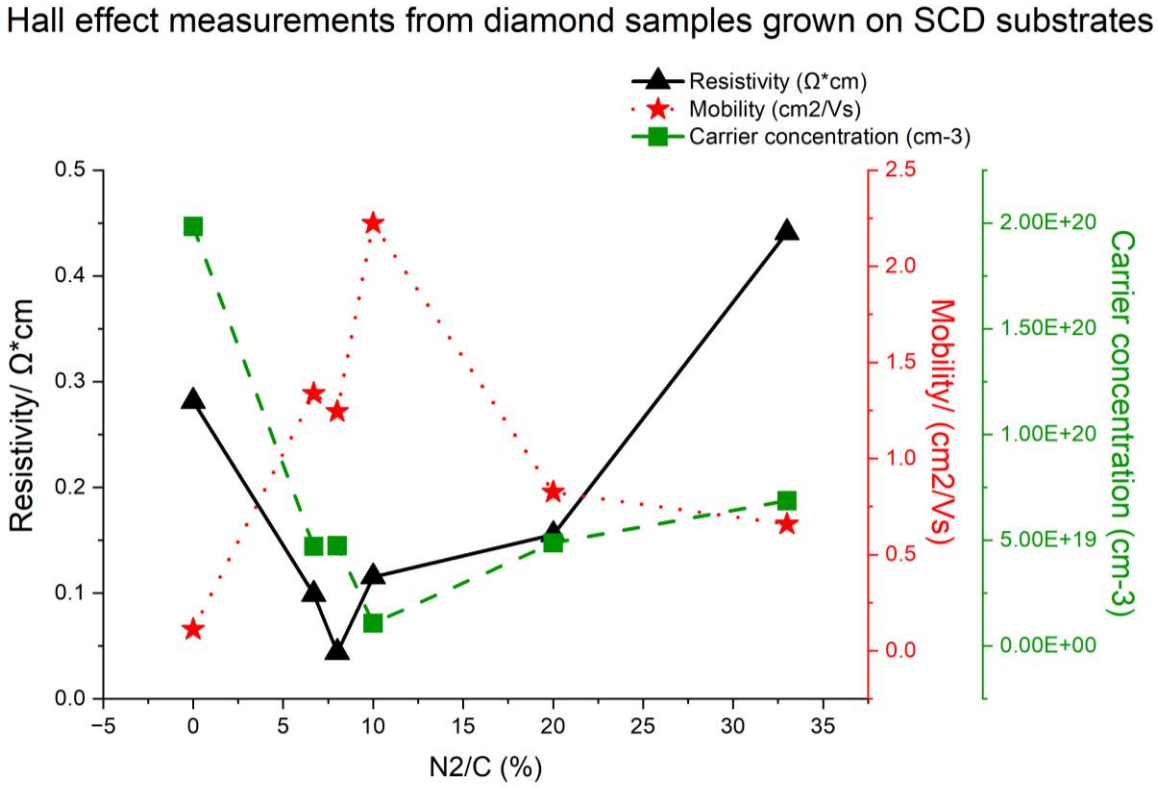

Figure 47: Graph with three different Y axis, showing results from the Hall effect measurements taken of diamond samples grown on SCD substrates. The graph shows the values and trends of the resistivity measured in Ω*cm, the mobility of the carriers measured in cm^2/Vs and the carrier concentration measured in cm^{-3}.

As shown in the graph, the mobility of all samples increase in comparison with the BDD sample (0% N_2/C). There is a maximum in mobility for the sample of 10% N_2/C, but this could be due to a lower dopant introduction in this particular sample, as the carrier concentration is lower than for other samples, ~77% lower. From the graph, the mobilities of the samples are much lower (more accurate) than the samples grown on Si substrates, as these samples did not have many inaccuracies for Hall effect measurements regarding carrier concentrations and mobility. Looking only at the co-doped samples, the trend in mobility is a decrease from low levels of Nitrogen to higher levels (apart from the sample with 10% N_2/C), as expected with higher levels of dopant in the films. The carrier concentrations for co-doped samples, stays approximately stable for all the films, apart from the sample 10% N_2/C, which was already discussed.

5. Conclusion and future work

Based on the evidence presented, the synthesis of an n-type conductive diamond film at room temperature, using Boron and Nitrogen co-doping was unsuccessful, as all the samples showed p-type carriers. Nevertheless, the experiments showed unforeseen results, manifesting a decrease in resistivity on films co-doped with low levels of Nitrogen, up to 8% N_2/C for SCD samples. These results led to the conclusion that Boron-Nitrogen clusters were forming in substitutional positions in the lattice, with Nitrogen atoms bonding to Boron atoms in interstitial positions and taking them into substitutional positions, allowing a longer mean free path in the semiconductor. An increase in the mean free path in the semiconductor meant a higher mobility for the carriers which led to a decrease in resistivity, as seen in the results. As discussed, the control of the type of clusters formed in the lattice is a complex technique, as diamond only allows to introduce these impurities during growth. During this step, many types of BN-clusters can form, and not only the desired ones that theoretically show better results for n-type conductivity, so the sole action that can be managed, is to change the N/B ratio in the growth parameters.

A comparison of the N/B ratios of this experiment with the ratios from the work of Liu, D.Y. *et al.* was made (Figure 48), showing lower ratios for the experiment carried out, hence suggesting that the clusters formed in the films synthesised may not be Nitrogen-rich clusters, like BN_2, which were the clusters showing n-type conductivity in past computational studies.

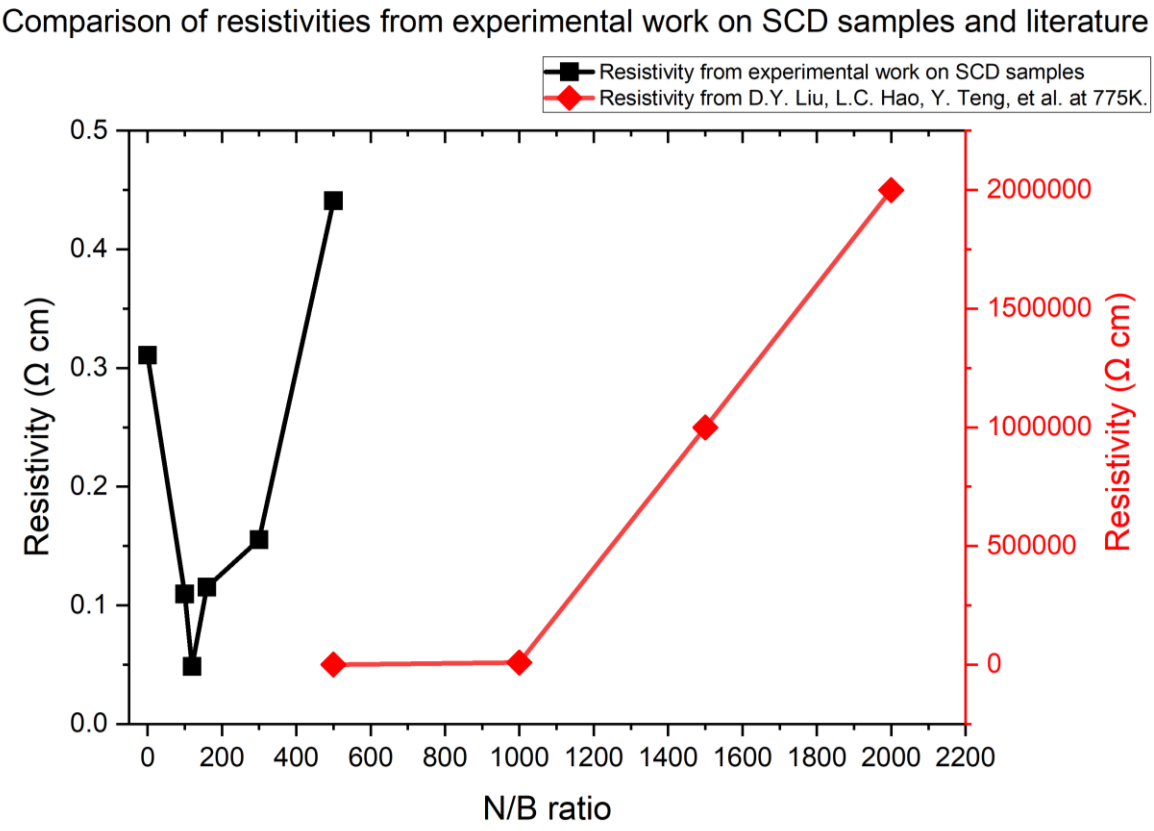

Figure 48: Graph showing a comparison in resistivity vs N/B ratio from the experiments carried out for this project on SCD samples and by Liu, D.Y. *et al.* The measurements taken by Liu, D.Y. *et al.* were at a temperature of 775K, while the ones taken for this project were taken at room temperature.

As a result, future work should be focused on increasing the N/B ratio to levels closer to the work from Liu, D.Y. *et al.,* although this may lead to various issues as the N_2/C ratio would be too elevated which could lead to a very high resistance from the films, making them essentially impracticable for any device operating at room temperature. The films synthesised for this experiment showed lower resistivity at room temperature than the samples from Liu, D.Y. *et al.* at 775K, manifesting rousing results for the films synthesised. The decrease in resistivity manifested in the samples with low percentage of Nitrogen over Carbon could also be used as a potential process to optimise the production of more conductive p-type diamond films for various applications, but more work should be done with similar parameters, to confirm the results.

Aside from the work that should focus on the N/B ratios of the films, a further study using Secondary Ion Mass Spectrometry (SIMS) would be helpful to understand the dopant distribution in the films, as the results from SEM suggested a non-uniform distribution of the dopants. Further study is needed to comprehend the 'edge effect' reported in the films grown on SCD substrates, which reported very low dopant levels around the edges.

This project has overviewed the co-doping of Boron and Nitrogen for diamond films, as an attempt to achieve an n-type material at room temperature. While further work is needed, the results shown in this study should prompt for other studies regarding co-doping of diamond to be done in the future, and even attempt co-doping of diamond with other elements that have shown better results than Boron-Nitrogen clusters in past computational studies, as discussed.

6. Appendix

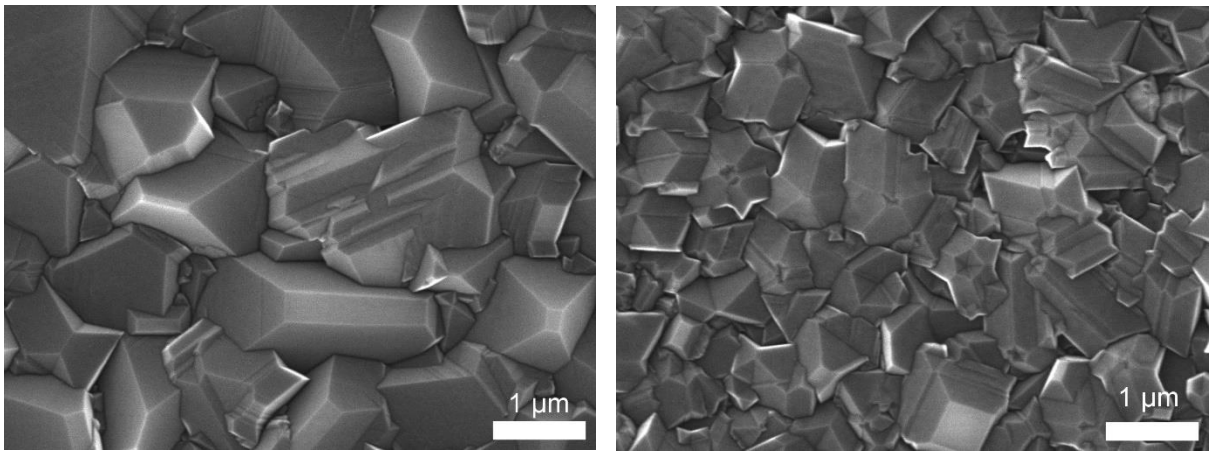

Figure 49: On the left, image of 2% N_2/C sample. On the right, image of 3% N_2/C sample. All pictures have a magnification of x20000, and an applied potential of 15.0 kV.

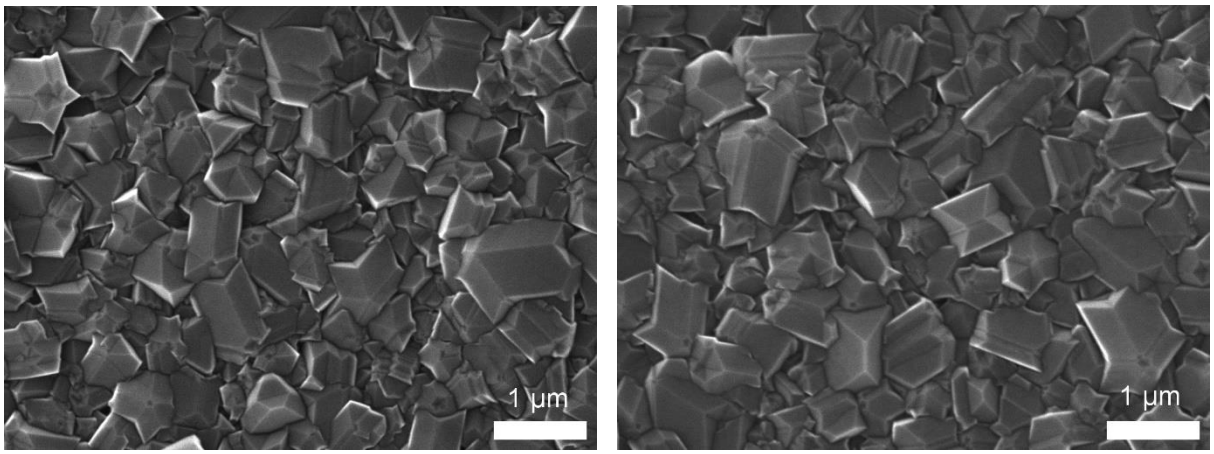

Figure 50: On the left, image of 3.5% N_2/C sample. On the right, image of 4% N_2/C sample. All pictures have a magnification of x20000, and an applied potential of 15.0 kV.

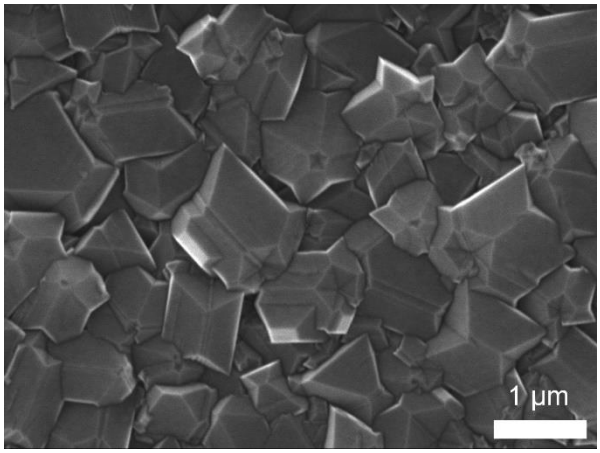

Figure 51: Image of 4.5%% N_2/C sample. The picture has a magnification of x20000, and an applied potential of 15.0 kV.

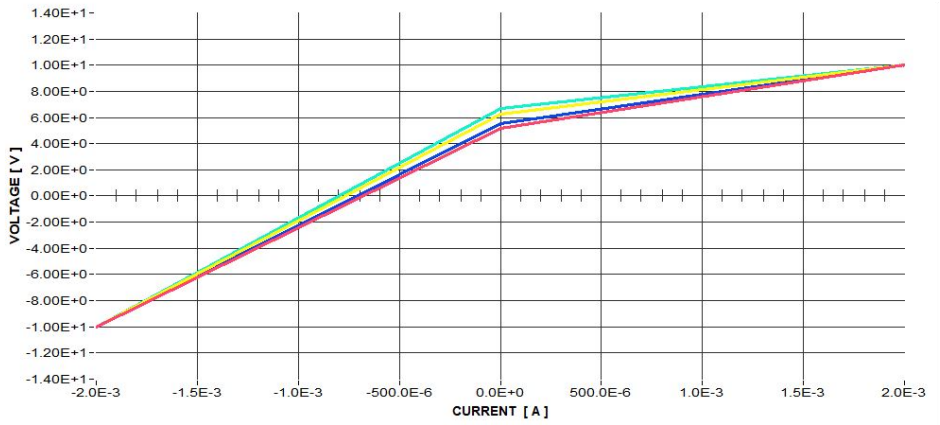

Figure 52: I/V graph of BDD sample grown on a Si substrate, showing non-Ohmic contacts but being consistent on all four contacts.

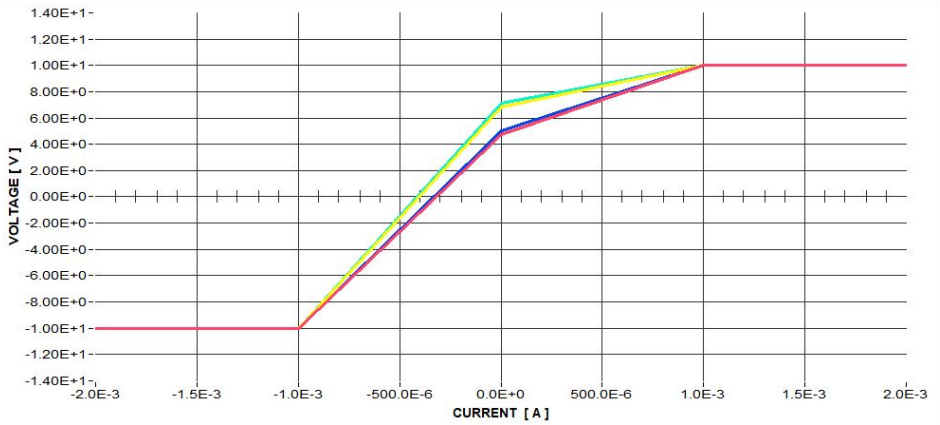

Figure 53: I/V graph of BN co-doped sample (2% N_2/C) grown on a Si substrate, showing non-Ohmic contacts but being consistent on all four contacts.

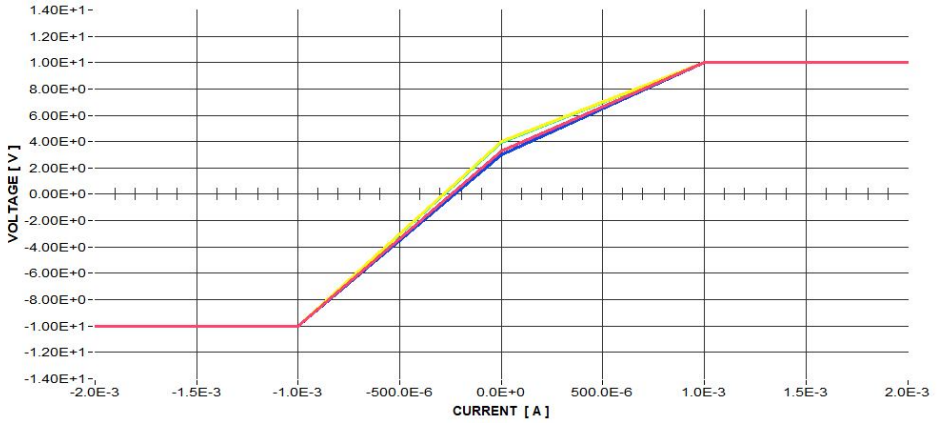

Figure 54: I/V graph of BN co-doped sample (2.5% N_2/C) grown on a Si substrate, showing non-Ohmic contacts but being consistent on all four contacts.

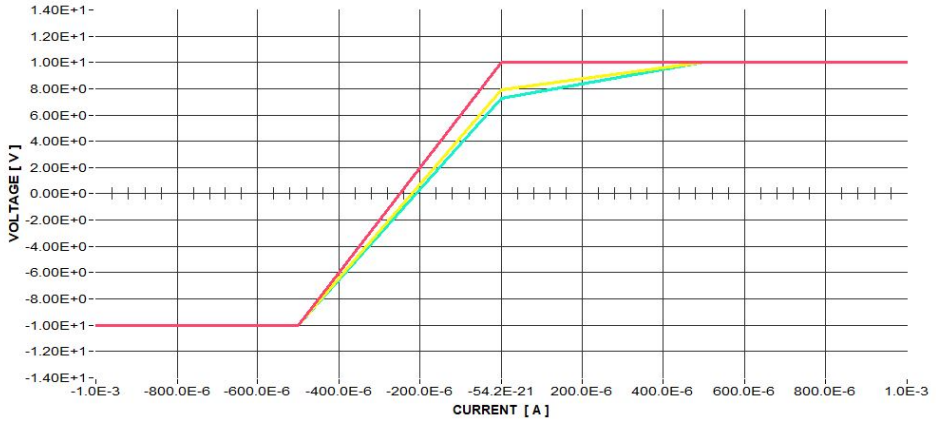

Figure 55: I/V graph of BN co-doped sample (3% N_2/C) grown on a Si substrate, showing non-Ohmic contacts but being consistent on all four contacts.

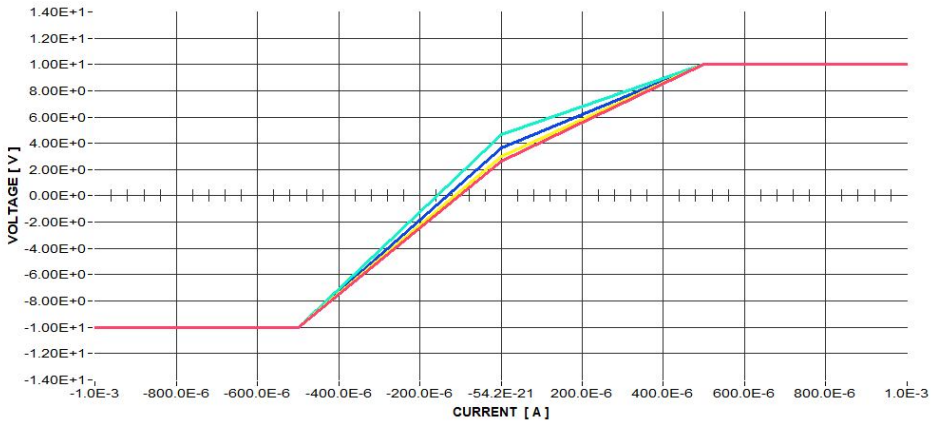

Figure 56: I/V graph of BN co-doped sample (3.5% N_2/C) grown on a Si substrate, showing non-Ohmic contacts but being consistent on all four contacts.

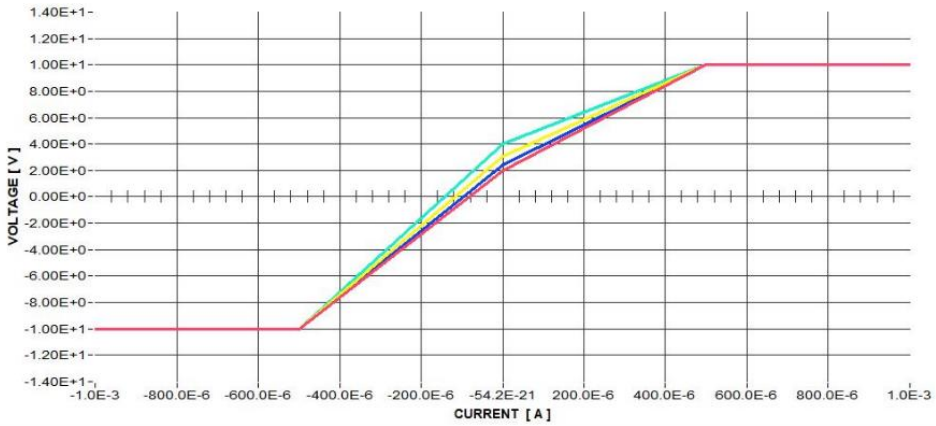

Figure 57: I/V graph of BN co-doped sample (4% N_2/C) grown on a Si substrate, showing non-Ohmic contacts but being consistent on all four contacts.

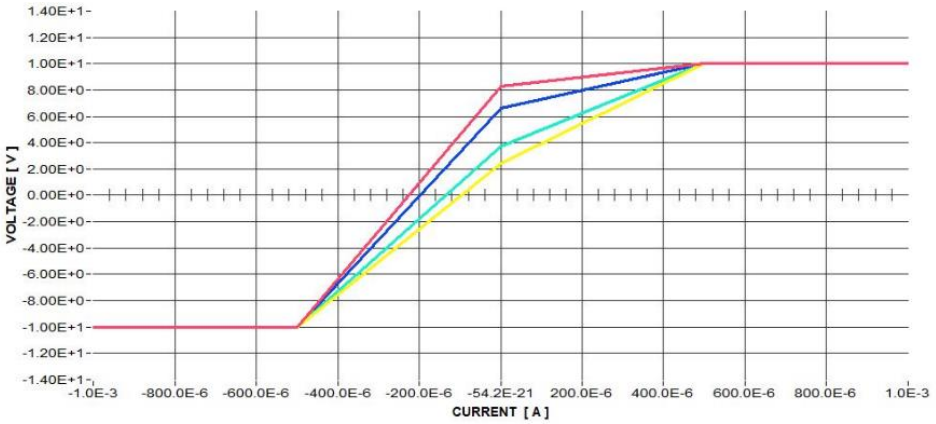

Figure 58: I/V graph of BN co-doped sample (4.5% N_2/C) grown on a Si substrate, showing non-Ohmic contacts but being consistent on all four contacts.

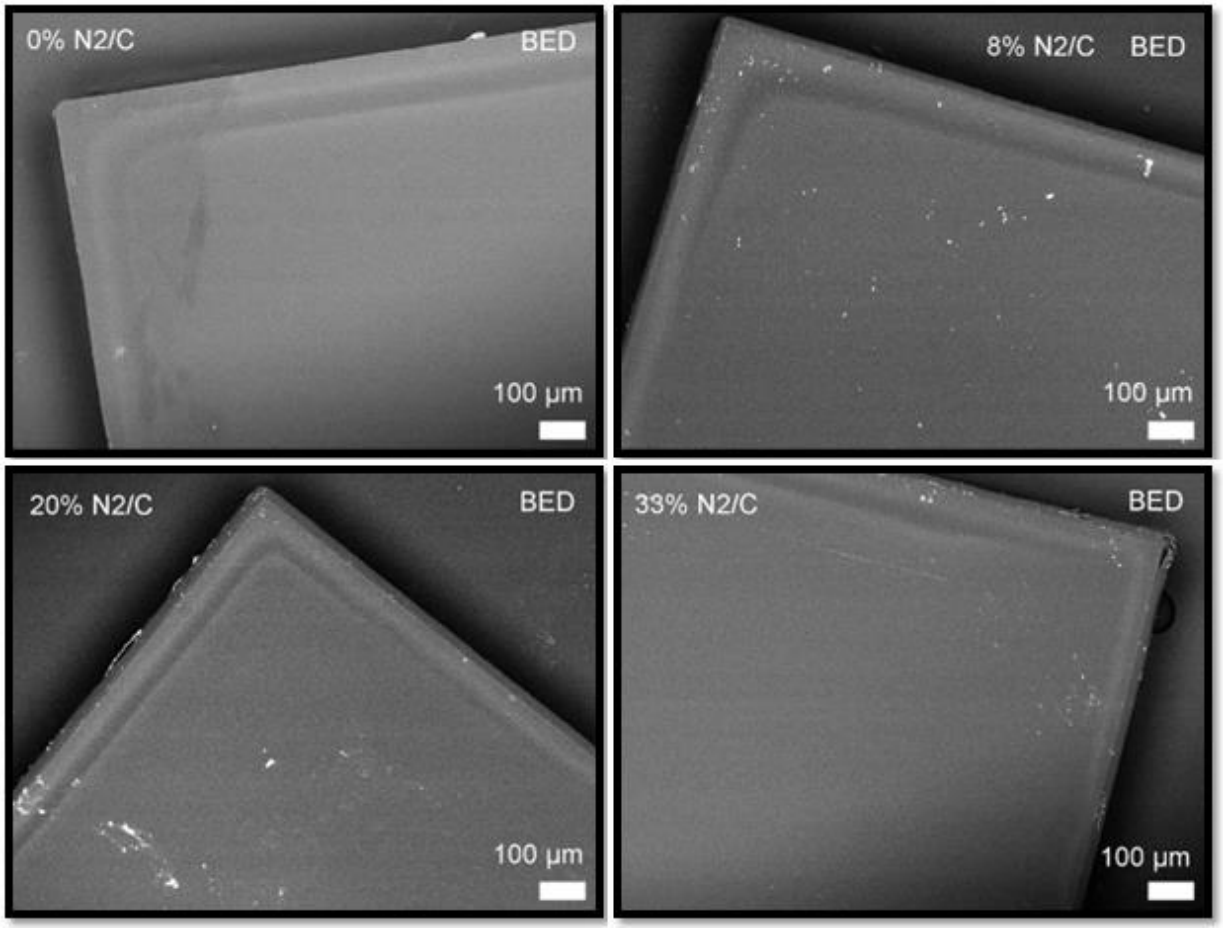

Figure 59: Four different images taken with BED on SEM facility, showing smooth surfaces with few scratches which are not enough to explain the 'edge effect'. All images were taken with an acceleration voltage of 15 kV and a magnification of x100.

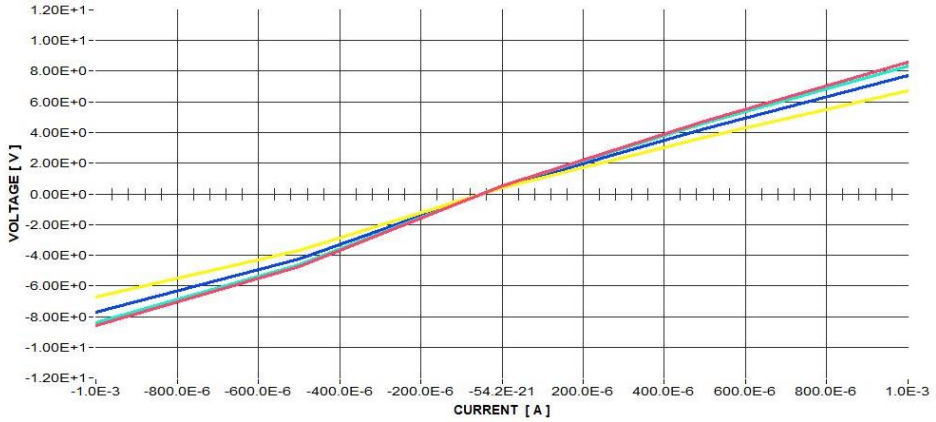

Figure 60: I/V graph of BDD sample grown on SCD, showing Ohmic contact in all four contacts.

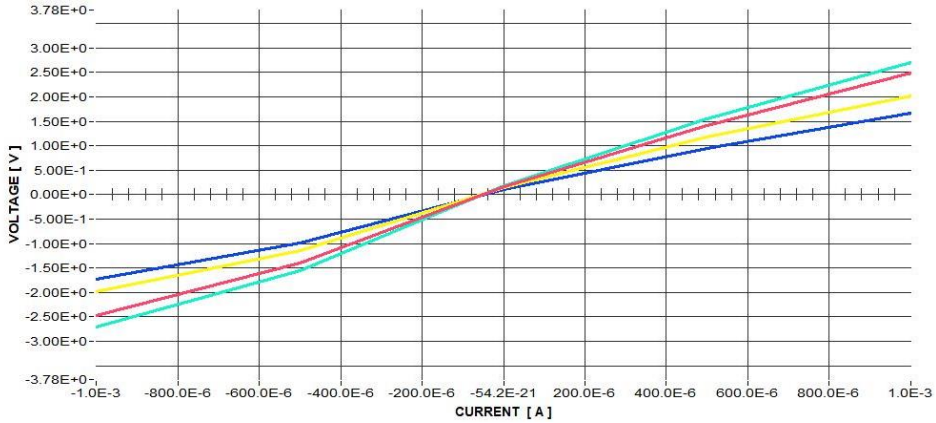

Figure 61: I/V graph of BN-6.7% on SCD, showing Ohmic contact in the Hall effect measurements.

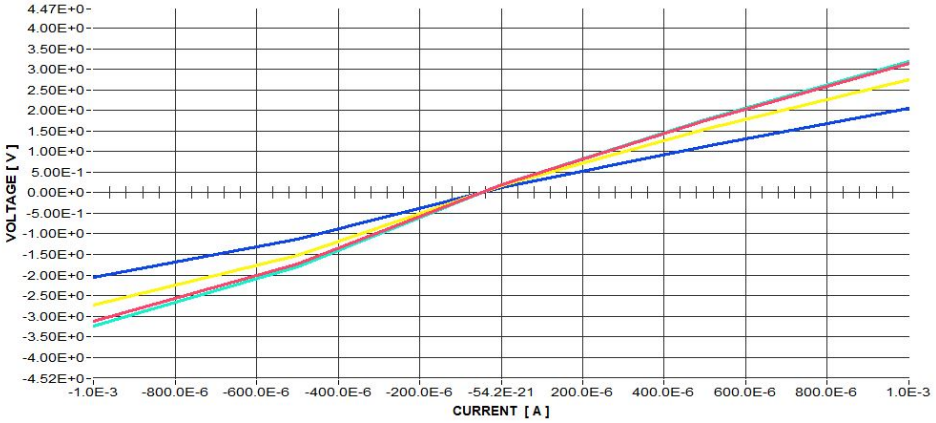

Figure 62: I/V graph of BN-8% on SCD, showing Ohmic contact in the Hall effect measurements.

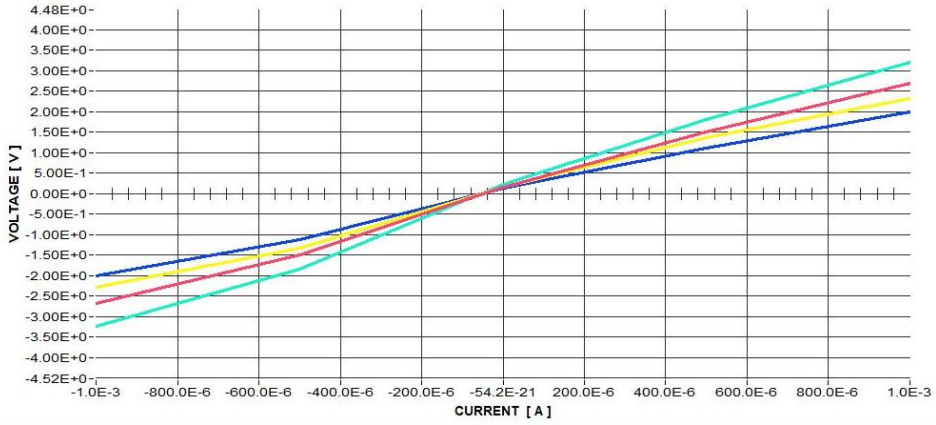

Figure 63: I/V graph of BN-10% on SCD, showing Ohmic contact in the Hall effect measurements.

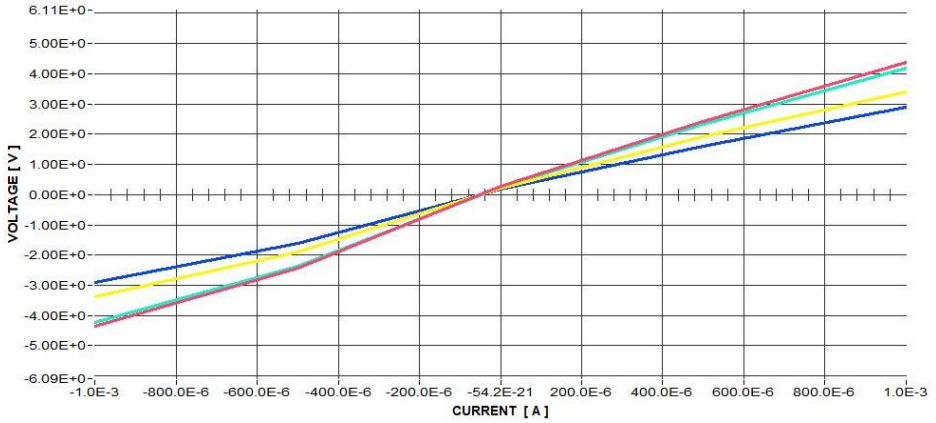

Figure 64: I/V graph of BN-20% on SCD, showing Ohmic contact in the Hall effect measurements.

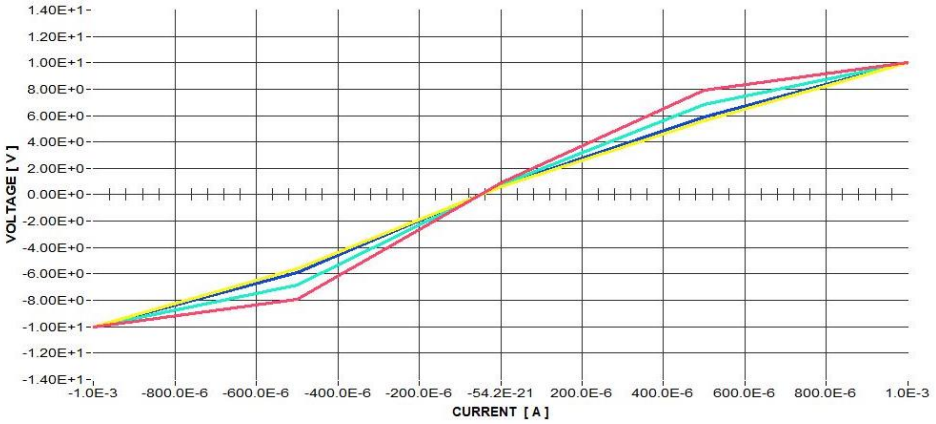

Figure 65: I/V graph of BN-30% on SCD, showing less Ohmic contact in the Hall effect measurements than the previous samples.

7. Bibliography

[i] Ashfold, M.N. et al. (1994) “Thin film diamond by chemical vapour deposition methods,” Chemical Society Reviews, 23(1), p. 21.

[ii] Chen, M. et al. (2018) “Natural diamond formation by self-redox of Ferromagnesian carbonate,” Proceedings of the National Academy of Sciences, 115(11), pp. 2676–2680..

[iii] Hall, H.T. (1961) “The synthesis of diamond,” Journal of Chemical Education, 38(10), p. 484.

[iv] Linares, R. (2013) ‘‘CVD-Grown Synthetic Diamonds,’’ Integrated Diamond Technologies, LLC.

[v] Kharisov, B.I. and Kharissova, O.V. (2019) “Conventional carbon allotropes,” *Carbon Allotropes: Metal-Complex Chemistry, Properties and Applications*, pp. 9–33.

[vi] Ristein, J. (2006) “Surface science of diamond: Familiar and amazing,” Surface Science, 600(18), pp. 3677–3689.

[vii] Wang, J. *et al.* (2021) “A review of tool wear mechanism and suppression method in diamond turning of ferrous materials,” *The International Journal of Advanced Manufacturing Technology*, 113(11-12), pp. 3027–3055.

[viii] Mortet, V. *et al.* (2015) “Properties of boron-doped epitaxial diamond layers grown on (110) oriented single crystal substrates,” *Diamond and Related Materials*, 53, pp. 29–34.

[ix] Breeding, C.M. and Shigley, J.E. (2009) “The ‘Type’ Classification System of Diamonds and its importance in gemology,” Gems & Gemology, 45(2), pp. 96–111.

[x] Blank, V. et al. (1999) “Mechanical properties of different types of diamond,” Diamond and Related Materials, 8(8-9), pp. 1531–1535.

[xi] Piekarczyk, W. (1998) “How and why CVD diamond is formed: a solution of the thermodynamic paradox,” Journal of Materials Science, 33(13), pp. 3443–3453.

[xii] D’Haenens-Johansson, U.F., Butler, J.E. and Katrusha, A.N. (2022) “Synthesis of diamonds and their identification,” Reviews in Mineralogy and Geochemistry, 88(1), pp. 689–753.

[xiii] Sonin, V. et al. (2022) “The composition of the fluid phase in inclusions in synthetic hpht diamonds grown in system Fe–ni–ti–c,” Scientific Reports, 12(1).

[xiv] Wood, G.F. et al. (2021) “High pressure high temperature synthesis of highly boron doped diamond microparticles and porous electrodes for electrochemical applications,” Carbon, 171, pp. 845–856.

[xv] Tu, E. (2009) “Diamonds: For ever or for everyone?,” Berkeley Scientific Journal, 13(1) (Ashfold, 1994).

[xvi] Fang, C. et al. (2017) “Synthesis and characterization of HPHT large single-crystal diamonds under the simultaneous influence of oxygen and hydrogen,” CrystEngComm, 19(38), pp. 5727–5734.

[xvii] Shenderova, O.A. et al. (2019) “Review article: Synthesis, properties, and applications of fluorescent diamond particles,” Journal of Vacuum Science & Technology B, 37(3), p. 030802.

[xviii] Kiflawi, I., Kanda, H. and Lawson, S.C. (2002) “The effect of the growth rate on the concentration of nitrogen and transition metal impurities in HPHT Synthetic Diamonds,” Diamond and Related Materials, 11(2), pp. 204–211.

[xix] Nemanich, R. J., Carlisle, J. A., Hirata, A., & Haenen, K. (2014). CVD diamond—Research, applications, and challenges. MRS Bulletin, 39(6), 490–494.

[xx] Matsumoto, S., Sato, Y., Kamo, M., & Setaka, N. (1982). Vapor Deposition of Diamond Particles from Methane. Japanese Journal of Applied Physics, 21(Part 2, No. 4), L183–L185.

[xxi] Matsumoto, S., Sato, Y., Tsutsumi, M., & Setaka, N. (1982). Growth of diamond particles from methane-hydrogen gas. Journal of Materials Science, 17(11), 3106–3112.

[xxii] Choy, K. (2003) “Chemical vapour deposition of coatings,” Progress in Materials Science, 48(2), pp. 57–170.

[xxiii] May, P.W. (no date) Modelling CVD diamond growth, CVD Diamond Group - School of Chemistry - Bristol University.

[xxiv] Gracio, J. J., Fan, Q. H., & Madaleno, J. C. (2010b). Diamond growth by chemical vapour deposition. Journal of Physics D: Applied Physics, 43(37), 374017.

[xxv] Degutis, G. et al. (2016) “CVD diamond growth from nanodiamond seeds buried under a thin chromium layer,” Diamond and Related Materials, 64, pp. 163–168.

[xxvi] Das, D., & Singh, R. N. (2007). A review of nucleation, growth and low temperature synthesis of diamond thin films. International Materials Reviews, 52(1), 29–64.

[xxvii] Pastor-Moreno, G. (2002) Electrochemical applications of CVD Diamond. thesis. University of Bristol.

[xxviii] Williams, O.A. et al. (2006) “Comparison of the growth and properties of ultrananocrystalline Diamond and Nanocrystalline Diamond,” Diamond and Related Materials, 15(4-8), pp. 654–658.

[xxix] Williams, O.A. (2011) “Nanocrystalline Diamond,” Diamond and Related Materials, 20(5-6), pp. 621–640.

[xxx] Haubner, R. (2021) “Low-pressure diamond: From the unbelievable to technical products,” ChemTexts, 7(2)..

[xxxi] Kamo, M., Sato, Y., Matsumoto, S., & Setaka, N. (1983). Diamond synthesis from gas phase in microwave plasma. Journal of Crystal Growth, 62(3), 642–644.

[xxxii] Weller, M. T., Overton, T., Rourke, J., & Armstrong, F. A. (2018). Inorganic Chemistry. Oxford: Oxford University Press.

[xxxiii] Canadell, E., Doublet, M., & Iung, C. (2016). Orbital approach to the electronic structure of Solids. Oxford: Oxford University Press.

[xxxiv] *Electrical resistivity and conductivity* (2019) *Michael Pilgaard's Web Chemistry*. Available at: https://pilgaard.info/Conductivity/ConductivityResistivity.htm (Accessed: March 24, 2023).

[xxxv] Averill, G., & Eldredge, P. (2007). Chemistry: Principles, patterns, and applications. San Francisco, CA: Pearson Benjamin Cummings.

[xxxvi] McKelvey, J. P. (1966). Solid state and semiconductor physics. Florida: Harper.

[xxxvii] https://en.wikipedia.org/wiki/Electronic_band_structure

[xxxviii] Ohashi, H. (2012). Power devices now and future, strategy of Japan. 2012 24th International Symposium on Power Semiconductor Devices and ICs.

[xxxix] Araujo, D., Suzuki, M., Lloret, F., Alba, G., & Villar, P. (2021). Diamond for Electronics: Materials, Processing and Devices. Materials, 14(22), 7081.

[xl] Wort, C. J., & Balmer, R. S. (2008). Diamond as an electronic material. Materials Today, 11(1–2), 22–28.

[xli] Kalish, R. (2007). Diamond as a unique high-tech electronic material: difficulties and prospects. Journal of Physics D: Applied Physics, 40(20), 6467–6478.

[xlii] Post author By mattk (2022) *Home*, *IQS Directory*. IQS Resource Center. Available at: https://www.iqsdirectory.com/resources/everything-you-ever-wanted-to-know-about-semiconductors/ (Accessed: December 18, 2022).

[xliii] Trucchi, D.M. et al. (2006) “Feasibility of CVD diamond radiation energy conversion devices,” Diamond and Related Materials, 15(11-12), pp. 1980–1985.

[xliv] Wort, C.J.H. and Balmer, R.S. (2008) “Diamond as an electronic material,” Materials Today, 11(1-2), pp. 22–28.

[xlv] Macpherson, J.V. (2015) “A practical guide to using boron doped diamond in electrochemical research,” Physical Chemistry Chemical Physics, 17(5), pp. 2935–2949.

[xlvi] Sartori, A.F. and Stritzker, B. (2016) Heteroepitaxial boron-doped diamond: from synthesis to application. PhD dissertation. Augsburg University.

[xlvii] Diamond doping (no date) Applied diamond, Inc.. Available at: http://usappliedddiamond.com/capabilities/doping/?gclid=Cj0KCQiA4aacBhCUARIsAI55maHO-VYtt_y-Ol_eXLi0zYwklyD-F-7bzXeG3SSWTNt6jw2oOUQNKfoaAvPTEALw_wcB (Accessed: December 20, 2022).

[xlviii] Lagrange, J.-P., Deneuville, A. and Gheeraert, E. (1998) “Activation energy in low compensated homoepitaxial boron-doped diamond films,” Diamond and Related Materials, 7(9), pp. 1390–1393.

[xlix] Watanabe, T. et al. (2018) “The local structure in heavily boron-doped diamond and the effect this has on its electrochemical properties,” Carbon, 137, pp. 333–342.

[l] Yao, Y. et al. (2020) “Review on the properties of boron-doped diamond and one-dimensional-metal-oxide based P-N Heterojunction,” Molecules, 26(1), p. 71.

[li] Roychoudhury, R. et al. (1997) “Growth and characterization of phosphorus doped diamond films using trimethyl phosphite as the doping source,” Journal of Applied Physics, 81(8), pp. 3644–3646.

[lii] Farrer, R.G. (1969) “On the substitutional nitrogen donor in diamond,” Solid State Communications, 7(9), pp. 685–688.

[liii] Fang, C. et al. (2018) “Preparation of ‘natural’ diamonds by HPHT annealing of synthetic diamonds,” CrystEngComm, 20(4), pp. 505–511.

[liv] Zaitsev, A.M. et al. (2020) “Nitrogen-doped CVD diamond: Nitrogen concentration, color and internal stress,” Diamond and Related Materials, 105, p. 107794.

[lv] Doherty, M.W. et al. (2013) “The nitrogen-vacancy colour centre in diamond,” Physics Reports, 528(1), pp. 1–45.

[lvi] Baranauskas, V. *et al.* (1999) “Nitrogen-doped diamond films,” *Journal of Applied Physics*, 85(10), pp. 7455–7458.

[lvii] Jensen, K., Kehayias, P. and Budker, D. (2016) “Magnetometry with Nitrogen-Vacancy Centers in Diamond,” Smart Sensors, Measurement and Instrumentation, pp. 553–576.

[lviii] Katagiri, M. et al. (2004) “Lightly phosphorus-doped homoepitaxial diamond films grown by chemical vapor deposition,” Applied Physics Letters, 85(26), pp. 6365–6367.

[lix] Liu, D.Y. et al. (2021) “Nitrogen modulation of boron doping behavior for accessible n-type diamond,” APL Materials, 9(8), p. 081106.

[lx] Kalish, R. (1997) “Ion-implantation in diamond and diamond films: doping, damage effects and their applications,” Applied Surface Science, 117–118, pp. 558–569.

[lxi] Pinault, M.-A. et al. (2007) “The n-type doping of diamond: Present status and pending questions,” Physica B: Condensed Matter, 401–402, pp. 51–56.

[lxii] Conejeros, S. et al. (2021) “Hunting the elusive shallow n-type donor – An ab initio study of Li and N co-doped diamond,” Carbon, 171, pp. 857–868.

[lxiii] Katayama-Yoshida, H. et al. (2001) “Codoping method for the fabrication of low-resistivity wide band-gap semiconductors in p-type GaN, p-type AlN and n-type diamond: prediction versus experiment,” Journal of Physics: Condensed Matter, 13(40), pp. 8901–8914.

[lxiv] Segev, D. and Wei, S.-H. (2003) “Design of Shallow Donor Levels in Diamond by Isovalent-Donor Coupling,” Physical Review Letters, 91(12).

[lxv] Miyazaki, T., Okushi, H. and Uda, T. (2002) “Shallow Donor State Due to Nitrogen-Hydrogen Complex in Diamond,” Physical Review Letters, 88(6).

[lxvi] Shen, S. et al. (2020) “First-principles calculations of co-doping impurities in diamond,” Materials Today Communications, 23, p. 100847.

[lxvii] Dr. Jonathan Goss, 'n-type doping of diamond'. Available at: https://www.staff.ncl.ac.uk/j.p.goss/Research/NtypeDiamond/.

[lxviii] Balmer, R.S. et al. (2007) "Unlocking diamond's potential as an electronic material," Philosophical Transactions of the Royal Society A: Mathematical, Physical and Engineering Sciences, 366(1863), pp. 251–265.

[lxix] Liou, Y., Inspektor, A., Weimer, R. et al. The effect of oxygen in diamond deposition by microwave plasma enhanced chemical vapor deposition. Journal of Materials Research 5, 2305–2312 (1990).

[lxx] Tallaire, A. et al. (2016) "Growth of thick and heavily boron-doped (113)-oriented CVD diamond films," Diamond and Related Materials, 66, pp. 61–66.

[lxxi] A. Croot, "Boron and nitrogen in diamond: An ab initio simulation, plasma emission spectroscopy and material deposition and characterisation study," Ph.D. thesis, University of Bristol, 2018.

[lxxii] Croot, A. et al. (2018) "A theoretical study of substitutional boron–nitrogen clusters in diamond," Journal of Physics: Condensed Matter, 30(42), p. 425501.

[lxxiii] Prawer, S. and Nemanich, R.J. (2004) "Raman spectroscopy of diamond and Doped Diamond," Philosophical Transactions of the Royal Society of London. Series A: Mathematical, Physical and Engineering Sciences, 362(1824), pp. 2537–2565.

[lxxiv] Knight, D.S. and White, W.B. (1989) "Characterization of diamond films by Raman Spectroscopy," Journal of Materials Research, 4(2), pp. 385–393.

[lxxv] Dychalska, A. *et al.* (2015) "Study of CVD diamond layers with amorphous carbon admixture by Raman scattering spectroscopy," *Materials Science-Poland*, 33(4), pp. 799–805.

[lxxvi] Zhuang, H. *et al.* (2012) "Nanoscale integration of SiC/SIO2 core-shell nanocables in diamond through a simultaneous hybrid structure fabrication," *Applied Physics Letters*, 100(19), p. 193102.

[lxxvii] Fortunato, W. *et al.* (2007) "Crystalline quality and phase purity of CVD Diamond Films studied by Raman Spectroscopy," *Journal of Materials Science*, 42(17), pp. 7331–7336.

[lxxviii] Larkins, E.C. and Harris, J.S. (1995) "Molecular beam epitaxy of high-quality gaas and AlGaAs," *Molecular Beam Epitaxy*, pp. 114–274.

[lxxix] *Resistivity and hall measurements* (2022) *NIST*. NIST. Available at: https://www.nist.gov/pml/nanoscale-device-characterization-division/popular-links/hall-effect/resistivity-and-hall (Accessed: February 22, 2023).

[lxxx] Vernon-Parry, K.D. (2000) "Scanning electron microscopy: An introduction," *III-Vs Review*, 13(4), pp. 40–44.

[lxxxi] Gleichmann, N. (2020) *Sem Vs Tem*, *Analysis & Separations from Technology Networks*. Technology Networks. Available at: https://www.technologynetworks.com/analysis/articles/sem-vs-tem-331262 (Accessed: February 22, 2023).

[lxxxii] Mohammed, A. and Abdullah, A. (2018) “Scanning electron microscopy (SEM): A Review,” *Proceedings of 2018 International Conference on Hydraulics and Pneumatics.*

[lxxxiii] Nanakoudis, A. (2022) *SEM: Types of electrons and the information they provide*, *Advancing Materials*. Thermofisher scientific. (Accessed: March 21, 2023).

[lxxxiv] Yiming, Z., Larsson, F. and Larsson, K. (2013) “Effect of CVD diamond growth by doping with nitrogen,” *Theoretical Chemistry Accounts*, 133(2).

[lxxxv] Nakano, Y. *et al.* (2022) “Impact of nitrogen doping on homoepitaxial diamond (111) growth,” *Diamond and Related Materials*, 125, p. 108997.

[lxxxvi] Werner, F. (2017) “Hall measurements on low-mobility thin films,” *Journal of Applied Physics*, 122(13), p. 135306.